LA-13424-T
Thesis

A Viscoplastic Model of Expanding Cylindrical Shells Subjected to Internal Explosive Detonations

Los Alamos
NATIONAL LABORATORY

Los Alamos National Laboratory is operated by the University of California for the United States Department of Energy under contract W-7405-ENG-36.

This thesis was accepted by the Department of Mechanical Engineering, Colorado State University, Fort Collins, Colorado, in partial fulfillment of the requirements for the degree of Doctor of Philosophy. The text and illustrations are the independent work of the author and only the front matter has been edited by the CIC-1 Writing and Editing Staff to conform with Department of Energy and Los Alamos National Laboratory publication policies.

An Affirmative Action/Equal Opportunity Employer

This report was prepared as an account of work sponsored by an agency of the United States Government. Neither The Regents of the University of California, the United States Government nor any agency thereof, nor any of their employees, makes any warranty, express or implied, or assumes any legal liability or responsibility for the accuracy, completeness, or usefulness of any information, apparatus, product, or process disclosed, or represents that its use would not infringe privately owned rights. Reference herein to any specific commercial product, process, or service by trade name, trademark, manufacturer, or otherwise, does not necessarily constitute or imply its endorsement, recommendation, or favoring by The Regents of the University of California, the United States Government, or any agency thereof. The views and opinions of authors expressed herein do not necessarily state or reflect those of The Regents of the University of California, the United States Government, or any agency thereof. Los Alamos National Laboratory strongly supports academic freedom and a researcher's right to publish; as an institution, however, the Laboratory does not endorse the viewpoint of a publication or guarantee its technical correctness.

LA-13424-T
Thesis

UC-741
Issued: April 1998

A Viscoplastic Model of Expanding Cylindrical Shells Subjected to Internal Explosive Detonations

Rick L. Martineau

Los Alamos
NATIONAL LABORATORY
Los Alamos, New Mexico 87545

ACKNOWLEDGMENTS

A statement of appreciation is due to several of people at Los Alamos National Laboratory who assisted me during the course of this dissertation with technical advice and financial support.

I would like to thank Chuck Anderson for his help, patience, and guidance. Chuck's professionalism, knowledge, and vision have been a motivation for me throughout this research. His insight into the mechanics of this problem was extremely valuable.

I would like to thank Professor Fred Smith for all of his help and guidance throughout this program. His insight, enthusiasm, and devotion to the field of engineering is enlightening and inspirational.

I would also like to thank my other committee members Professor Donald Radford, Professor Michael Peterson, and Professor Bogusz Bienkiewicz for the time they spent with me discussing and reviewing my dissertation.

I am grateful for the insightful conversations and opportunity to work with Mike Prime. His suggestions and support of this project are greatly appreciated. I really appreciate his time and enthusiasm with all aspects of this project especially during the cylinder experiments.

I would like to thank Val Hart, Allan Anderson, Mike Burns, Kirk Christensen, and Will Fox for their support and assistance in helping me to develop and promote this research program.

I am grateful to my upper management Jim Straight, Steve Girrens, Larry Goen, Kirk Christensen, Will Fox, and Don Rabern for their support while I've been researching this topic. Their support and vision allowed me to concentrate the majority of my efforts on this research which was greatly appreciated.

I am grateful to Tim Neal, Carmelo Spirio, Alan Patterson, and Tom Alexander for their financial support of my education while at Colorado State University and during the course of this research.

I am thankful to Eric Ferm for our countless conversations regarding shock physics and stress wave behavior. I really appreciate all of the time Eric has spent with me over the years discussing hydrocodes and the behavior of shock waves.

I would like to thank Larry Hill for the copper tubes and C-4 used in the explosive bulge test. The results of this test proved to be insightful and an important part of this research.

I am grateful to Carl Necker for the conversations we have had regarding copper, microvoids, and metallurgy in general. I really enjoyed working with Carl and am grateful for all of his assistance from the heat-treatment procedures to the photomicrographs.

I would like to thank Mike Christian for all of his suggestions and ideas regarding explosive cylinder tests. Mike's vast experience, suggestions, knowledge, and enthusiasm in this area were a great asset in developing the experiments and analyzing the data.

I am also thankful for the support from Christopher Romero. I really appreciate his programmatic support during the course of this research.

I am grateful to Jim Johnson and Stan Marsh for helping me to understand hydrocodes and high pressure shock waves and their relevance to this research. I would also like to thank Stan for his suggestions and insights regarding experimental configurations.

I am grateful to John Balog for his assistance with machining. I really appreciate John's extra efforts in obtaining high quality mechanical hardware.

I would like to thank Manny Chavez and Ernst Christen for their help and guidance regarding high explosives, high explosive machining, and shot assembly. Their professionalism and dedication is greatly appreciated.

I am grateful to Will Hemsing and Mike Shinas for their time and expertise with the Fabry-Perot equipment. Will's knowledge and expertise in this area was insightful and very valuable.

I am thankful to Steve Ellis for helping me expedite the layouts and release of the mechanical drawings used to fabricate the hardware for the experiments and in general for all of our discussions regarding mechanical hardware.

I am grateful to Ron Boat for his guidance and direction during the high explosive experiments. I appreciate his time and suggestions regarding the fast framing camera equipment and the overall set-up of the experiment.

I am grateful to Keith Haberman and Joel Bennett for our discussions regarding cutting plane techniques and continuum mechanics.

I am grateful to Mike Catanach and Dan Custer for their support with the mechanical drawings used to fabricate the hardware and set-up the experiments.

TABLE OF CONTENTS

Title Page iii
Acknowledgements v
Table of Contents vii
List of Tables ix
List of Figures x
List of Symbols and Their Dimensions xii
Abstract xv

1.0 Introduction and Problem Definition 1
- 1.1 Why Study Expanding Shells 2
- 1.2 Background on Experimental Studies 5
- 1.3 Background on Numerical Studies 10
- 1.4 Shortcomings in Existing Literature 12
- 1.5 Scope of Work Presented in this Dissertation 15

2.0 Constitutive Models 17
- 2.1 Material Strength Models 18
- 2.2 Shock Waves and the Equation of State 21
- 2.3 Microvoid Damage Model 37

3.0 Numerical Model 43
- 3.1 EOS Subroutine 45
- 3.2 GTN Subroutine 47
- 3.3 Strength Subroutine 53
- 3.4 Void Subroutine 53
- 3.5 "Element Remove" Subroutine 55
- 3.6 HE Burn Model 56
- 3.7 Preliminary Results 57

4.0 Cylinder Experiments 65
- 4.1 Cylinder Material and Design 66
- 4.2 High Explosive Type and Design 67
- 4.3 Firing Point Set-Up 70
- 4.4 Preliminary Observations 74

5.0 Model Verifications 78
5.1 Axisymmetric Numerical Model and Parameters. 78
5.2 Comparison of Numerical Results with Experimental Data 83

6.0 Dynamic Instabilities 92
6.1 Plane Strain Numerical Model 93
6.2 Instability Development 95
6.3 Sensitivity Study 103

7.0 Summary and Conclusions 114

8.0 References 119

9.0 Appendix A – Fabrication Drawings 124

10.0Appendix B – Fortran Source Code for VUMAT Subroutine 128

List of Tables

Table

1.1 Classification of Strain-Rates and Testing Methods 5

2.1 Material Constants for the Johnson-Cook Strength Model 20
2.2 Longitudinal Velocity of Elastic Waves 31
2.3 Shock and Thermodynamic Properties of Metals 32

3.1 JWL Parameters for PBX-9501 56
3.2 User Parameters Supplied to the Constitutive Model for the Copper Ring 59

4.1 Dimensions of the Two Cylinders Used for the Experiments 67

5.1 Number of Elements Used in Axisymmetric Model of HE and Copper Cylinder. . 79
5.2 User Parameters Supplied to the Axisymmetric Model 81
5.3 Gurney Velocity for Cylindrical Shell Experiments 88
5.4 Number of Instabilities for Each Cylinder as Determined from the Fast Framing Camera Photographs 90

6.1 Impulse and Number of Elements for Four Cylinders with 50.8 mm Inside Radius 104
6.2 Results from Mesh Sensitivity Study 112
6.3 Results from Void Range Sensitivity Study 113

List of Figures

Figures

1.1 Compressive and Tensile Stresses on Expanding Ring 7
1.2 Exaggerated Fractures from a High and Low Pressure Detonation 9

2.1 Johnson-Cook Flow Stress for OFE Copper as a Function of Strain. 21
2.2 Profile of a Shock Front Propagating Through a Material 23
2.3 Plot of the Hugoniot Curve and Rayleigh Line on the P-V Plane 25
2.4 Formation of a Stable Shock Wave 26
2.5 One-dimensional and Hydrostatic Compression of Solids. 28
2.6 Wave Structure in Relation to the Hugoniot Curve and Rayleigh Line. 30

3.1 Flow Chart for VUMAT Subroutine 45
3.2 Mesh for Preliminary Axisymmetric Ring Model 57
3.3 Shock and EOS Effects on the Bulk Modulus 60
3.4 Temperature Effects from High Pressure Shock and Plastic Work 61
3.5 Hoop Stress on the ID and OD of Expanding Ring from 0-30 Microseconds. 62
3.6 Hoop Stress on the ID and OD of Expanding Ring from 30-100 Microseconds . . 62
3.7 Strain Rate on the ID with and without EOS Model 63
3.8 Hoop Strain with and without EOS Model 64
3.9 Void Volume Fraction on the OD with and without EOS Model 64

4.1 Microstructure of the Copper Material Before and After Heat Treat 66
4.2 Copper Cylinder and HE Assemblies 70
4.3 Elevation View of the Experimental Set-Up 71
4.4 Plan View of the Experimental Set-Up 72
4.5 Shot Stand Used in Experimental Set-Up 73
4.6 Experimental Set-Up 74
4.7 Framing Camera Images for the Thin Cylinder. 75
4.8 View of Instabilities on Expanding Thin Cylinder 76
4.9 Firing Point Following Explosive Detonation of the Thick Cylinder 77
4.10 Fragments Obtained from Explosive Detonation of Copper Cylinders 77

5.1 Axisymmetric Mesh of HE and Copper Cylinder 79
5.2 Deformed Axisymmetric Edge of the Copper Cylinder Computed
from the Numerical Model 82
5.3 Deformed Geometry for the 2.54 mm Thick Copper Cylinder 84
5.4 Deformed Geometry for the 5.08 mm Thick Copper Cylinder 85

5.5 Radial Displacement as a Function of Time at Eight Locations Along the Longitudinal Axis of the 2.54 mm Thick Cylinder 87
5.6 Radial Displacement as a Function of Time at Eight Locations Along the Longitudinal Axis of the 5.08 mm Thick Cylinder 87
5.7 Radial Velocity as a Function of Time for the 2.54 mm Thick Cylinder 89
5.8 Radial Velocity as a Function of Time for the 5.08 mm Thick Cylinder 89

6.1 Plane Strain Mesh for Instability Investigation 94
6.2 Pressure Time History for the 2.54 mm Thick Cylinder 95
6.3 Bulged Tube from C-4 Experiment 96
6.4 Exaggerated Illustration of Quasi-Periodic Instabilities 97
6.5 Shear Band from Bulged Tube Experiment 97
6.6 Equivalent Plastic Strain and Surface Features from the Numerical Model 99
6.7 Equivalent Plastic Strain at 7.6 Microseconds 100
6.8 Equivalent Plastic Strain Rate at 7.6 Microseconds 101
6.9 Temperature at 7.6 Microseconds 101
6.10 Volumetric Void Fraction at 7.6 Microseconds 102
6.11 Illustration of Failure Criterion for Expanding Shell 105
6.12 Change in Wall Thickness for Expanding Cylinder 107
6.13 Failure Time vs Shell Thickness for Three Values of q_1 108
6.14 Strain at Failure vs q_1 for Four Cylinders with Different Shell Thickness 108
6.15 Maximum Equivalent Plastic Strain Rate at Failure vs Shell Thickness for Three Values of q_1 109
6.16 Maximum Volumetric Void Fraction at Failure vs Shell Thickness for Three Values of q_1 109
6.17 Maximum Equivalent Plastic Strain Rate at Failure vs Shell Thickness for Three Values of q_1 110
6.18 Number of Circumferential Instabilities vs Shell Thickness 110

LIST OF SYMBOLS AND THEIR DIMENSIONS

U_s – Shock Velocity [L/T]

U_p – Particle Velocity [L/T]

P – Pressure [M/LT^2]

P_H – Pressure on Hugoniot Curve [M/LT^2]

ρ – Density [M/L^3]

V – Specific Volume [L^3/M]

η – First Strain Invariant [None]

λ – Lamé Constant [M/LT^2]

G – Shear Modulus [M/LT^2]

K – Bulk Modulus [M/LT^2]

D – Elastic Constant Matrix [M/LT^2]

f – Void Volume Fraction [L^3/L^3]

f_c – Critical Void Volume Fraction [L^3/L^3]

f_f – Final Void Volume Fraction [L^3/L^3]

f_N – Volume Fraction for Void Nucleation [L^3/L^3]

S_N – Standard Deviation for Void Nucleation [None]

$\dot{f}_{gr}$ – Void Growth [L^3/L^{3}T]

$\dot{f}_{nucl}$ – Void Nucleation Rate [L^3/L^{3}T]

σ_f – Flow Stress [M/LT^2]

σ_y – Yield Stress [M/LT^2]

σ_n – Normal Stress [M/LT^2]

σ_t – Transverse Stress [M/LT^2]

σ_{ij} – Stress Tensor [M/LT^2]

σ – Effective Stress [M/LT^2]

S_{ij} – Deviatoric Stress Tensor [M/LT^2]

δ_{ij} – Kronecker Delta [None]

$\dot{W}_p$ – Rate of Plastic Work [ML^2/T^2]

T – Temperature [θ]

T_s – Shock Temperature [θ]

Y – Yield Stress [M/LT^2]

$\tau_{\max}$ – Maximum Shear Stress [M/LT^2]

C_e – Longitudinal Elastic Wave Speed [L/T]

C_{pl} – Plastic Wave Speed [L/T]

C_o – Isentropic Sound Speed [L/T]

γ – Grüneisen Gamma [None]

η – Normal Strain [None]

ε_v – Volumetric Strain [None]

ε – Strain [None]

ε^{el} – Elastic Strain [None]

ε^{pl} – Plastic Strain [None]

$\dot{\varepsilon}$ – Strain Rate [1/T]

$\bar{\varepsilon}_m^{pl}$ – Mean Plastic Strain [None]

E – Energy [L^2/T^2]

Q – Heat [L^2/T^2]

W^{pl} – Plastic Work [L^2/T^2]

C_v – Constant Volume Specific Heat [L^2/T^2 θ]

S – Specific Entropy [L^2/T^2 θ]

ϕ – Yield Function [None]

ζ – Relative Material Density [ML^3/ML^3]

Unless otherwise noted, the letter '*d*' preceding a symbol indicates the incremental value.

A VISCOPLASTIC MODEL OF EXPANDING CYLINDRICAL SHELLS SUBJECTED TO INTERNAL EXPLOSIVE DETONATIONS

by

Rick L. Martineau

ABSTRACT

Magnetic flux compression generators rely on the expansion of thin ductile shells to generate magnetic fields. These thin shells are filled with high explosives, which when detonated, cause the shell to expand to over 200% strain at strain-rates on the order of 10^4 s^{-1}. Experimental data indicate the development and growth of multiple plastic instabilities which appear in a quasi-periodic pattern on the surfaces of the shells. These quasi-periodic instabilities are connected by localized zones of intense shear that are orientated approximately 45° from the outward radial direction. The quasi-periodic instabilities continue to develop and eventually become through-cracks, causing the shell to fragment.

A viscoplastic constitutive model is formulated to model the high strain-rate expansion and provide insight into the development of plastic instabilities. The formulation of the viscoplastic constitutive model includes the effects of shock heating and damage in the form of microvoid nucleation, growth, and coalescence in the expanding shell. This model uses the Johnson-Cook strength model with the Mie-Grüneisen equation of state and a modified Gurson yield surface. The constitutive model

includes the modifications proposed by Tvergaard and the plastic strain controlled nucleation introduced by Needleman. The constitutive model is implemented as a user material subroutine into ABAQUS/Explicit, which is a commercially available non-linear explicit dynamic finite element program. A cylindrical shell is modeled using both axisymmetric and plane strain elements.

Two experiments were conducted involving plane wave detonated, explosively filled, copper cylinders. Instability, displacement, and velocity data were recorded using a fast framing camera and a Fabry-Perot interferometer. Good agreement is shown between the numerical results and experimental data. An additional explosively bulged cylinder experiment was also performed and a photomicrograph of an instability is shown to provide a qualitative comparison between the experimental observations and the numerical predictions.

Observations from this research indicate the onset of a quasi-periodic pattern in the through-thickness equivalent plastic strain, which occurs early in the deformation process before the stress waves have attenuated. This quasi-periodic pattern continues to develop, eventually connecting the inner and outer surfaces, at which time quasi-periodic instabilities are observed on the surfaces of the shell. In addition, parameter studies performed as part of this research indicate relationships between the shell thickness, the number of instabilities, and the approximate time to failure.

1.0 Introduction and Problem Definition

The high strain-rate deformation of ductile materials subjected to high dynamic pressures is of great fundamental importance to physicists and engineers. High pressure dynamic loading which results in large impulses with short rise times can generate shock waves in a material. These high pressure shock waves, which are often generated by explosives, can destroy, modify or enhance materials. Experimental data have shown that when ductile shells are subjected to internal pressure loading from high explosives, they experience large plastic deformation prior to fragmenting. These shells expand at strain rates on the order of 10^4 sec^{-1}. At approximately 150% strain, multiple plastic instabilities are observed on the outer surface of these shells in a quasi-periodic pattern. These quasi-periodic instabilities continue to develop and eventually form cracks that progress in a way that causes the shell to break into fragments. The entire process takes less than 100 microseconds from detonation to complete fragmentation.

Developing the modeling and constitutive relationships for predicting these plastic instabilities and the overall deformation of the shell are the motivation for this dissertation. Although others have worked on limited constitutive models demonstrating plastic instabilities on rings and cylinders, few have compared their results with experimental data. An experimentally verified finite element model incorporating the constitutive relationships for large plastic deformation, void growth, inertia, strain-rate,

high pressure equation of state effects, and thermal effects will be a valuable tool for analyzing rapidly expanding shells.

1.1 Why Study Expanding Shells

The elastic/viscoplastic behavior of materials is an area of study that encompasses a variety of scientific disciplines with industrial and military applications. Industrial applications typically produce a structure or improve a material. Military applications are generally intended to defeat or protect a structure. In either case, the response of structures subjected to rapidly changing loads is considerably different from those under quasi-static conditions. Applications for this research include hypervelocity accelerators, magnetic flux compression generators, explosive power generating plants, and containment vessels.

In 1948, the first hypervelocity accelerator was developed at the New Mexico School of Mines. This accelerator consisted of a combustion chamber which when ignited, accelerated a solid projectile to velocities as high as 11 km/s. The mechanical behavior of this projectile during the acceleration phases of the machine is critical in understanding the machine limitations (Kinslow, 1970). Scientists at General Electric and the Stanford Research Institute continued this research and in particular investigated applications for explosively driven guns and shaped charges. During the 1980's, research in the area of rail guns became popular as scientists continued to look at hypervelocity accelerators. This work is continuing at the University of Texas (Persad et al., 1997) and at other research institutions around the world. In a recent report by Trucano and Chhabildas, (1995), it was recognized that preventing the fracture and failure of the flier

plates which are subjected to extraordinary accelerations is crucial to the functionality of the machine.

A magnetic flux compression generator uses explosives to amplify electromagnetic fields. This device consists of a thin cylindrical shell filled with high explosives and a low inductance coil (Prishchepenko, 1994). Understanding the high-strain-rate expansion and deformation of the shell is important in improving the functionality and reliability of this type of generator.

Several countries including the USA, Russia, Japan, and UK are working on explosive generator plants (Shchegolevskii, 1983). While this process does not involve the large plastic deformation of materials, understanding the dynamic response of materials is important in the design of the hardware used to contain the explosive detonations.

Large thin walled vessels are often used to contain high explosive detonations in the reduction and elimination of high explosive materials. Police and antiterrorist personnel around the world rely on these vessels to save lives and eliminate potential hazards. Containment vessels are also important in the design and operation of nuclear power plants. These vessels are re-used many times and may sustain damage. Predicting the damage, structural integrity, ultimate load capability, and remaining life are important applications for which the research of this dissertation is needed. A detailed understanding of the dynamic response of the material in the plastic region of behavior is critical to ensure structural integrity.

An understanding of the dynamic response and high strain-rate behavior of materials is also important for other applications. In space, micrometeorites can travel at

velocities as high as 30 km/sec before impacting space structures. Damage to these structures may result from the impact itself, shock waves, or excitation of destructive vibrational modes.

The energy associated with shock waves is also instrumental in industry to harden materials. Techniques like explosive hardening and explosive forming are important in the production of large complex parts. Materials undergoing large plastic deformation at high strain-rates demonstrate enhanced formability allowing engineers to design and produce complicated structures and moldings. Industry also relies on the dynamic behavior of materials to explosively weld dissimilar metals. More recently, explosives are being used for shock synthesis and shock consolidation. Shock synthesis is used to produce diamond powder from carbon, while shock consolidation uses the energy of shock waves to bond fine metal powders.

There is an ongoing need to understand the behavior of materials subjected to high strain-rate deformation. Numerical models capable of predicting the deformation and failure of materials subjected to high strain rates could substantially reduce costs and improve structural reliability. The research presented here provides an investigation into developing this capability for ductile materials such as oxygen free electronic (OFE) grade copper.

The strain rates of interest in this investigation are on the order $10^4\ s^{-1}$, which are easily obtainable with conventional high explosives. Meyers (1994) described five strain-rate categories. These categories are presented below in Table 1.1.

Table 1.1: Classification of Strain-Rates and Testing Methods

Strain-rate, s^{-1}	Category	Testing Method
$10^7 - 10^5$	Ultra High Velocity Impact	Explosives, Impact, Laser
$10^5 - 10^3$	Dynamic-High	Explosives
$10^3 - 10^0$	Dynamic-Low	High Velocity Machines
$10^0 - 10^{-5}$	Quasi-Static	Hydraulic, Screw Driven Machines
$10^{-5} - 10^{-9}$	Creep and Stress Relaxation	Conventional Testing Machines

Materials research in the Dynamic-Low, Quasi-Static, and Creep categories is fairly advanced. However, research in the Dynamic-High and Ultra-High areas is still in its infancy, further justifying the scientific importance of this study.

High explosives are typically used to obtain strain rates above 10^3 s^{-1} and at sufficiently high strain-rates; material can behave like a fluid. Shock physicists, who thoroughly understand the high explosive detonations, have sometimes underestimated the importance of classical engineering plasticity in the high strain-rate deformation of solid materials. This has resulted in the use of hydrocodes to analyze the deformation process. Hydrocodes typically treat the material as a fluid and assume shear effects are negligible or in some cases model the behavior of the material without strength. A summary of previous experimental and numerical work regarding the expansion of thin shells and their failure is provided in the next two sections.

1.2 Background on Experimental Studies

When a thin-walled circular cylinder is subjected to an internal explosion, the walls of the cylinder expand radially. For ductile materials this radial expansion occurs at very high velocities prior to failure by fragmentation. In 1943, Gurney (1943) derived a widely used model for predicting the terminal velocities of fragments from shells

subjected to internal explosive detonations. His expression is based on an energy balance that assumes the potential energy characterizing the explosive charge before the detonation is equal to the kinetic energy of the gases from the detonation products and the metal after detonation and expansion. Gurney's model provides an equation for determining the terminal velocity of common configurations, but provides no information regarding the deformation process itself. In addition, his model does not consider the energy consumed in the deformation of the shell.

The failure of cylindrical structures was first examined in 1944 as a fragmentation problem by Taylor (1963a). G. I. Taylor was concerned with the formation of longitudinal cracks on the outer surface of cylindrical shells subjected to an internal explosive detonation. Taylor proposed that longitudinal cracks in the axial plane will open out into regions where the circumferential stress is tensile, but will not penetrate into regions where this stress is compressive. He concluded that the cracks will not penetrate to the inner wall of the cylinder until the compressive region is reduced to zero thickness and in some cases, the cylinder has nearly doubled its initial diameter. In addition, Taylor observed that for copper tubes with a 3.8 mm wall thickness, the hoop strain at failure by fragmentation was on average 2.4. The research presented in this dissertation is compared with Taylor's conclusions and observations. An expanding circular ring illustrating Taylor's conclusions is shown below in Figure 1.1, where P, represents the internal pressure, t the shell thickness, and r the expanded radius.

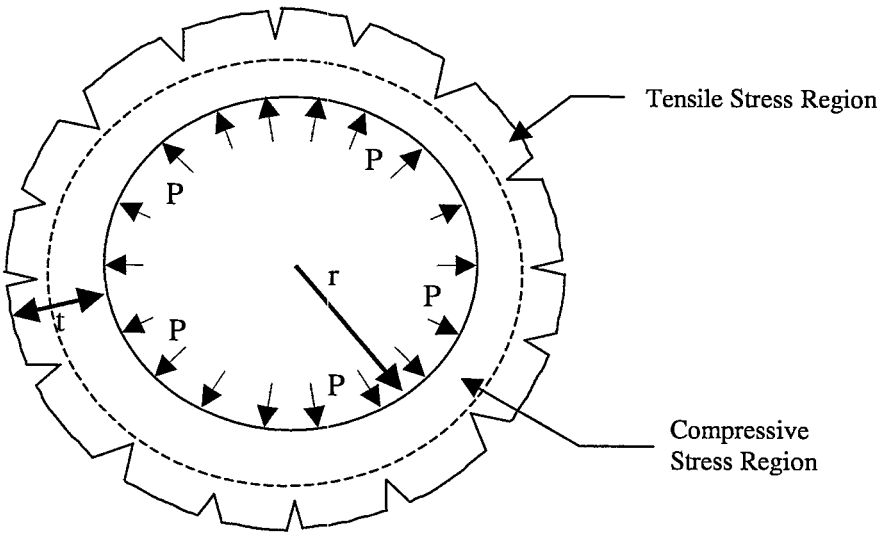

Figure 1.1: Compressive and Tensile Stresses on Expanding Ring

About the same time, Mott (1947), attempted to predict the distribution and size of fragments from a tubular structure based on the assumptions of a perfectly plastic material model and probability theory. Mott examined fragments from expanding shells and concluded that considerable plastic deformation occurs prior to case fragmentation. He also concluded that by the time fracture occurs, the case is traveling at some terminal velocity and the internal pressures for the high explosive have dropped to a small fraction of their original value. Mott observed two types of fractures; shear fractures and cup and cone type fractures. Mott also concluded that initiation of the fracture is not necessarily a surface phenomenon as reported by Taylor, but may occur inside the wall of the shell as in the case of a tensile specimen where high triaxial tensile stress causes the initiation of fracture.

G. I. Taylor (1963b) continued his research in this area and in 1963, another paper was published on the expansion of cylindrical shells detonated on one end. In this paper, Taylor developed analytical expressions for estimating the velocity profile of the shell.

In 1967, Slate and others (Slate et al., 1967) experimentally examined the behavior of several thin spherical shells subjected to internal explosive detonations. These shells were fabricated from various materials including copper, aluminum, and titanium. Their report indicated that for copper shells with a thickness to radius ratio of 0.02, the shells fragmented early with the formation of bubbles on the surface indicating a fluid like response. A more ductile response occurred for a radius ratio of 0.04. At this ratio, they observed what appeared to be local thinning between the fragments before the detonation products pierced through the surface. Finally, a more brittle response was observed for copper shells with a ratio of 0.08. At this ratio, the surface ripples became more obvious and eventually these ripples developed into lines of fracture. They felt this pattern was a result of heterogeneities in the density or crystalline structure of the material, thus providing a potential pattern for rupture under circumferential strain. In summary, their observations indicate that the thicker the shell, the more evident the surface cracking and in addition, the higher the strain to rupture.

Hoggatt and Recht (1968) furthered the experimental study of fragmenting cylinders and developed a mathematical model assuming the fractures occur along lines of maximum shear. In addition, Hoggatt and Recht observed different types of fractures based on the amount of HE and the detonation pressures. At low detonation pressures, deep cracks formed on the outer surface before unstable shear zones began to develop. This resulted in fragments with deep radial cracks on the surface and shear zones only near the inner diameter. Hoggatt and Recht define shear zones as cracks that lie along shear planes, which are rotated approximately 45 degrees from the outward radial direction. At high detonation pressures, the compressive hoop stress from the detonation

retards the growth of cracks and the unstable shear zones form earlier. As a result, larger shear zones are observed on the fragments. An illustration of the fracture resulting from a high and low pressure detonation is shown in Figure 1.2

Figure 1.2: Exaggerated Fractures from a High and Low Pressure Detonation

Later, Al-Hassani and others (1969a) determined from experiments that the radial expansion of the vessel walls continues long after attenuation of the shock waves in the material. In addition, they provide an analytical expression for the hoop and radial stress in the vessel wall assuming a perfectly plastic material and confirmed the behavior observed by Taylor. In a separate report by Al-Hassani and Johnson (1969b), they concluded that the strain-rate, strain hardening, and deformation induced temperature are important to the yield behavior and that they influence both the fracture radius and velocity, although they did not include them in their analysis.

Wesenberg and Sagartz (1977) analyzed the expansion of thin cylindrical shells at strain rates of 10^4 sec^{-1}. They discuss the radial expansion of the cylinders and their subsequent fracture by providing a numerical solution to Mott's fracture equation (Mott, 1947). Wesenberg and Sagartz compared Mott's probabilistic analysis with experimental

data, which were reasonably close. They also observed that the number of fragments decreases with material density and decreasing strain-rate or detonation pressure.

The research presented in this dissertation will verify G. I. Taylor's conclusions and observations regarding failure and the tensile and compressive stress regions in an expanding shell. Reports by Mott, Slate, Hoggatt, Recht, and others indicate fragment variations are based on material thickness or detonation pressures. This dissertation will also provide numerical and experimental results for cylinders of different thicknesses, which will dispute or confirm the thickness dependent effects observed by Mott, Slate, Hoggatt, and Recht.

1.3 Background on Numerical Studies

In the late 1970's experimental research into the high strain-rate expansion of explosively loaded shells began to taper off. Experiments probably became more costly and the advent of the super computer provided a numerical means to investigate the high strain-rate expansion phenomena. As a result, scientists conducted more numerical studies in an effort to understand the development of plastic instabilities in dynamically loaded structures and dynamic fragmentation. Early numerical studies were limited to the expansion of rings and axially detonated cylinders. In both of these cases the entire geometry expands uniformly in the radial direction in the absence of a longitudinal stress component. The research presented in this dissertation considers this and the more complicated end detonated cylinder where the expansion varies along the longitudinal axis of the cylinder.

Early results by Hoggatt and Recht (1968), suggest that thermoplastic instabilities occur when the local flow stress decreases with increasing strain. This occurs when the rate of thermal softening exceeds the rate of work hardening. In general, the loss of stability is assumed to take place when an increment in strain occurs with no simultaneous increase in pressure or load (Duffey, 1989). Duffey examined the effects of work hardening and mentions that work hardening effectively spreads out the deformation to a point that prevents strain localization. Neglecting inertia effects, materials with greater strain hardening exhibit higher instability strains.

A formulation for modeling dynamic plastic instabilities in a thin sheet was developed by J. W. Taylor (Taylor et al., 1978). Their approach is based on hydrodynamic principles where they assume that the shear effects are negligible. They introduced a thickness perturbation in thin sheets and demonstrated that the size and appearance of the instabilities are dependent on the strain-rate and work hardening. Their analysis does not include porosity or temperature effects, nor does it consider multi-axial stresses.

In 1983, Johnson (1983) examined the ductile failure of rapidly expanding rings. Johnson describes the time dependent heterogeneous plastic deformation in terms of the differential equations of thermoplasticity, conservation of mass, and conservation of momentum. Johnson's model uses a small perturbation in the wall thickness or porosity to create the instability. He also examines the influence of work hardening and thermal softening and suggests that thermal effects can not be ignored. However, Johnson's constitutive model focuses on the response of the material using a high pressure equation of state formulation and not the accepted theory of plasticity. In addition, his paper

considers only the one-dimensional case and thus can not be easily extended to cylindrical shells under a multi-axial state of stress.

Anderson, Predebon, and Karpp (1985) developed a two-dimensional finite difference code to model expanding cylinders. They felt typical hydrodynamic codes over-predicted the fragment velocities and attempted to obtain a more complete solution. Their model includes gas leakage and results for the velocity and expansion angle are compared with experimental data. However, their model assumes elastic-perfectly-plastic material behavior and does not consider instabilities.

In 1997, Hao and Brocks (1997) implemented a void nucleation and growth constitutive model into a numerical finite element code. The constitutive model they developed was written as a user subroutine for the ABAQUS/Standard code. Their model was capable of analyzing low strain-rate problems involving creep and quasi-static type loading, rather than the high strain-rate problems considered in this dissertation.

1.4 Shortcomings in Existing Literature

Considering the results of the literature cited here, it is clear that strain-rate, material density, temperature, and inertial effects are important in large strain plastic deformation and development of instabilities when materials are subjected to high strain rates. These instabilities may result from inadequate thermal diffusion and excessive plastic flow and may include the effects of damage in the material. Several authors have examined instabilities associated with both uniaxial and bi-axial stress under quasi-static conditions, but most have not considered materials subjected to multiaxial stress states at strain rates on the order of 10^4 s^{-1}.

The previous experimental and numerical work leaves several shortcomings. In the early literature, the material used in experiments was not carefully characterized or documented. As a result, little is known about the grain size and hardness of the materials used, which makes it difficult to duplicate experimental results. The size of copper grains can be quite large resulting in perhaps one grain through the thickness of the tube. The microstructure, particularly the hardness and number of grains through the thickness of the tube, could significantly affect high strain-rate deformation. The work presented here examines the microstructure of the material before and after the experiment.

Much of the current numerical literature only considers one stress component or at most the trace of the stress tensor. Furthermore, the geometries considered in the current literature are typically one-dimensional. The research presented here considers the entire stress and strain tensor according to the fundamental constitutive formulations for three-dimensional plasticity. This complexity advances the current state of the art. In addition, it allows researchers to consider not only the complex expansion of shells, but also provides the foundation to examine large strain plastic instabilities.

From a review of the numerical literature, very few authors have included the high pressure equation of state effects, which could be important in the formulation of the constitutive equations. Those that have included these effects examined situations with strain rates much higher than 10^4 sec^{-1} or provided formulations that are limited to one-dimensional calculations. Most of the authors who have implemented equation of state type formulations are typically concerned with 1-dimensional fragmentation or spall and do not focus on the evolution of large strain plastic instabilities.

In some cases, researchers have neglected the strength of the material, which could be significant for predicting instabilities for rapidly expanding shells. In other cases, they assume a perfectly-plastic material where the flow stress is constant and the strength model for the material is independent of the material behavior. The strength model typically relates the current state of the material, most often strain, to some allowable state of stress. Numerous strength models exist in the current literature and a few of them are examined in Chapter 2. The Johnson-Cook strength model is arguably the most widely used in both the previous and current literature for high strain-rate plasticity. The underlying principles of the Johnson-Cook model and its implementation are discussed in Chapters 2 and 3.

Shock physicists contend that numerical codes can not completely characterize the shock front or detonation front due to processor limitations even with the world's fastest super computers. However, this research is not concerned with the microscopic behavior at either front, but rather treats the materials as a continuum and is concerned only with the average microscopic behavior. Curran et al. (1987) describe the average microscopic behavior in terms of state variables in the constitutive relations of materials. This continuum mechanics approach is referred to as "Microstatistical Fracture Mechanics" (MSFM).

The MSFM approach is considered in the development of the damage model. Damage, which results from the effects of microdefects in the material, is incorporated in the form of a void model. This void model includes the effects of microvoid nucleation, growth, and coalescence in the material and is an important aspect in this constitutive model. In summing up the current literature, no one has formulated a model that includes

the 3-dimensional fundamental equations for high strain-rate plasticity with a high pressure equation of state model, a microvoid damage model, and a high strain-rate material strength model to study the expansion of thin ductile shells.

1.5 Scope of Work Presented in this Dissertation

The purpose of this research is to develop an experimentally verified finite element model capable of predicting the high strain-rate expansion of explosively loaded cylindrical shells. In addition, the constitutive model developed in this research provides insight into the initiation and development of plastic instabilities on the surfaces of the shell. The constitutive model is based on the Johnson-Cook strength model, Mie-Grüneisen equation of state (EOS) model, and the GTN or modified Gurson void model.

The constitutive model is verified with experimental data from two plane wave detonated copper cylinders filled with high explosive. The material for these cylinders is carefully characterized and state-of-the-art diagnostic equipment is used to record the cylinder wall displacement and velocity during the experiments.

The numerical model is written to allow future modifications to the constitutive equations and additional damage criteria. The model is multi-dimensional and assumes void nucleation and growth is the main damage mechanism leading to the onset of plastic instabilities. As with most Lagrangian finite element models, the accuracy of the of the results diminishes with large element distortions and as a result the user must be cautious of extensive element warping, strain, and aspect ratios. In addition, the explicit finite element code used in this research limits the user to single integration point elements and as a result requires high mesh densities. At strain rates above 10^6 s^{-1}, the accuracy of the

Johnson-Cook model tends to diminish and result from this numerical model may no longer be accurate. Finally, this is a newly developed model and further limitations may be observed as the code is exercised with new applications.

The remaining chapters of this dissertation focus on the numerical model, the experimental and numerical results, and the onset of instabilities. Chapter 2 discusses the constitutive equations used in the development of the numerical model. The implementation of the constitutive equations in the numerical model is discussed in Chapter 3. Chapter 4 discusses the material characterization and set-up of the experiment used for verifying the numerical model. A comparison of experimental data with the results from the numerical model is provided in Chapter 5. Chapter 6 focuses on the development of the quasi-periodic instabilities for cylinder of different thickness. Finally Chapter 7 provides a summary, a list of conclusions, and recommendations for future work.

2.0 Constitutive Models

Typical hydrodynamic calculations neglect the strength of the material and treat the material as a fluid. This simplification is reasonable in the case of fluids or solids undergoing high compression shocks resulting in a fluid type behavior. The copper cylinders considered in this study are subjected to high pressures, but are not believed to behave as a fluid. Instead, as the material strains, thermal energy is deposited in the material as a result of shock loading and plastic work. This thermal energy has an effect on the flow surface and resultant stress state of the material. In addition, damage accumulates in the material as it yields. This damage, which is modeled in the form of microvoids accumulating in the material, leads to the onset of the instabilities in the material. Recent literature suggests that constitutive models for modeling this high strain-rate behavior should be composed of at least three models: a strain-rate and temperature dependent material strength model, an equation of state, and a microvoid damage model. The research presented here includes all three of these models.

This chapter is divided into three sections. Each section discusses or formulates a particular part of the constitutive model used to describe the deformation of the expanding cylindrical shells. The first section describes the material strength model, which predicts the flow stress of the material based on temperature, strain, and strain-rate. The second section provides an overview of the shock and stress waves propagation in solids and presents the background information regarding the equation of state, Rayleigh

line, and Hugoniot curve. In addition, this section formulates the equations used to model the shock wave effects on the bulk modulus and material temperature. The third section provides an overview of the damage model. The damage model used in this work is based on the nucleation, coalescence, and growth of microvoids in the material as a result of plastic strain.

2.1 Material Strength Models

Several strength models exist in the current literature. Strength models like the Zerrilli-Armstrong and Mechanical Threshold Stress (MTS) model are considered to be physically based models, while the Johnson-Cook model is an empirically based model. Numerous experiments have been conducted using each of these models, and all show reasonable agreement for dynamic strain rates below 10^5 s^{-1}.

Zerilli and Armstrong proposed a microstructural based constitutive model based on the framework of thermally activated dislocation motion (Zerilli and Armstrong, 1986). Their model results in equations that are very similar to the stress function proposed by Hall (1951) and Petch (1953) and contains terms for the flow stress, the grain size dependence, and a stress correction factor that is slightly different for FCC and BCC metals. For FCC metals the correction factor couples the plastic strain with the strain rate and temperature, while for BCC metals, the plastic strain is uncoupled from the strain rate and temperature.

The Mechanical Threshold Stress Model (Follansbee and Kocks, 1988) uses the same concepts as the Zerilli-Armstrong Model. In the MTS model, the thermally activated dislocation interactions are described by the linear summation of three different

terms. The first term represents the internal stress resulting from the dislocation interactions, perhaps with grain boundaries. The second term represents the strain rate and temperature effects on the yield stress. The final term represents the dislocation interactions from deformation and accounts for work hardening and thermal softening.

A number of empirically based strength models have been proposed in the literature, and most of these show reasonable agreement with experimental data. Typically, these models define the flow stress as some function of strain raised to a power. Johnson and Cook (1983) used this principle in formulating their model. The strength model presented by Johnson and Cook has five experimentally determined parameters (A, B, C, n, m) coupled together in an easily identified form. Their model expresses the flow stress as a function of the equivalent plastic strain, strain rate, and temperature. The Johnson-Cook equation for the flow stress is expressed as

$$\sigma_f = \left(A + B\varepsilon^n\right)\left(1 + C\ln\dot{\varepsilon}^*\right)\left(1 - T^{*m}\right), \tag{2.1}$$

where ε is the equivalent plastic strain,

$$\dot{\varepsilon}^* = \frac{\dot{\varepsilon}}{\dot{\varepsilon}_o}, \tag{2.2}$$

is the dimensionless plastic strain-rate for a reference strain-rate $\dot{\varepsilon}_o = 1.0\ \mathrm{s}^{-1}$ and

$$T^* = \frac{(T - T_{room})}{(T_{melt} - T_{room})} \tag{2.3}$$

is what Johnson and Cook refer to as the homologous temperature.

The five material constants in eqn. (2.1) are separated into three multiplicative terms. The first term in eqn. (2.1) represents the strain hardening with A interpreted as the initial yield stress, B the strain hardening coefficient, and n the strain hardening

exponent. The second term in eqn (2.1) represents the strain-rate effect with C interpreted as the strain-rate hardening coefficient. The last term in eqn. (2.1) represents the thermal softening with m interpreted as the thermal softening exponent. The five material constants A, B, C, n, and m were determined by Johnson and Cook from a series of tensile and torsion tests evaluated at various temperatures and strain rates ranging from 10^3-10^5 s^{-1} (Johnson and Cook, 1983). Specific values for these constants as reported by Johnson and Cook are given in Table 2.1. Strain-rate dependent plots of the adiabatic flow stress from eqn. (2.1) as function of strain are shown in Figure 2.1 for OFE (Oxygen-Free Electronic) copper. Adiabatic effects were accounted for in eqn (2.1) by including the increase in temperature resulting from plastic work. The formulation for this increase in temperature is discussed later in this chapter.

Table 2.1. Material Constants for the Johnson-Cook Strength Model

Material	A (MPa)	B (MPa)	n	C	m
OFE Copper	90	292	0.31	0.025	1.09
Cartridge Brass	112	505	0.42	0.009	1.68
Nickel 200	163	648	0.33	0.006	1.44
Armco Iron	175	380	0.32	0.060	0.55
1006 Steel	350	275	0.36	0.022	1.00
2024-T351 Aluminum	265	426	0.34	0.015	1.00
7039 Aluminum	337	343	0.41	0.010	1.00
4340 Steel	792	510	0.26	0.014	1.03
Tungston Alloy	1506	177	0.12	0.016	1.00
S-7 Tool Steel	1539	477	0.18	0.012	1.00
Uranium-.75Ti	1079	1120	0.25	0.007	1.00

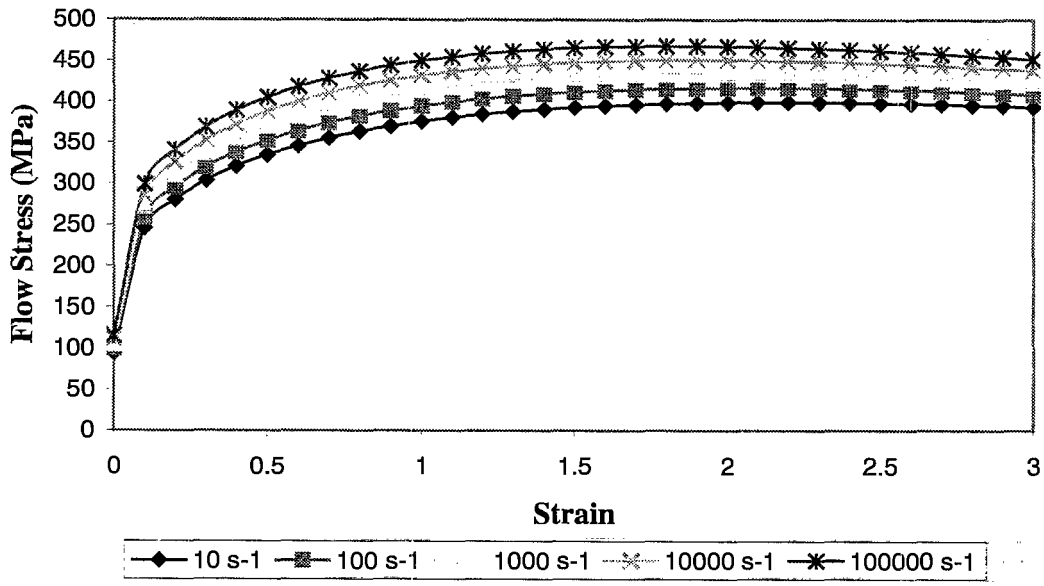

Figure 2.1: Johnson-Cook Flow Stress for OFE Copper as a Function of Strain

The Johnson-Cook model (Johnson and Cook, 1983) has several desirable features. One of the most obvious is its ease of implementation. In addition, it can be readily applied to a variety of materials and the constants are easily obtainable for several materials of interest. The effects of various parameters in the equations are easily identifiable and the Johnson-Cook strength model does not require an extraordinary amount of computer time. However, since it has no physical basis, caution must be used when extrapolating ε, $\dot{\varepsilon}$, and T beyond the limits of the data from which the constants were determined. The equations and implementation of the Johnson-Cook model into the plasticity model will be further examined in Chapter 3.

2.2 Shock Waves and the Equation of State

Shock wave studies examine the behavior of materials that are subjected to intense short term loading which forces the material into states not usually encountered.

The pressures attained from this loading can be two orders of magnitude larger than those attainable by conventional methods (Skidmore, 1965). This loading is typically a result of explosive detonations, the duration of which is on the order of microseconds. High speed diagnostic equipment is required to experimentally observe shock waves and as a result investigations in this area are limited.

The study of shock waves in solids was first introduced in the UK by Pack and others in 1948 (Pack et al. 1948). Later in 1955, similar work was reported in the USA by Gorason et al. (1955). In addition, Walsh and Christian (1955) made significant contributions in this area while working at Los Alamos National Laboratory. During the 1960's scientists began focusing on shock waves resulting from high velocity impact (Duvall, 1961). Interest in shock waves has recently expanded in industry as engineers recognize the value of using explosive techniques for welding and plastic forming. In addition, metallurgists are studying the changes in the microstructure of solids following intense transient loading. Intense quantities of energy are deposited into materials from shock loading. This energy and the resulting temperatures are included as an integral part of the work presented in this study.

Arguably, when the solid is subjected to intense hydrodynamic forces, the shear stresses are relatively small, and the stress system is effectively hydrostatic (Skidmore, 1965). Therefore, the effects of shear stress are typically not included in hydrodynamic methods and it is possible to treat the material as a fluid when attempting to understand shock wave propagation in solids. The fundamental requirement for establishing a shock wave is that the velocity of the disturbance increases with an increase in pressure.

Understanding of the concept of shock wave propagation in a material can be aided by considering the simplified analogy of the flow of snow in front of a snowplow. As the snowplow moves into a fresh new snow, a layer of packed snow begins to build up in front of the plow. The snow immediately in front of the blade of the snowplow travels faster than the snow further ahead of the blade. Eventually the wave front becomes infinitely steep, forming a mathematical discontinuity (Graham, 1993). This discontinuous wave front is called a shock wave.

In a shock wave, the material changes discontinuously from one side of the front to the other and the expressions governing sound wave behavior are no longer strictly applicable. Instead scientists use what are called the Rankine-Hugoniot relations or jump conditions. A schematic of the profile of shock front is shown below in Figure 2.2 where U_s is the shock velocity, U_p is the particle velocity, ρ is the density of the material, E is the energy, and P is the pressure. The subscript 'o' indicates the properties of the material ahead of the shock front.

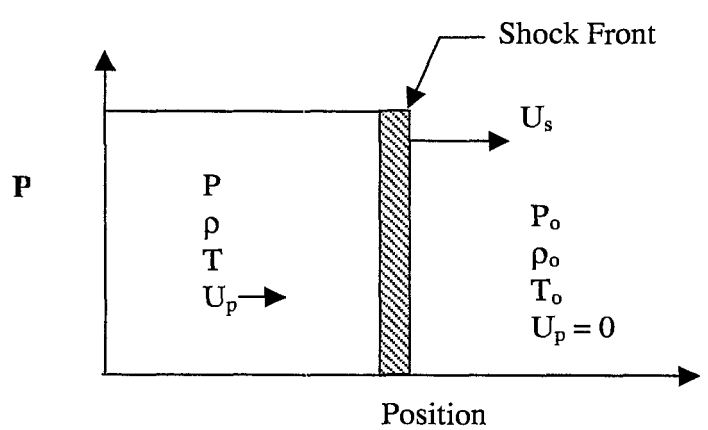

Figure 2.2: Profile of a Shock Front Propagating Through a Material

The useful form of Rankine-Hugoniot relations result from writing the conservation equations in their discrete forms. The conservation of mass becomes,

$$\rho_0 U_s = \rho \left(U_s - U_p\right). \tag{2.4}$$

While the conservation of energy becomes,

$$E - E_o = \frac{1}{2}\left(P + P_0\right)\left(V_0 - V\right), \tag{2.5}$$

and the conservation of momentum becomes,

$$P - P_o = \rho_o U_s U_p . \tag{2.6}$$

This results in three equations and five unknown parameters.

A fourth equation known as the equation of state (EOS) is necessary to determine any of the parameters as a function of one parameter. The EOS, which will be discussed later, defines all of the equilibrium states that can exist in a material. If the state of the material behind the shock is an equilibrium state, then it too satisfies the EOS. If both the Rankine-Hugoniot conditions and the EOS are satisfied simultaneously, then the energy terms between them may be eliminated and it is possible to obtain a P-V (Pressure-Volume) relation that is unique for the material represented by the EOS. The curve represented by this relation is called the Hugoniot curve, which simply represents a unique curve in the P-V plane representing the locus of all shocked states attainable behind the shock.

The conservation of momentum defines a straight line of slope $(P - P_0) / (V - V_0)$ in the P-V plane. This line is called the Rayleigh line. A graphical representation of the Hugoniot curve, and Rayleigh line is shown in Figure 2.3. The adiabats in Figure 2.3 represent lines of constant entropy on the pressure-volume plane.

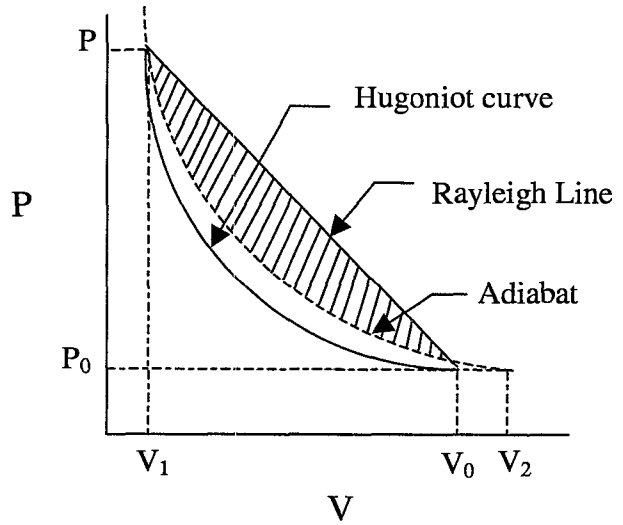

Figure 2.3: Plot of the Hugoniot Curve and Rayleigh Line on the P-V Plane

When the pressure in the shock front is increased, it does not follow the adiabat or the Hugoniot Curve. Instead it follows along the Rayleigh line from P_0 to P. The unloading process behind the shock front is usually assumed to be adiabatic and as result takes place along the adiabatic curve from V_1 to V_2. The initial specific volume, V_o, is different than V_2 due to an increase in the temperature from the energy deposited in the material. The irreversibility of the process is shown graphically in Figure 2.3 as the hatched area between the Rayleigh line and the release adiabat. In practice, physicists often assume the unloading takes place along the Hugoniot. This is a reasonable approximation since the Hugoniot and the adiabat have close proximity. However, recall the Hugoniot curve represents the locus of end states, not the shock path.

The concept of shock stability is important in understanding wave propagation in a material. Using an "Eulerian" coordinate system, consider a compression wave resulting from two small compressional disturbances as shown in Figure 2.4.

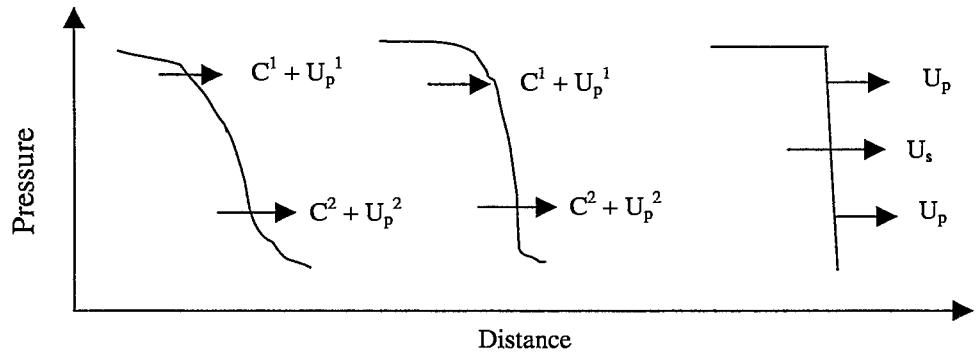

Figure 2.4: Formation of a Stable Shock Wave

The first wave moves at a speed of $C^1 + U_p^1$, where C^1 is the pressure dependent sound speed. The second wave moves at a speed of $C^2 + U_p^2$ where again C^2 is the local sound speed. In general, the local sound speed of a material increases with pressure. The high pressure wave travels faster than the low pressure wave so that the combined compression wave becomes steeper. Eventually, the first wave overtakes the second. This results in a discontinuous disturbance or shock wave, which travels at the speed U_s. In general, for a stable shock to exist, the velocity of the disturbance, $C + U_p$, must always be greater than or equal to the shock velocity, U_s. Otherwise, the disturbance will not be able to catch up to the shock and the shock will decay, develop an elastic precursor, or cause a phase transformation in the material. Thus a necessary condition for shock stability is

$$U_p + C \geq U_s . \tag{2.7}$$

Three different stress wave configurations can exist in a solid and understanding the Rayleigh line and Hugoniot curve provides insight into the structure of the wave. Consider the stress system behind a one-dimensional compressive stress wave where the volumetric strain, ε_v which is defined as positive in compression, is described by

$$\varepsilon_v = \frac{V_0 - V}{V_0} = 1 - \frac{V}{V_0}, \tag{2.8}$$

for small strain elasticity. The normal and transverse elastic stress for an element subjected to uniaxial strain can be respectively written as

$$\sigma_n = (\lambda + 2G)\,\varepsilon_v \tag{2.9}$$

and

$$\sigma_t = \lambda\,\varepsilon_v \tag{2.10}$$

where λ is the Lamé constant and G is the shear modulus. The Lamé constant is related to the bulk modulus, K, (Love, 1944) as

$$\lambda = K - \frac{2}{3}G. \tag{2.11}$$

For the case of hydrostatic pressure, P, the bulk modulus can be defined as

$$K = \frac{P}{\varepsilon_v}. \tag{2.12}$$

Using eqns. (2.9), (2.10), and (2.11), the equations for the elastic response of the material can now be written as

$$\sigma_n = \left(K + \frac{4}{3}G\right)\varepsilon_v \tag{2.13}$$

and

$$\sigma_t = \left(K - \frac{2}{3}G\right)\varepsilon_v. \tag{2.14}$$

These elastic relations remain valid provided the yield criterion is not violated. In this case, the yield criteria can be written in terms of the maximum shear stress as

$$Y = 2\tau_{\max} = (\sigma_n - \sigma_t), \tag{2.15}$$

When yielding occurs, $(\sigma_n - \sigma_t)$ remains constant and as a result,

$$\sigma_n - \sigma_t \leq Y. \tag{2.16}$$

or

$$2G\varepsilon_v \leq Y \tag{2.17}$$

Combining eqn. (2.12), (2.13), and (2.17), the normal yield stress, σ_y, can be written as

$$\sigma_y = P + \frac{2}{3}Y \tag{2.18}$$

The stress wave behavior of a material subjected to shock loading can be understood with these equations. First consider the plot of stress vs. strain shown in Figure 2.5. This plot is similar to the plot shown by Skidmore (1965).

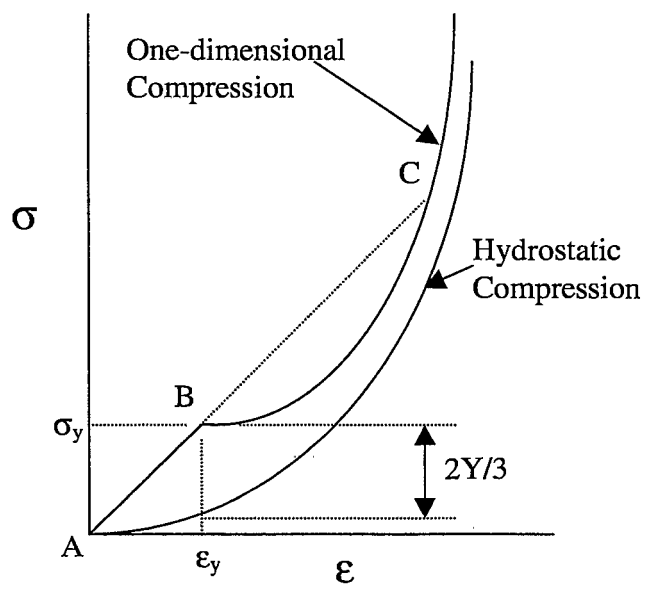

Figure 2.5: One-dimensional and Hydrostatic Compression of Solids

Point B in Figure 2.5 is called the Hugoniot Elastic Limit (HEL). The stresses below this limit are elastic and propagate through the material as a single wave. The

velocity of the elastic wave, C_e, is determined by substituting the equation for the normal stress into a combination of the conservation of mass and momentum equations given in eqns. (2.4) and (2.6), where $\sigma_n = P$ and $P_0 = 0$. The resultant

$$C_e = \left(\frac{\lambda + 2G}{\rho_0}\right)^{1/2} = \left(\frac{K + \frac{4}{3}G}{\rho_0}\right)^{1/2} = \left(\frac{E}{\rho_o}\right)^{1/2}, \tag{2.19}$$

is the equation for longitudinal elastic waves in an unbounded medium. At point B, the material yields and plastically deforms along the solid curve from B to C.

Experimental data have shown that the bulk modulus, K, slowly increases with pressure. At point B, the discontinuous decrease in slope violates the condition for shock stability. As a result, the shock breaks up into two waves, an elastic and a plastic wave. The elastic wave propagates with a stress of σ_y moving with a velocity of C_e, followed by the plastic wave moving with a velocity C_{pl},

$$C_{pl} = \left(\frac{d\sigma/d\varepsilon}{\rho_o}\right)^{1/2}. \tag{2.20}$$

At point C, the Rayleigh line for the plastic shock is an extension of the elastic line from point A to B and the velocity of the plastic wave is equal to or greater than the elastic wave. At this point the shock is stable and the stress wave travels through the material as a single wave. Shocks of this magnitude are described as strong shocks or overdriven shocks. Notice that at point B in Figure 2.5, the difference between the hydrostatic compression curve and the one-dimensional compression curve is *2/3 Y*, which is also shown in eqn. (2.18). As the pressure and normal stress increases, the difference between the two curves becomes negligible. Therefore, at very high shock

pressures, the stress system can be regarded as hydrostatic thus justifying the simplified approach of hydrocodes.

Figure 2.6 shows a graphical representation summarizing the resulting stress waves, which can propagate through a material, in relation to the Hugoniot curve and Rayleigh line. At a shock pressure equal to P_1, a single elastic stress wave propagates through the material. At a higher pressure of P_2, the stress wave is unstable and breaks up into two waves. This results in an elastic stress wave followed by a plastic stress wave. In general, a stable wave can not exist unless the Hugoniot curve is steeper than the Rayleigh line at the final state. At an even higher pressure of P_3, the velocity of the plastic wave overtakes the elastic wave and a single stress wave propagates through the material.

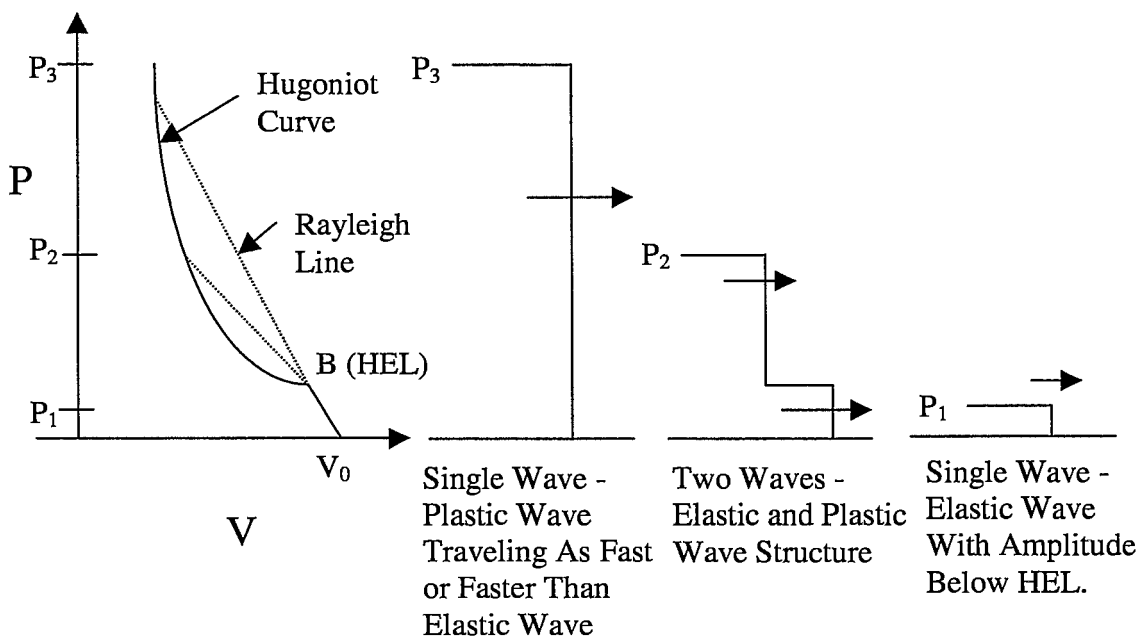

Figure 2.6: Wave Structure in Relation to the Hugoniot Curve and Rayleigh Line

A table with the mechanical properties and the velocity of elastic waves for five different materials is given in Table 2.2.

Table 2.2: Longitudinal Velocity of Elastic Waves

Material	Density (kg/m$^{3)}$	G (GPa)	K (GPa)	Elastic Velocity (m/s)
Iron	7,850	81.6	170.1	5,960
Copper	8,930	48.3	137.8	4,760
Aluminum	2,700	26.1	75.6	6,400
Alumina	3,900	140.4	304.2	11,230
Uranium	18,950	66.1	143.26	3,490

Any time a material experiences high pressure loading, which may result from a shock wave, the effects of the pressure can be described with the use of the EOS for the material. If the state behind the shock wave is in equilibrium, then both the Rankine-Hugoniot and EOS relations must be satisfied. A common experimental form for the EOS is know as the $U_s - U_p$ form which can be expressed as

$$U_s = C_o + S_e U_p, \tag{2.21}$$

where C_o, is the isentropic sound speed and S_e is the slope of the U_s - U_p curve.

In the study of shock waves, there are several different types of EOS equations. The Mie-Grüneisen EOS is common form used in numerical codes, which relates a state of pressure, volume, and energy to the state energy and pressure at a reference state. This reference state could, for example, be a point on the Hugoniot at the same volume (Meyers, 1994). In this case, the Mie-Grüneisen EOS can be written as,

$$P = P_H + \frac{\gamma}{V}(E - E_H), \tag{2.22}$$

where P_H is the Hugoniot pressure and E_H is the specific internal energy along the Hugoniot line on the P-V plane. The Grüneisen constant, γ, can then be expressed as

$$\gamma = V\left(\frac{\partial P}{\partial E}\right)_V \tag{2.23}$$

The shock and thermodynamic properties for different materials is given in Table 2.3 (Meyers, 1994), where C_p is the constant pressure specific heat.

Table 2.3: Shock and Thermodynamic Properties of Metals

Material	ρ_0 (kg/cm^3)	C_0 (mm/μs)	S_e	C_p (J/g-K)	γ
Be	1.85	8.00	1.12	0.18	1.2
Cu	8.93	3.94	1.49	0.40	2.0
Fe	7.85	3.57	1.92	0.45	1.8
Ni	8.87	4.60	1.44	0.44	2.0
Pb	11.35	2.05	1.46	0.13	2.8
U	18.95	2.49	2.20	0.12	2.1
W	19.22	4.03	1.24	0.13	1.8

At this point, a detailed explanation of the relationship between shock waves and stress waves has been provided. The loading in this dissertation is not considered in the range of a strong shock and once a shock propagates through a material, numerous waves are released and developed (Ferm, 1998). In the absence of strong shocks, it is quite common to see the terminology of shock waves and stress waves used interchangeably in the literature depending on the author, the audience, and the loading conditions.

The previous explanation included an introduction to the Hugoniot curve, Rayleigh Line, and equation of state. These principles will now be used to formulate the equations representing the effects of the high pressure shock on the bulk modulus and

temperature in the material. The formulation for this part of the constitutive model closely follows the work of Johnson (1981) and Wallace (1980b).

Recall that the isentropic bulk modulus, K, is defined as

$$K = \left(\frac{\partial P}{\partial \varepsilon_v} \right)_s , \tag{2.24}$$

where ε_v is the volumetric strain and P is the pressure. Under shock loading, the pressure in the material can be found from the Hugoniot curve. Therefore, the modified bulk modulus is found by taking the partial derivative of the Hugoniot pressure with respect to the volumetric strain.

The formulation to find the Hugoniot pressure as a function of the volumetric strain begins with the conservation of momentum equation given in eqn. (2.6),

$$P - P_o = \rho_o U_s U_p . \tag{2.25}$$

The pressure on the Hugoniot, P_H is then found by applying the $U_s - U_p$ form of the EOS (eqn. (2-21)) to eqn. (2.25) with $P_o = 0$,

$$P_H = \rho_o U_p \left(C_o + S_e U_p \right). \tag{2.26}$$

Recall from eqn (2.4), the conservation of mass may be written as,

$$\rho_o U_s = \rho \left(U_s - U_p \right). \tag{2.27}$$

Substituting the $U_s - U_p$ form of the EOS into eqn. (2.27) gives,

$$U_p \left[1 + S_e \left(\frac{\rho_o}{\rho} - 1 \right) \right] = C_o \left[1 - \frac{\rho_o}{\rho} \right]. \tag{2.28}$$

Recall, the volumetric strain, ε_v, is defined as the trace of the stress tensor or,

$$\varepsilon_v = 1 - \frac{V}{V_o} = 1 - \frac{\rho_o}{\rho} = (-1)\, \varepsilon_{ii} . \tag{2.29}$$

Substituting eqn. (2.29) into (2.28) and simplifying gives an equation for the particle velocity as a function of volumetric strain.

$$U_p = \frac{C_o \varepsilon_v}{1 - S_e \, \varepsilon_v} \tag{2.30}$$

Substituting eqn. (2.30) into eqn. (2.26) gives the following equation representing the Hugoniot pressure as a function of the volumetric strain.

$$P_H = \frac{\rho_o C_o^2 \varepsilon_v}{(1 - S_e \varepsilon_v)^2} \tag{2.31}$$

The partial derivative is then

$$\frac{\partial P_H}{\partial \varepsilon_v} = \frac{\rho_o C_o^2 (1 + S_e \varepsilon_v)}{(1 - S_e \varepsilon_v)^3}. \tag{2.32}$$

Therefore the factor by which the bulk modulus is modified from the high pressure shock is simply

$$\frac{(1 + S_e \varepsilon_v)}{(1 - S_e \varepsilon_v)^3}. \tag{2.33}$$

Next, a thermodynamic equation will be formulated to determine the change in temperature in the material as a result of plastic work and the high pressure shock. This formulation begins with the first law of thermodynamics for a closed system,

$$\delta Q - \delta W = dE, \tag{2.34}$$

where the work is defined as

$$\delta W = P \, dV \tag{2.35}$$

and the heat flux is defined as

$$\delta Q = T \, dS. \tag{2.36}$$

Substituting eqns. (2.35) and (2.36) into eqn. (2.34) yields

$$dE = T\,dS - P\,dV\,. \tag{2.37}$$

Recall, entropy S, is a function of temperature and volume and therefore

$$dS = \left(\frac{\partial S}{\partial T}\right)_V dT + \left(\frac{\partial S}{\partial V}\right)_T dV\,. \tag{2.38}$$

Multiplying the eqn. (2.38) by the temperature, T, gives

$$T\,dS = T\left(\frac{\partial S}{\partial T}\right)_V dT + T\left(\frac{\partial S}{\partial V}\right)_T dV\,. \tag{2.39}$$

The specific heat at constant volume is defined as

$$C_V = \left(\frac{\partial E}{\partial T}\right)_V = T\left(\frac{\partial S}{\partial T}\right)_V, \tag{2.40}$$

which when substituted into eqn. (2.37) above gives

$$T\,dS = C_V\,dT + T\left(\frac{\partial S}{\partial V}\right)_V dV\,. \tag{2.41}$$

Using the following form of Maxwell's Equations,

$$\left(\frac{\partial S}{\partial V}\right)_T = \left(\frac{\partial P}{\partial T}\right)_V, \tag{2.42}$$

eqn. (2.41) can be written as

$$T\,dS = C_V\,dT + T\left(\frac{\partial P}{\partial T}\right)_V dV\,, \tag{2.43}$$

or

$$T\,dS = C_V\,dT + T\left(\frac{\partial P}{\partial E}\right)_V \left(\frac{\partial E}{\partial T}\right)_V dV\,. \tag{2.44}$$

Substituting eqns. (2.22) and (2.23) from the Hugoniot and Grüneisen relations into

eqn (2.44) gives

$$T\,dS = C_V\,dT - T\,\gamma\left(\frac{\partial E}{\partial T}\right)_V d\varepsilon_v\,, \tag{2.45}$$

or

$$T\,dS = C_V\,dT - T\,\gamma\,C_V\,d\varepsilon_v\,. \tag{2.46}$$

Solving for dT gives,

$$dT = T\,\gamma\,d\varepsilon_v + \frac{T\,dS}{C_v} \tag{2.47}$$

For adiabatic solids, $\dot{Q} = 0$, and as a result

$$dW^{pl} = T\,dS = \frac{\sigma_{ij}\,d\varepsilon_{ij}^{pl}}{\rho} \tag{2.48}$$

Substituting eqn. (2.48) into (2.47) gives the equation for calculating the temperature rise in the material due to the high pressure shock and plastic work.

$$dT = T\,\gamma\,d\varepsilon_v + \frac{\sigma_{ij}\,d\varepsilon_{ij}^{pl}}{C_V\,\rho} \tag{2.49}$$

The increase in temperature as a result of the shock loading and the plastic work is given by the first and second respective terms on the right side of eqn. (2.49). The term that accounts for the shock heating, along with eqn. (2.33) which represents the change in the bulk modulus, are determined in the EOS subroutine of the constitutive model. These values are then passed back to the constitutive model to be used in the Gurson subroutine. The details of their implementation into the constitutive model will be discussed in the next chapter.

2.3 Microvoid Damage Model

The rate dependent plastic deformation that occurs during radial expansion of a ductile cylindrical shell causes material bonds to be broken which nucleates voids in the previously intact material. These voids are thought to nucleate predominantly at secondary phase particles in the material because of their stress raising effect or low bond strength with the surrounding material during plastic deformation (Shockey et al. 1980). Voids can also nucleate prior to, or as a result of, instabilities in the material. The voids continue to grow by means of local plastic flow or diffusion and coalescence with neighboring voids. It is therefore important to understand and account for void nucleation and void kinetics in the failure of ductile materials.

Fracture by the growth of microvoids in materials was observed by Tipper (1949) in 1949 and later by Puttick (1959) and Rogers (1960). Early work on the growth of voids and microstructural damage in the plastic region of behavior for ductile materials under combined loading was performed in the late 1960's (McClintock, 1968; Rice and Tracey 1969). Rice and Tracey derive a growth law for a spherical void that depends on both the plastic strain and the mean tensile stress. They considered only a single void in an infinite medium and thus void growth does not affect the imposed stress field. Later Gurson (1977), extended their model to consider a finite block of material with a continuum approach. Gurson's model depends on the plastic strain and mean tensile stress and demonstrates the effects of the voids on the surrounding stress field. By assuming the material behaves as a continuum, voids appear in the model indirectly and their effects are averaged through the material.

In addition to the strain, entropy, and temperature in the constitutive relations, functions for the distribution, orientation, and size of the microvoids are introduced to describe the current state of the material. This MSFM type of constitutive approach is justified for two reasons. First, the specimen size is large in comparison to the size of the flaws. Secondly, the flaws are distributed throughout the material and are numerous enough that their behavior can be averaged like molecular collisions in a material.

Curran et al. (1987) categorize failure in polycrystalline solids by either ductile void growth or brittle crack extension. The bulk of existing literature assumes ductile void growth occurs by either diffusion or plastic flow from spherically symmetric tension or by a combination of symmetric tension and shear stress. Chadwick (1959) and Hopkins (1960) provided early results on the growth of voids subjected to spherically symmetric tension. Carrol and Holt (1972) continued this work and now much of the current literature considers only the effects of spherically symmetric tension, which is a simplification of the combined loading problem.

Gurson's model was observed to greatly over predict failure strains in real materials, which prompted Tvergaard (1981, 1982) to adjust Gurson's constitutive equations. His modification was to include an effective void volume fraction in the constitutive model. In addition, Tvergaard introduced several coefficients to account for void interaction effects. Needleman and Rice (1978) proposed a general equation to represent the nucleation rate of voids in the material. This rate is controlled by either the maximum normal stress or maximum plastic strain (Chu and Needleman,1980; Needleman, 1987; Tvergaard, 1987).

The Gurson model is more comprehensive and computationally intensive than the model proposed by Carrol and Holt. However, it appears to be more commonly used in the recent literature. The modifications by Tvergaard and Needleman have greatly improved the model and in recent literature, this model has been referred to as the Gurson-Tvergaard-Needleman (GTN) model. Its numerical implementation is a major part of this dissertation.

The yield condition for the GTN model can be expressed as:

$$\phi = \left(\frac{\sigma}{\sigma_f}\right)^2 + 2q_1 f^* \cosh\left(-\frac{3q_2 P}{2\sigma_f}\right) - \left(1 + q_3 f^{*2}\right) = 0 \tag{2.50}$$

where

$$\sigma = \sqrt{\frac{3}{2} S_{ij} S_{ij}} \tag{2.51}$$

is the effective Mises stress,

$$S_{ij} = \sigma_{ij} - \frac{1}{3}\sigma_{ij}\delta_{ij} \tag{2.52}$$

is the deviatoric stress,

$$P = -\frac{1}{3}\sigma_{ii} \tag{2.53}$$

is the hydrostatic pressure and σ_f is the flow stress. The original model derived by Gurson was formulated for a perfectly plastic material with spherically symmetric deformations around a single void. This model can be recovered by setting $q_1 = q_2 = q_3 = 1$ in eqn (2.50). The variables q_1, q_2, and q_3 are the material parameters introduced by Tvergaard (1981, 1982). Tvergaard's modifications considerably improved the model by demonstrating closer agreement with experimental data. The

GTN model is usually applied to ductile materials like OFE copper and aluminum. Typical values for q_1, q_2, and q_3 are q_1 = 1.0-1.5, q_2 = 1.0, and $q_3 = q_1^2$ = 1.0 - 2.25.

The void volume fraction, f, is defined as a function of the relative density, ζ, of the material. The relative density, ζ, is defined as the ratio of the volume of solid material to the total volume of material. The void volume fraction and relative density are related by

$$f = 1 - \zeta = 1 - \frac{\rho_s}{\rho_o}. \tag{2.54}$$

The material is assumed to be fully dense if $f = 0$ ($\zeta = 1$), and in this case the Gurson yield surface reduces to the Von-Mises model. In the case of $f = 1$ ($\zeta = 0$), the material is assumed to be fully voided (100% voids) and the material has lost its stress carrying capacity.

The parameter f^*, which was introduced by Needleman and Tvergaard (1984), is the modified damage parameter that accounts for void coalescence. This parameter is a function of the void volume fraction f and is defined as

$$f^* = \left\{ \begin{array}{cc} f & \text{if } f \le f_c \\ f_c + \dfrac{\bar{f}_F - f_c}{f_F - f_c}(f - f_c) & \text{if } f_c < f < f_F \\ \bar{f}_F & \text{if } f \ge f_F \end{array} \right\} \tag{2.55}$$

where f_c is the critical value of the void volume fraction and f_F is the final value of void volume fraction at which the material has completely lost its stress carrying capacity. The function for $\bar{f}_F$ is defined as

$$\bar{f}_F = \frac{q_1 + \sqrt{q_1^2 - q_3}}{q_3} \tag{2.56}$$

The total increment in the void volume fraction is the sum of the increment due to void growth and the increment due to void nucleation, or

$$df = df_{gr} + df_{nucl}. \tag{2.57}$$

The growth of existing voids is based on the conservation of mass and is expressed as

$$df_{gr} = (1 - f)\, d\varepsilon_{ii}^{pl}, \tag{2.58}$$

where $d\varepsilon_{ii}^{pl}$ is the trace of the plastic strain tensor. The nucleation of voids occurs by decohesion of the interface between second phase particles and the matrix, by particle fracture, or from broken material bonds. The nucleation model suggested in the current literature can include strain or stress based nucleation. At this time, the work in this dissertation considers only strain based nucleation. The strain based nucleation rate is expressed as,

$$df_{nucl} = A\, d\bar{\varepsilon}_m^{pl}, \tag{2.59}$$

where

$$A = \frac{f_N}{s_N\sqrt{2\pi}} \exp\left[-\frac{1}{2}\left(\frac{\bar{\varepsilon}_m^{pl} - \varepsilon_N}{s_N}\right)^2\right], \tag{2.60}$$

and the mean plastic strain, $d\bar{\varepsilon}_m^{pl}$, is found from,

$$(1 - f)\sigma_f\, d\bar{\varepsilon}_m^{pl} = \sigma_{ij}\, d\varepsilon_{ij}^{pl}. \tag{2.61}$$

In eqn. (2.60), f_N is the volume fraction for nucleating particles, ε_N is the main strain for nucleation, and s_N is the corresponding standard deviation. Recent literature

(ABAQUS, 1997) suggests the following range of values for typical metals: $f_N = 0.04$, $s_N = 0.05 - 0.1$, $\varepsilon_N = 0.1 - 0.3$.

Several of the equations presented in this chapter will reappear in the next chapter as the implementation of the constitutive model is discussed. The method used to determine the increment in plastic strain is also discussed in Chapter 3. In short, an increment in total strain is passed to the constitutive model. The constitutive model then iterates to determine the elastic strains and stresses to remain on the yield surface and not violate the yield condition presented in eqn (2.50). The iteration technique, which is occasionally called the cutting plane algorithm, is discussed in Chapter 3. In addition, Chapter 3 discusses other aspects of the constitutive model such as the optional "element remove" subroutine, which may be used to prevent elements from inverting and stopping the computation by removing them from the calculation.

3.0 Numerical Model

This chapter describes the implementation of the constitutive model into the ABAQUS (1997) code through what ABAQUS calls a VUMAT subroutine. The constitutive model for this analysis is divided into four basic modules: shock effects, GTN plasticity, void growth and strength (Johnson-Cook). In general, the VUMAT subroutine is used to define the mechanical constitutive behavior of the material and if necessary update or use solution dependent state variables to track the material response.

Finite element codes such as ABAQUS Explicit are widely used in industry and at government laboratories such as Los Alamos National Laboratory. These codes are capable of analyzing highly non-linear structural dynamics problems. ABAQUS is a commercially available Lagrangian finite element package. It offers post processing capabilities and a significant amount of user flexibility. Johnson (1981) demonstrated the implementation of his constitutive model using a finite difference approach. However, since numerical codes exist at Los Alamos National Laboratory to preprocess and post process finite element results from ABAQUS along with a strong experience base, ABAQUS was chosen for the numerical code. Enhancement of ABAQUS with additional code development in the form of a VUMAT subroutine will expedite the implementation of new constitutive models and provide a platform to analyze complex geometries.

During the solution process, ABAQUS calculates an increment in strain based on the boundary conditions (such as an increment in load) and the previous state of stress.

This increment in strain is passed to the VUMAT subroutine. The subroutine then returns the state of stress for the material. A large number of parameters can be passed into the VUMAT subroutine. Most of these parameters are either user defined material properties or solution variables, which provide information regarding the last state of the solution and the increment in strain. The user definable variables include the updated stress tensor, state variables, internal energy, and inelastic energy.

The VUMAT subroutine developed for this dissertation consists of a main subroutine and five other smaller subroutines: an equation of state (EOS) subroutine, a GTN subroutine, a Johnson-Cook subroutine, a void growth subroutine, and an element remove subroutine. The EOS and element remove subroutines are optional and can be activated by the user. This allows the code to skip those calculations.

Initially, the main VUMAT subroutine is called. Then if activated, the main subroutine calls the EOS subroutine to modify the bulk modulus and determine the shock heating effects. These results are then returned to the main VUMAT subroutine. Next the main subroutine calls the GTN subroutine. The GTN subroutine calculates the necessary parameters for the strength model and then calls the Johnson-Cook subroutine to determine the flow stress. This flow stress is returned back to the GTN subroutine where the code iterates to converge to a point on the yield surface. At this point, the stresses, energies, and temperatures are updated and passed back to the main subroutine. Next the main VUMAT subroutine calls the void subroutine. The void subroutine determines the nucleation and growth rate for the voids and passes back the new volumetric void concentration in the material. Finally, at the user's discretion, the code enters the element remove subroutine. This subroutine eliminates elements from the

computation based on user specified parameters like volumetric void concentrations or equivalent plastic strain. A flow chart of the VUMAT subroutine is shown in Figure 3.1. It is important to understand that once the code enters the VUMAT subroutine, which is indicated by the dotted oval in Figure 3.1, it does not return to ABAQUS until the stresses and state variables are updated. The circled numbers in Figure 3.1 indicate the calling order for each subroutine. The entire VUMAT subroutine consists of approximately 2300 lines of commented Fortran source code. The implementation of the constitutive model into the VUMAT subroutine is explained in more detail in the remaining sections of this chapter.

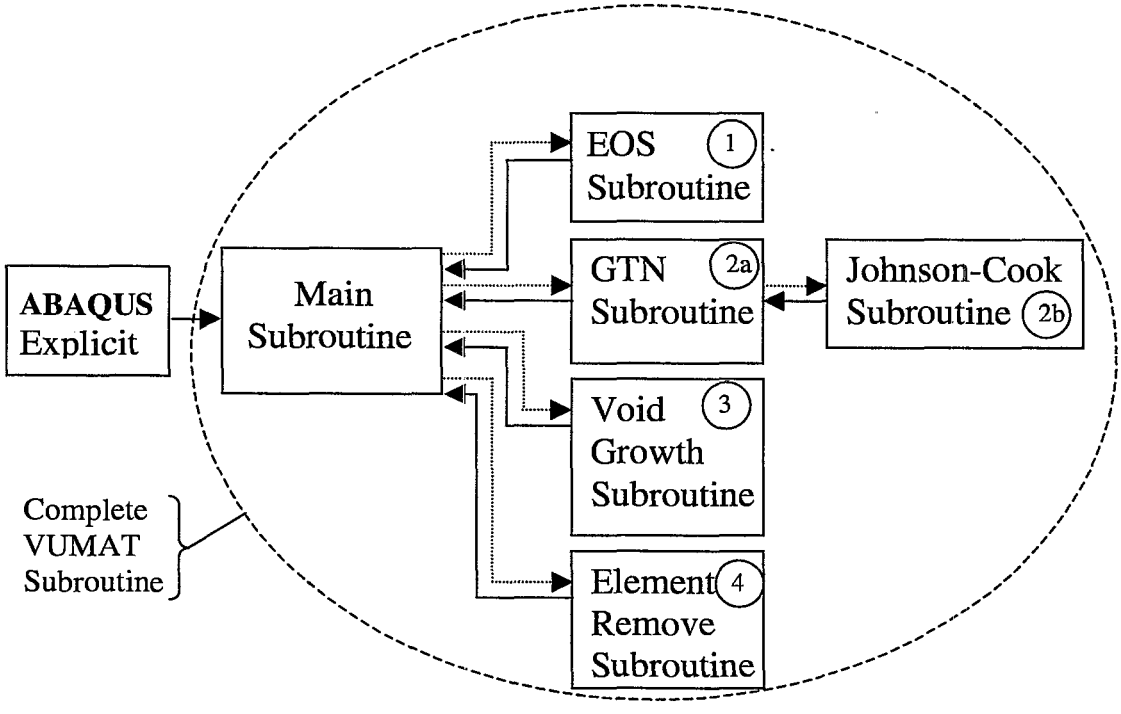

Figure 3.1 Flow Chart for VUMAT Subroutine

3.1 EOS Subroutine

As mentioned earlier, the first subroutine called from the main VUMAT subroutine is the equation of state subroutine. This subroutine determines the

temperature change and the modified bulk modulus resulting from the high pressure shock. Recall that the increment in strain is passed into this subroutine and as a result, this subroutine begins by calculating the volumetric strain increment, where compression is defined as being positive in this subroutine,

$$d\varepsilon_v = (-1.0)\, d\varepsilon_{ii}\,. \tag{3.1}$$

This increment is then added to the total volumetric strain at previous increment,

$$\varepsilon_v = \varepsilon_v^{old} + d\varepsilon_v \tag{3.2}$$

Recall from Chapter 2, the particle velocity, shock velocity, and Hugoniot pressure are calculated with

$$U_p = \frac{C_o \varepsilon_v}{1 - S_e \varepsilon_v} \tag{3.3}$$

$$U_s = C_o + S_e U_p \tag{3.4}$$

$$P_H = \frac{\rho_o C_o^2 \varepsilon_v}{(1 - S_e \varepsilon_v)^2} \tag{3.5}$$

The shock velocity is not specifically needed for the constitutive model. However, its value is stored as a solution dependent variable. If the particle velocity is positive, then the bulk modulus and material temperatures are modified based on the volumetric strain. For positive particle velocities $(U_p > 0)$, the new bulk modulus, K_{new}, and shock temperature, T_s, are found using

$$K_{new} = K_o \frac{(1.0 + S_e \varepsilon_v)}{(1.0 - S_e \varepsilon_v)^3}\,, \tag{3.6}$$

$$T_s = T_o\, \gamma\, \varepsilon_v\,, \tag{3.7}$$

otherwise, the default bulk modulus, K_o, remains unchanged and the shock temperature is set to zero,

$$K_{new} = K_o \tag{3.8}$$

$$T_s = 0.0. \tag{3.9}$$

At this point, the solution dependent variables are updated and the computation returns to the main VUMAT subroutine. The next subroutine called updates the stresses based on the yield surface calculations defined by the GTN model.

3.2 GTN Subroutine

As mentioned in Chapter 2, the form of the GTN model implemented in this dissertation is a combination of the work completed by Gurson, Tvergaard and Needleman. This model has been implemented into other numerical codes like ABAQUS/Standard (Hao & Brocks, 1997) and NIKE (Engelmann & Whirley, 1992).

An iterative technique must be used to obtain the stresses and not violate the yield conditions. The technique adopted for this dissertation is called the cutting-plane algorithm and is described by Ortiz and Popov (1985) and Ortiz and Simo (1986). This algorithm is based on linearization of the plastic consistency condition for the current iteration and satisfaction of the plastic consistency for the new iteration. The cutting plane algorithm is very efficient and demonstrates reasonable accuracy (Ortiz and Simo, 1986). However, it is necessary to take the derivative of the yield function, which is not always straightforward.

The first operation this subroutine performs is to reformulate the elastic constant matrix, zero temporary variables, and set the convergence tolerance. Recall the EOS

subroutine may have modified the bulk modulus. The updated elastic constant matrix, D_{ij}, becomes,

$$D_{ij} = \begin{bmatrix} \left(K_{new} - \frac{2}{3}G\right) + 2G & \left(K_{new} - \frac{2}{3}G\right) & \left(K_{new} - \frac{2}{3}G\right) & 0 & 0 & 0 \\ \left(K_{new} - \frac{2}{3}G\right) & \left(K_{new} - \frac{2}{3}G\right) + 2G & \left(K_{new} - \frac{2}{3}G\right) & 0 & 0 & 0 \\ \left(K_{new} - \frac{2}{3}G\right) & \left(K_{new} - \frac{2}{3}G\right) & \left(K_{new} - \frac{2}{3}G\right) + 2G & 0 & 0 & 0 \\ 0 & 0 & 0 & G & 0 & 0 \\ 0 & 0 & 0 & 0 & G & 0 \\ 0 & 0 & 0 & 0 & 0 & G \end{bmatrix} \tag{3.10}$$

Next, the subroutine performs a few preliminary calculations, which are required to determine the flow stress in the Johnson-Cook subroutine. The increment in plastic strain is found from

$$d\varepsilon_{ij}^{pl} = d\varepsilon_{ij} - \frac{1}{3} d\varepsilon_{kk} \delta_{ij}, \tag{3.11}$$

where $d\varepsilon_{ij}$ is the strain increment and $d\varepsilon_{ij}^{pl}$ is the plastic strain increment. The incremental equivalent plastic strain is found from,

$$d\varepsilon^{pl} = \sqrt{\frac{2}{3} d\varepsilon_{ij}^{pl} \, d\varepsilon_{ij}^{pl}}, \tag{3.12}$$

and the equivalent plastic strain rate is calculated using,

$$\dot{\varepsilon}^{pl} = \frac{d\varepsilon^{pl}}{dt}, \tag{3.13}$$

where dt is the current time step. The equivalent plastic strain rate and the total plastic strain are passed to the Johnson-Cook subroutine along with the current material temperature. The Johnson-Cook subroutine, which is discussed in the next section, returns the flow stress.

The iteration begins with the computation of the plastic strain increment,

$$d\varepsilon_{ij}^{pl} = d\varepsilon_{ij}^{pl} + \Delta\lambda\, D_{ij}\psi_i\,. \tag{3.14}$$

Initially, $\Delta\lambda$ and $d\varepsilon_{ij}^{pl}$ are zero, so the plastic strain increment is also zero. The equivalent plastic strain increment is recalculated in the iteration loop using,

$$d\varepsilon^{pl} = \sqrt{\frac{2}{3} d\varepsilon_{ij}^{pl} d\varepsilon_{ij}^{pl}} \tag{3.15}$$

Next the total elastic strain is calculated using,

$$\varepsilon_{ij}^{el} = \varepsilon_{ij}^{el_{old}} + \left(d\varepsilon_{ij} - d\varepsilon_{ij}^{pl}\right), \tag{3.16}$$

where $\varepsilon_{ij}^{el_{old}}$ is the total elastic strain at the previous converged increment and $d\varepsilon_{ij}^{pl}$, is found from eqn. (3.14). At this point the new trial stresses are computed,

$$\sigma_{ij}^{tr} = D_{ik}\, \varepsilon_{kj}^{el}\,. \tag{3.17}$$

For compressive shock loading, the hyperbolic cosine part of the yield function given in eqn. (2.50) becomes unstable at large hydrostatic pressures. As a result, a pressure cutoff was implemented to modify q_2 and stabilize the yield function. The concept of a pressure cutoff is unique to this dissertation and is based on the assumption that the GTN yield surface is not applicable to materials subjected to high hydrostatic compression. A cut-off pressure, which is set as a user supplied parameter, will ensure stability and not affect the resultant stresses. If the trace of the stress tensor is more compressive than allowed by the user defined cut-off pressure, then,

$$q_2^{new} = abs\left(\frac{\sigma_f}{\sigma_{ii}}\right), \tag{3.18}$$

otherwise, q_2, remains unchanged and the yield function is evaluated. Recall the yield function (see eqn. 2.50) is defined as

$$\phi = \left(\frac{\sigma}{\sigma_f}\right)^2 + 2q_1 f^* \cosh\left(-\frac{3q_2 P}{2\sigma_f}\right) - \left(1 + q_3 f^{*2}\right) = 0. \tag{3.19}$$

If the yield function is less than or equal to zero, then the trial stresses become the new stresses. Otherwise, the yield surface is extended and the iteration loop continues until it determines the elastic-plastic solution.

If an elastic-plastic solution exists, the iteration loop calculates the change in the plastic consistency parameter, $\Delta\lambda$. This new $\Delta\lambda$, is then used to recalculate the plastic strains in eqn. (3.14). Based on the new plastic strains, the elastic strains given by eqn. (3.16) are updated and the new trial stresses are found using eqn. (3.17). These trial stresses are then used to reevaluate the yield function, eqn. (3.19), and convergence is checked. If the yield function is still not less than or equal to zero, the iteration continues.

The formulation for calculating change in the plastic consistency parameter closely follows reports by Engelmann and Whirley (1992) and Ortiz and Simo (1986), and is briefly summarized here. First let ψ_i be a vector of the equivalent plastic strain and void volume fraction,

$$\psi_i = \begin{Bmatrix} \varepsilon^{pl} \\ f \end{Bmatrix}, \tag{3.20}$$

and let the vector function $h_i(\sigma, \psi)$ be defined such that,

$$\Delta\psi_i(\sigma, \psi) = \Delta\lambda\, h_i(\sigma, \psi). \tag{3.21}$$

Next, define a vector function $\xi_i(\sigma, \psi)$ as the gradient of the yield function with respect to the history variables,

$$\xi_i(\sigma, \psi) = \frac{\partial\phi}{\partial\psi_i}(\sigma, \psi). \tag{3.22}$$

In addition, define a second order tensor $v_{ij}(\sigma,\psi)$ as the gradient of the yield function with respect to stress,

$$v_{ij}(\sigma,\psi)=\frac{\partial\phi}{\partial\sigma_{ij}}(\sigma,\psi). \tag{3.23}$$

The change in the plastic consistency parameter is then

$$\Delta\lambda=\frac{\phi}{v_{ij}D_{jk}v_{ik}-\xi_l h_l}, \tag{3.24}$$

where, ϕ, is the yield function. The specific definitions of ξ_l, v_{ik}, and h_l in terms of the stress components are:

$$\xi_1=\frac{\partial\phi}{\partial\varepsilon_{ij}^{pl}}=-\frac{2H}{\sigma_f^3}\left[\frac{2}{3}\sigma_{ij}\sigma_{ij}-\frac{1}{2}\sigma_{kk}\sigma_{ll}\right]-\frac{H f^* q_1\sigma_{kk}}{\sigma_f^2}\sinh\left(\frac{q_2\sigma_{kk}}{2\sigma_f}\right), \tag{3.25}$$

$$\xi_2=\frac{\partial\phi}{\partial f}=2q_1\cosh\left(\frac{q_2\sigma_{kk}}{2\sigma_f}\right)-2q_2 f^*, \tag{3.26}$$

$$v_{ik}=\frac{\partial\phi}{\partial\sigma_{ik}}=\frac{1}{\sigma_f^2}[3\sigma_{ik}-\sigma_{ll}\delta_{ik}]+\frac{f^* q_1}{\sigma_f}\sinh\left(\frac{q_2\sigma_{ll}}{2\sigma_f}\right)\delta_{ik}, \tag{3.27}$$

$$h_1=\sqrt{\frac{2}{3}v_{ij}v_{ij}}, \tag{3.28}$$

$$h_2=(1-f)v_{ii}, \tag{3.29}$$

where H is the tangent of the flow surface. The tangent of the flow stress equation given by Johnson and Cook is calculated as

$$H=\frac{(\sigma_f-\sigma_f^{old})}{d\varepsilon^{pl}}. \tag{3.30}$$

At this point, the iteration is complete and the elastic-plastic solution is known. Next the total plastic strain is updated with the new increments in plastic strain. The increment in plastic work is also calculated as,

$$dW^{pl} = \frac{\sigma_{ij}\, d\varepsilon_{ij}^{pl}}{\rho}. \tag{3.31}$$

Notice eqn. (3.31) is not written in terms of the deviatoric stress tensor but rather the total stress tensor. This is a result of incorporating microvoids, which makes the contribution of the spherical stress tensor important in the calculation of the plastic work. The increment in internal energy is simply,

$$dE = \frac{1}{2}\frac{\sigma_{ij}\, d\varepsilon_{ij}}{\rho}. \tag{3.32}$$

The total plastic work and total internal energy, whose units are for example J/kg, are then found by adding the respective increments from eqns. (3.31) and (3.32) to the values at the previously converged increment.

The new temperature of the material is calculated using both the temperature rise as a result of the shock heating and the temperature resulting from the plastic work.

$$T^{new} = T^{\text{int}} + T_s + \frac{\sum dW^{pl}}{C_v}, \tag{3.33}$$

where T^{init} is the initial temperature, $\sum dW^{pl}$ is the total increment in plastic work, and C_v is the specific heat. Recall that the shock temperature is passed into this subroutine from the EOS subroutine. Finally, the mean plastic strain is calculated from the increment in plastic work, the current void volume fraction, and the flow stress. This value, which is expressed as,

$$d\bar{\varepsilon}_m^{pl} = \frac{\sigma_{ij}\, d\varepsilon_{ij}^{pl}}{(1-f)\sigma_f}, \tag{3.34}$$

is needed to calculate the void nucleation rate in the void subroutine and is also shown as eqn. (2.61) in Chapter 2.

At the end of this subroutine, several variables are saved as solution dependent variables. Any variable saved as a solution dependent variable can be used in subsequent subroutines or during the next time step and the user can always plot the time history response of solution dependent variables during post processing.

3.3 Strength Subroutine

As mentioned in Chapter 2 and the previous section, the flow stress is based on the Johnson-Cook strength model and is calculated using the current plastic strain, strain-rate, and temperature. From eqn. (2.1), the equation for the flow stress is written as,

$$\sigma_f = \left(A + B\varepsilon^n\right)\left(1 + C\ln\dot{\varepsilon}^*\right)\left(1 - T^{*m}\right) \tag{3.35}$$

The five experimentally determined parameters (A, B, C, n, m) are supplied as constants to the VUMAT. The current plastic strain, strain-rate, and temperature are passed into this Johnson-Cook subroutine from the GTN subroutine. The Johnson-Cook subroutine then returns the allowable flow stress. By separating the flow stress calculations from the main body of the VUMAT, it is relatively easy to implement other strength models at a later time.

3.4 Void Subroutine

The implementation of the void model was separated from the GTN subroutine to allow the user to implement different constitutive laws involving other forms of void growth, nucleation, and coalescence. Recall from eqns (2.55) through (2.60) in Chapter 2, the rate of change in the void volume fraction can be written as,

$$df = df_{gr} + df_{nucl}, \tag{3.36}$$

where the growth rate is dependent on the trace of the plastic strain rate and the nucleation is based on the equivalent flow stress.

At the start of this subroutine, the first series of calculations set the constants that will be used in the subroutine. One of these constants is

$$\bar{f}_F = \frac{q_1 + \sqrt{q_1^2 - q_3}}{q_3} \tag{3.37}$$

which is the void volume fraction at which there is a complete loss of stress carrying capacity in the material. Next the increment in void growth,

$$df_{gr} = (1 - f)\, d\varepsilon_{ii}^{pl}, \tag{3.38}$$

is calculated using the trace of the increment in the plastic strain tensor from the GTN model. To determine the increment in nucleated voids, the parameter

$$A = \frac{f_N}{s_N\sqrt{2\pi}} \exp\left[-\frac{1}{2}\left(\frac{\bar{\varepsilon}_m^{pl} - \varepsilon_N}{s_N}\right)^2\right], \tag{3.39}$$

is determined and applied to

$$df_{nucl} = A\ d\bar{\varepsilon}_m^{pl}, \tag{3.40}$$

using the mean plastic strain from the GTN model. Combining eqns. (3.38) and (3.40) into (3.36) gives the total increment in the void volume fraction. The increment in the

void volume fraction is added to the total volume fraction from the previous increment to obtain f. The new void volume fraction, f^*, which is passed back from this subroutine is defined from the following equation as explained in eqn (2.55) from Chapter 2.

$$f^* = \begin{cases} f & \text{if } f \le f_c \\ f_c + \dfrac{\bar{f}_F - f_c}{f_F - f_c}(f - f_c) & \text{if } f_c < f < f_F \\ \bar{f}_F & \text{if } f \ge f_F \end{cases} \tag{3.41}$$

If this is the first increment, this subroutine initializes the void volume fraction in the material with either a constant or random distribution of voids. A constant distribution of voids is defined with the user defined variable, f^{init}, using

$$f^* = f^{init}, \tag{3.42}$$

and a random distribution of voids is defined using

$$f^* = f^{init} + 5.0\, r\, f^{init}, \tag{3.42}$$

where r is a randomly generated number from 0 to 1.0. For example, if f^{init} is 0.001, then the material will have a random distribution of voids ranging from 0.001-0.005.

3.5 "Element Remove" Subroutine

The element remove subroutine is simple and straightforward. ABAQUS allows the user to define a solution dependent variable that indicates the element is to be removed from the calculations. The corresponding stiffness of the targeted element is then significantly reduced to effectively remove this element from the calculations. The element does remain in the mesh, but does not interact any further with the surrounding elements. This allows the user to 'remove' elements based on a predetermined set of

specifications. For example, if the plastic strain or void volume fraction in the element reaches a selected critical value, the element is removed from the calculations. One negative aspect of this technique is that it does not allow for a gradual decrease in stiffness. However, this subroutine was written to allow the user to implement a stiffness degradation model at a later time. Currently, this subroutine removes elements based on either the accumulated equivalent plastic strain or void volume fraction.

3.6 HE Burn Model

The high explosive burn model used in this dissertation is developed and maintained by ABAQUS and is not part of the VUMAT developed in this dissertation. ABAQUS uses the Jones-Wilkens-Lee (JWL) equation of state to model the pressure generated by the release of chemical energy from the explosive. The reaction and initiation of the EOS is implemented using a program burn model. The program burn model determines the initiation time by a geometric construction using the detonation wave speed and the distance of the material points from the detonation point.

This model is simple to use and the parameters are widely available in the current literature. To activate this model, the user simply provides the detonation point(s) and the high explosive (HE) parameters for the JWL equation of state. The HE used throughout this dissertation is PBX-9501. This type HE was used because it is readily obtainable with a well documented EOS and it is easy to fabricate and machine to reasonable dimensional tolerances. The JWL parameters for PBX-9501 (Dobratz, 1981) are provided in Table 3.1, where C_d is the detonation wave speed, E_{mo} is the initial energy per unit mass, and P_{cj} is the cutoff pressure.

Table 3.1: JWL Parameters for PBX-9501

A (Pa)	B (Pa)	ω	R_1	R_2	C_d (m/s)	E_{mo} (J/kg)	P_{cj} (Pa)
8.545×10^{11}	2.049×10^{10}	0.25	4.6	1.35	8830.0	5.543×10^{6}	0.0

3.7 Preliminary Results

A small axisymmetric model was developed to demonstrate the capabilities of this constitutive model. This model consists of an axisymmetric ring of copper filled with high explosive. The mesh for this model is shown in Figure 3.2.

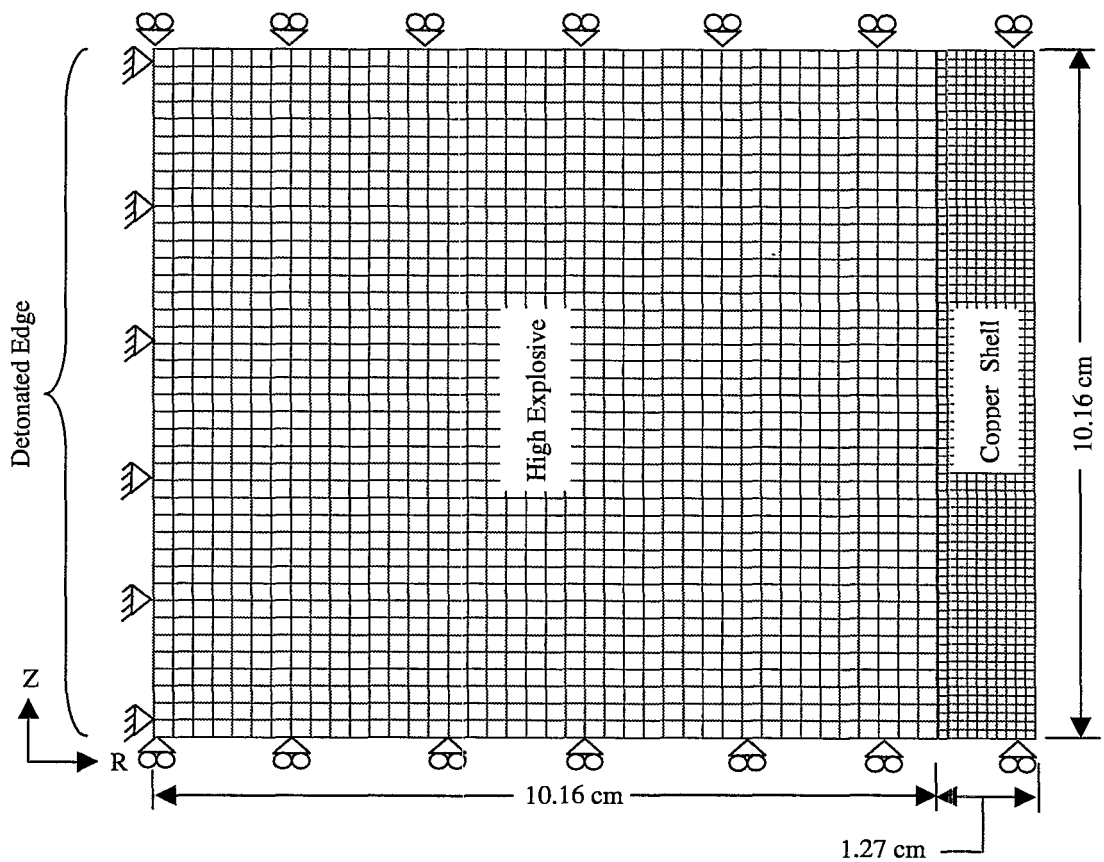

Figure 3.2: Mesh for Preliminary Axisymmetric Ring Model

The elements used in this model are four node, linear, axisymmetric elements. There are 1600 elements in the HE and 800 elements in the cylindrical shell. A 0.127 mm gap exists between the HE and the copper shell. A contact surface is prescribed between the HE and the shell. This contact surface allows the elements on the boundary to slide relative to one another without penetration. The effects of friction are not included in the model and thus only a normal force relative to the contact surface is transmitted across the HE-copper boundary. The HE is line detonated along the axis of symmetry (R = 0) to provide uniform radial expansion. A symmetry boundary condition is applied to the top and bottom of the mesh, as it appears in Figure 3.2. This allows the geometry to expand freely in the radial direction, away from the detonated axis, but with no displacement in the Z-direction, normal to the rollers. A table summarizing the user parameters supplied to the constitutive model is provided in Table 3.2.

Table 3.2: User Parameters Supplied to the Constitutive Model for the Copper Ring

Model	Description	Units	Value
Johnson-Cook Strength Model	Material Density	kg/m^3	8945.0
	Specific Heat	J/kg-K	383.5
	Initial Temperature	K	294.26
	Room Temperature	K	294.26
	Melt Temperature	K	1355.93
	Shear Modulus	Pa	4.63×10^{10}
	Yield Stress	Pa	8.963×10^{7}
	Hardening Coef.	Pa	2.916×10^{8}
	Hardening Exp.	-	0.31
	Strain-Rate Coef.	-	0.025
	Thermal Softening Exp.	-	1.09
	Pressure Hardening Term	Pa	0.0
	Strength Cut-off	Pa	6.895×10^{10}
	On/Off Flag (1-on, 0-off)	-	1.0
EOS Model	Bulk Modulus	Pa	1.372×10^{11}
	Sound Speed - C_0	m/s	3940.0
	Slope of U_s-U_p Curve - S	-	1.49
	Grüneisen Coef. - γ	-	1.96
	Tensile Pressure Cut-off	Pa	6.895×10^{10}
	On/Off Flag (1-on, 0-off)	-	1.0
GTN Void Model	q_1	-	1.5
	q_2	-	1.0
	q_3	-	2.25
	f_F	-	0.85
	f_c	-	0.85
	Init. Void Vol. Fract. - f^{init}	-	0.001
	E_n	-	0.3
	S_n	-	0.1
	F_n	-	0.04
	Void Nucleation On/Off	-	1.0
	Random Voids On/Off	-	1.0
	On/Off Flag (1-on, 0-off)	-	1.0
	Void Pressure Cut-off	Pa	-1.0×10^{6}

The effect of the shock on the bulk modulus is shown in Figure 3.3. This figure shows plots of the user supplied bulk modulus and modified bulk modulus vs. time for an

element on the ID and OD of the cylinder. When the EOS is not activated, the user supplied bulk modulus, given in Table 3.2, is used throughout the calculations and is constant with time. Otherwise when the EOS is activated, the bulk modulus in the material is modified to include the effects of the high pressure shock. Notice that the shock effect on the bulk modulus is much less for an element on the outside of the cylinder. This is a result of rarefraction waves, which diminish the magnitude of the shock as it travels through the cylinder wall.

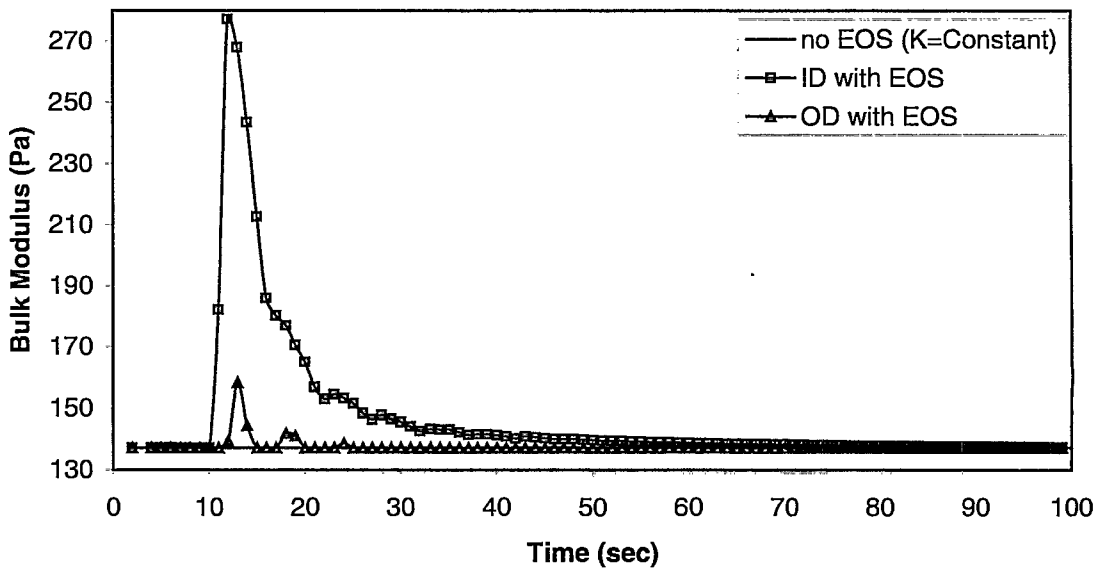

Figure 3.3: Shock EOS Effects on the Bulk Modulus

As expected, the temperature change resulting from the shock loading shows a similar effect. A graph of the temperature change from the high pressure shock and plastic deformation is shown in Figure 3.4. This figure shows the resulting temperature vs. time for an element on the OD and ID with and without the EOS model. The final temperature for a particular element is similar for either model. However, the shock does induce an initial temperature rise. As expected, the magnitude of this rise is larger on the

surface closest to the HE. The maximum increase in energy from the shock heating is approximately 0.1% of the total energy.

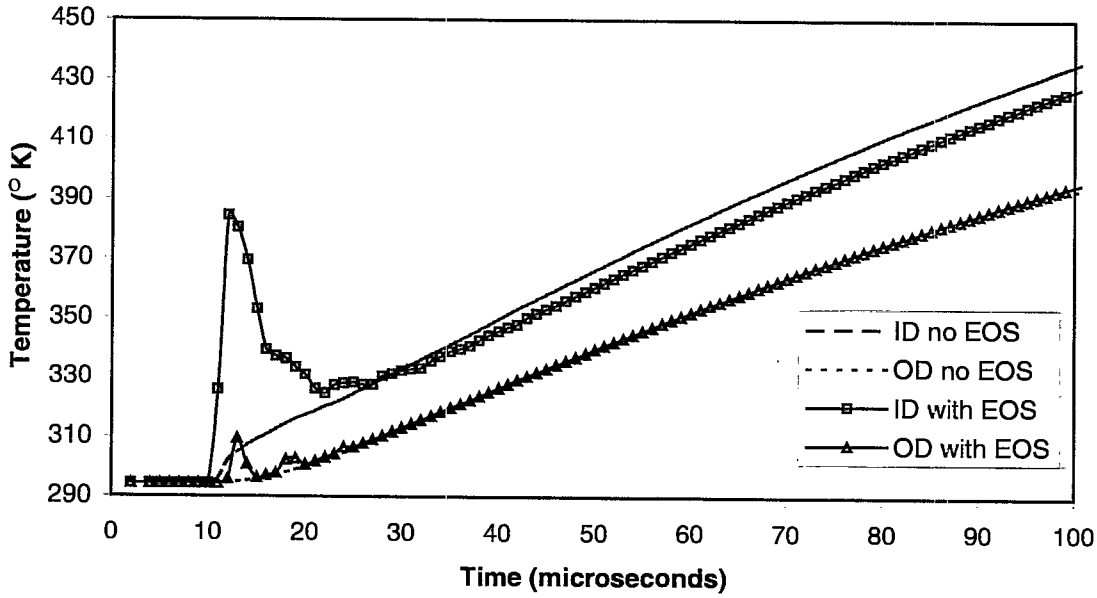

Figure 3.4: Temperature Effects from High Pressure Shock and Plastic Work

Early literature from Taylor (1963a) indicated that the hoop stress on the ID remains compressive after the hoop stress on the OD becomes tensile. This effect is illustrated in Figures 3.5 and 3.6. The hoop stress on the OD becomes tensile after 25 microseconds while the hoop stress on the ID becomes tensile after 54 microseconds. The early oscillations shown in Figures 3.5 and even more apparently in Figure 3.6 are a result of the reverberating elastic stress waves in the material. Several authors including Taylor (1963a) have shown that the hoop stress on the inner surface remains compressive until internal pressure is equal to yield stress. The radial stress, which is not shown here, remains negative long after the shock waves have attenuated and is still negative after 100 microseconds.

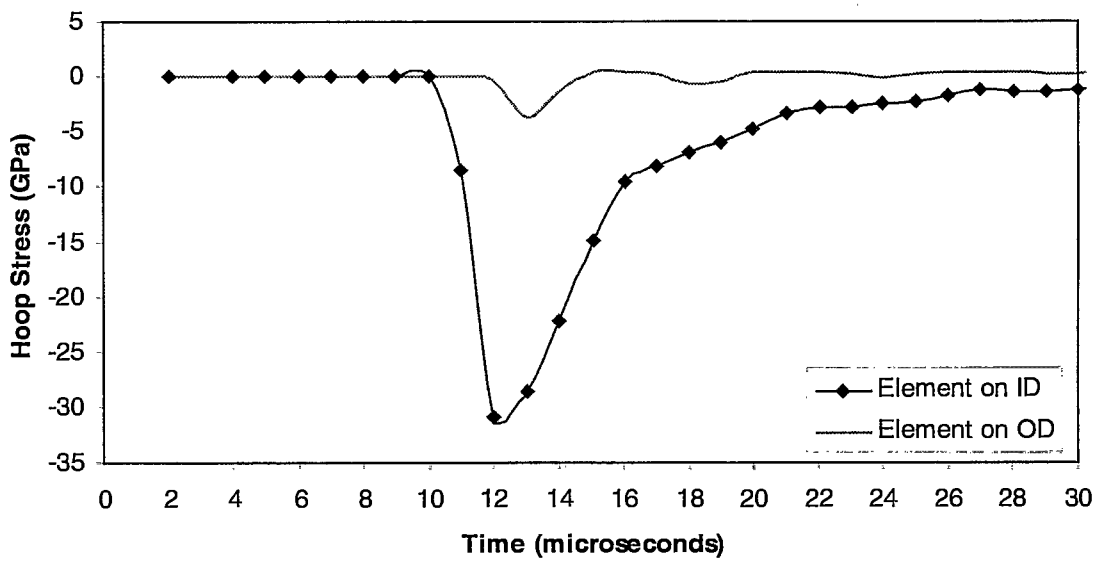

Figure 3.5: Hoop Stress on the ID and OD of Expanding Ring from 0-30 Microseconds

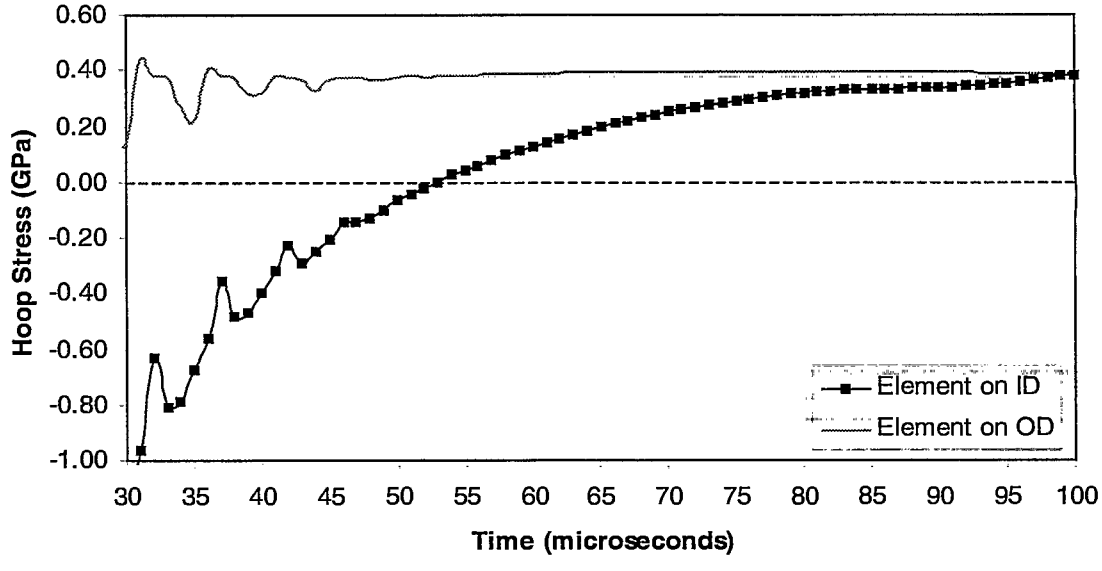

Figure 3.6: Hoop Stress on the ID and OD of Expanding Ring from 30-100 Microseconds

The numerical model predicts a maximum shock velocity in the copper that is approximately equal to the elastic wave speed. This indicates the presence of elastic stress wave and most likely a combination of elastic and plastic stress waves due to the magnitude of the loading. If the shock wave velocity was greater than the elastic wave

speed, a strong shock would propagate through the material as a single wave, which is shown for the case of P_3 in Figure 2.6.

The equivalent plastic strain rate for an element on the ID is shown in Figure 3.7. This figure indicates a maximum equivalent plastic strain rate of approximately 7.1×10^4 s^{-1} for calculations without the EOS and 6.6×10^4 s^{-1} for the calculations with the EOS subroutine. The equivalent plastic strain rate at 100 microseconds is 9.04×10^3 s^{-1} for calculations without the EOS and 9.18×10^3 s^{-1} for the calculations with the EOS model. The two curves are fairly close at this particular location on the mesh indicating that the EOS has a minor effect on the equivalent plastic strain rate. However, this observation is not conclusive in that the discrepancies between the two may be larger at other locations in the mesh and, as a result, additional comparisons should be performed.

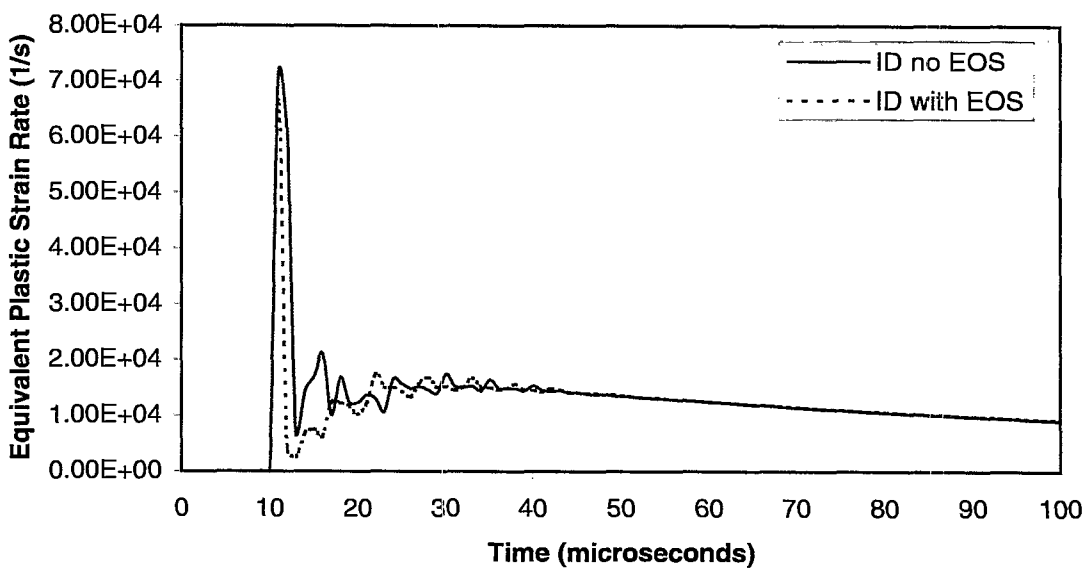

Figure 3.7: Strain Rate on the ID with and without EOS Model

The hoop strain for elements on the ID and OD with and without the EOS model is shown in Figure 3.8. From this figure, the strain on the OD is approximately the same

with and without the EOS model. However, the strain on the ID is slightly different which could be a result of compression in the shell material.

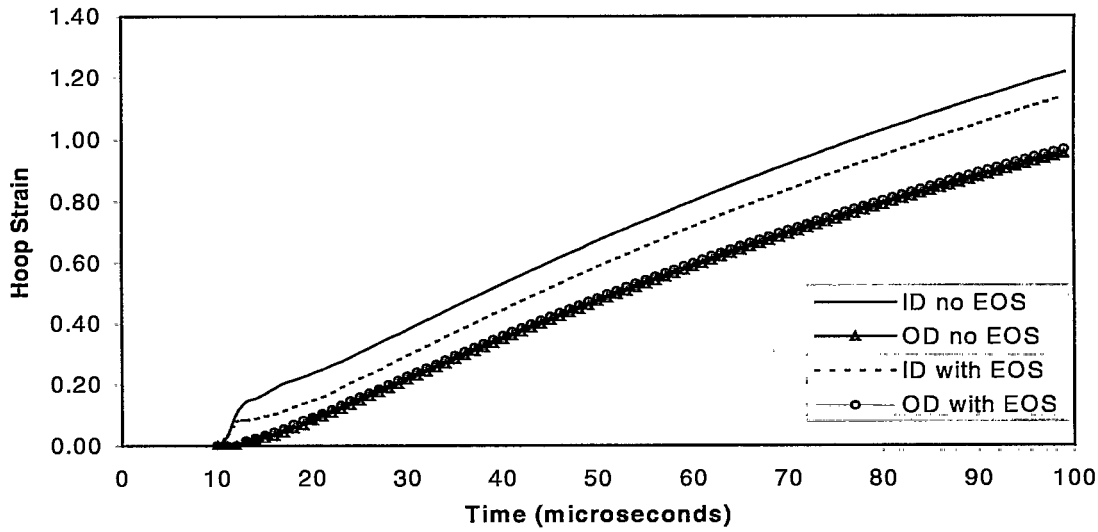

Figure 3.8: Hoop Strain with and without EOS Model

Finally, Figure 3.9 indicates the void volume fraction in the material for an element on the OD with and without the EOS model. The EOS model appears to have a minimal effect on this parameter. This trend is very similar for an element on the ID.

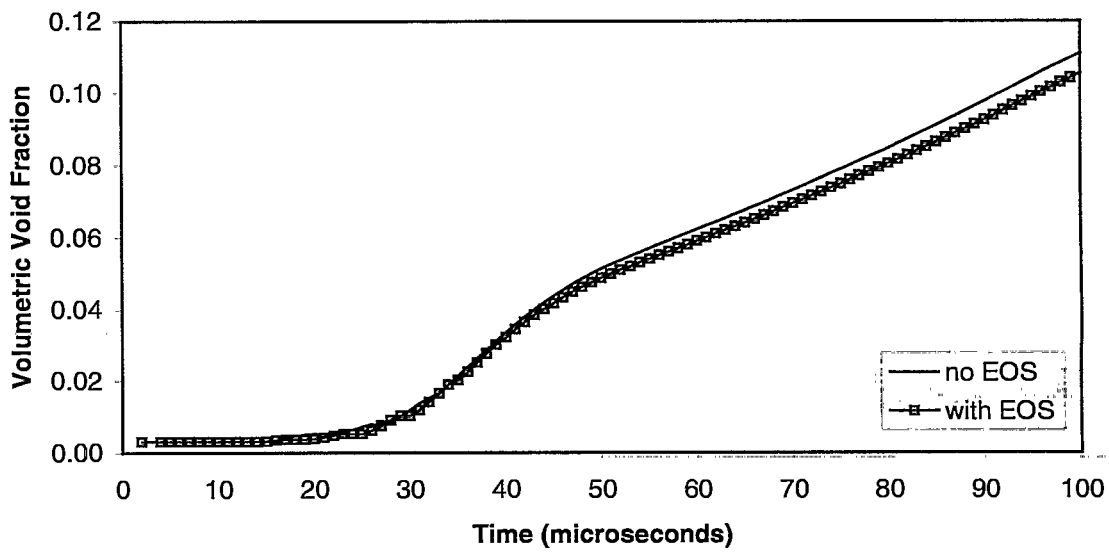

Figure 3.9: Void Volume Fraction on the OD with and without EOS Model

4.0 Cylinder Experiments

Two experiments were designed to benchmark the numerical model and to add credence to the formulation of the constitutive model. The geometry and the materials used for the experiments were determined from the current literature and conversations with experienced experimentalists at Los Alamos (Christian, 1997). This chapter describes the set-up, materials, and diagnostic equipment used for the experiments.

Numerous materials ranging from steel to 6061-T6 aluminum have been widely used in the literature for problems involving high strain-rate viscoplasticity. Most of these materials are not considered extremely ductile. A few experimenters have reported on the use of OFE (Oxygen-Free Electronic) copper, but in most cases they do not provide information regarding its hardness or grain size. In general, the bulk of existing literature, particularly before the 1970's, provides little or no information regarding the metallurgy or microstructure of the materials used.

OFE copper has been carefully characterized for a number of years. Its high strain-rate response and plastic deformation are well understood. Unlike uranium, for example, OFE copper does not undergo a phase transition at strain rates below 10^6 s^{-1}. Numerous strength models have used OFE copper for validation purposes. In addition, OFE copper is easy to obtain in a carefully controlled high purity form. The ductility, predictability, and purity of OFE copper make it the material of choice for studying the development of instabilities in problems involving large deformation plasticity.

4.1 Cylinder Material and Design

Alloy 101 OFE copper is 99.99% pure copper, and is considered extremely high purity copper. Locating alloy 101 copper in large diameter tubes or rods with a small grain size is a not trivial task. Numerous vendors advertise soft copper in large diameters but most have hot worked the material, which results in extremely large grains. However, Copper and Brass Sales Inc. located a batch of drawn copper tubing that proved to be adequate for the purposes of these experiments.

The initial grain size in the copper tubing was 35-40 μm with hardness on the Rockwell F scale of 80. A small sample of the material was sectioned off and heat treated to 350°C to determine the rate and degree of softening attainable in the material. After 60 minutes, the microstructure of the copper was approximately the same size. The hardness of the material was now 23 on the Rockwell F scale indicating the release of residual energy (Necker, 1997). The microstructure of the copper material before and after the heat treat is shown in Figure 4.1.

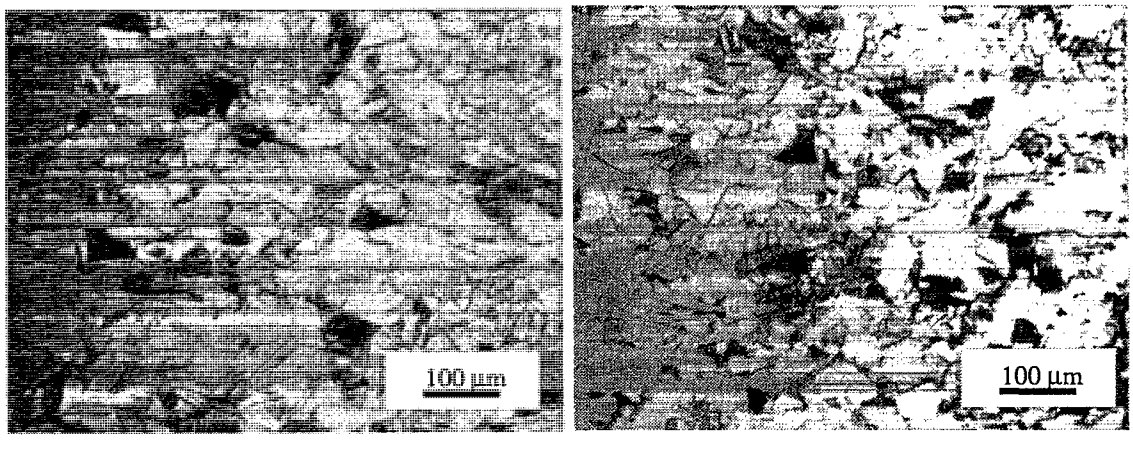

As Purchased Copper (Before Heat Treat) After Heat Treat at 350°C for 60 min.

Figure 4.1 Microstructure of the Copper Material Before and After Heat Treat

The largest diameter of copper tubing available from Copper and Brass Sales, Inc. had a 114.3 mm outer diameter with a 6.35 mm wall thickness. To a large degree this dictated the overall geometry of the experiments. The goal of the experiments was to test two different wall thicknesses using approximately the same amount of HE. After machining, the smallest inner diameter obtainable was 102.06 mm. This allowed for one tube to be 2.54 mm thick and the other to be 5.08 mm thick. Experimentalists at Los Alamos suggested the diameter to length ratio be at least 1:3 and preferably 1:4. This resulted in an overall tube length of 406.4 mm.

The surface finish of the cylinder was carefully controlled to minimize perturbations on the surface. A surface finish, as defined by ANSI B46.1-1962, of 16 and 32 was maintained on the outside and inside surfaces respectively. In addition, a concentricity tolerance of 0.05 mm was maintained during the fabrication process. The fabrication drawings for the cylinders are included in the Appendix A. The overall dimensions of the geometry for the two cylinders are shown below in Table 4.1.

Table 4.1: Dimensions of the Two Cylinders Used for the Experiments

	Length (mm)	Inner Diameter (mm)	Wall Thickness (mm)	Outer Diameter (cm)
Thin Cylinder	406.4	102.06	2.54	107.14
Thick Cylinder	406.4	102.06	5.08	112.22

4.2 High Explosive Type and Design

Numerous types of high explosives have been used in the past and several are still available. However, some are extremely sensitive and difficult to use, while others are not well characterized. The type of HE used in these experiments is known as PBX-

9501. This particular type of HE is very well characterized and predictable. In addition, the method used to detonate PBX-9501 is well understood (Ferm, 1998).

The finite element model used in the numerical analysis portion of this dissertation is not well suited for modeling large air gaps in the configuration. Therefore a solid cylinder of HE was designed to slide inside of the copper shell. A 0.127 mm clearance was prescribed between the HE and the cylinder to provide an adequate gap for assembly. The HE was centered in the cylinder and bonded to several small shims located at each end. This prevented the HE from falling out of the copper cylinder. The fabrications drawings for the HE are also included in Appendix A with the drawing for copper cylinders.

There are several possible detonation methods. The simplest and least expensive method is called an end-on detonation and uses a SE-1 type of detonator. In this method, the detonator is bonded to the HE in one place, which is typically at the axis of symmetry. This essentially detonates the cylinder of HE at a point. The detonation wave then propagates spherically from the point of detonation until it reaches the edges of the cylinder. At this point it begins propagating down the length of the cylinder and eventually becomes a planar detonation wave. This type of detonation is undesirable due to the complexity of the changing wave structure.

An alternative method uses a plane wave lens and a SE-1 detonator to develop a planar detonation front. A planar detonation is much simpler to model and as a result is more desirable. The plane wave lens is essentially a cone fabricated from two different types of HE. The cone is detonated at the apex with a SE-1 detonator and the detonation

front travels down the cone. The burn times of the two different types of HE produce a planer detonation wave by the time the front reaches the base of the cone.

The experiments presented in this dissertation used a plane wave lens and a SE-1 detonator to establish a plane wave detonation front. The plane wave lens and mounting ring for the SE-1 detonator are shown as the conical geometry above the copper cylinders in Figure 4.2. Once a plane wave front is established, it will remain planar as long as there are no significant material or geometric transitions. The transition from the plane wave lens to the solid cylinder of HE was improved in these experiments by extending the HE 5.08 cm beyond the end of the copper shell. This helped to ensure a stable plane wave detonation inside the copper cylinders. The weight of the HE was approximately 7.3 kg and the weight of the thick and thin copper cylinder were 6.2 kg and 3.0 kg respectively.

The assembly and inspection of both the cylinders and HE were carefully controlled. The final assemblies are shown below in Figure 4.2. Again, the mounting ring for the SE-1 detonator is shown at the top of the picture. This ring was bonded onto the plane wave lens, which in turn was bonded onto the cylinder of PBX-9501. The copper shells shown in Figure 4.2 have a grid with distinguishing marks on the outer surface. These marks provide a contrasting surface making it easier to identify the quasi-periodic instabilities. In addition, the grid is useful for determining the overall strain from the framing camera pictures.

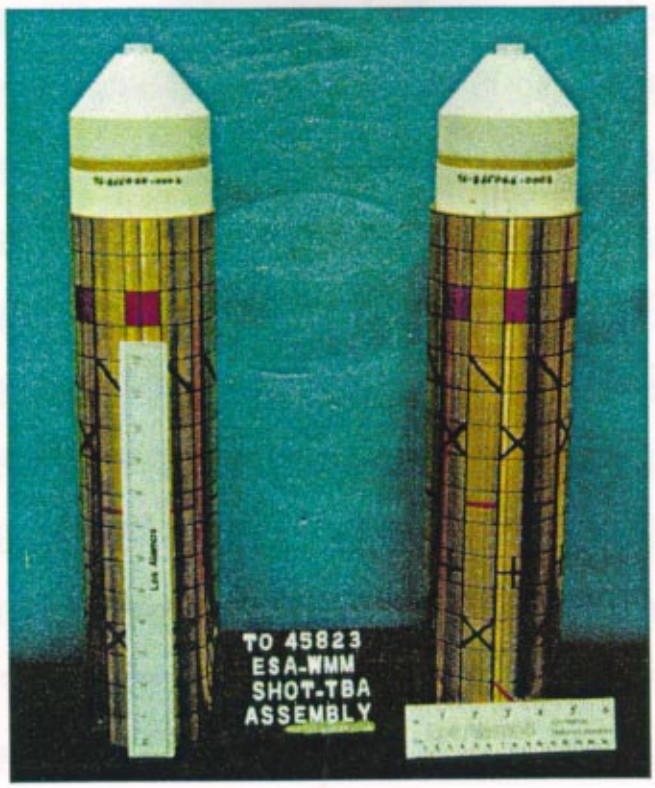

Figure 4.2: Copper Cylinder and HE Assemblies

4.3 Firing Point Set-Up

The types of diagnostics used in an experiment typically dictate the required experimental set-up. The experiments presented as part of this dissertation use two basic types of diagnostic equipment: Fabry-Perot and fast framing camera. Fabry-Perot is a type of laser or visar interferometer, which is capable of recording velocity information for a single point on the surface of the expanding shell. The fast framing camera diagnostic provides several images of the deformed shape at specified intervals in time. The strain and the development of the instabilities observed on the surface of the expanding shell can then be extracted from the photographs and plotted as a function of time.

Information regarding the damage mechanism in the material and strain at or near failure can sometimes be obtained from the fragments. This requires an extensive effort to minimize additional damage or 'soft catch', while decelerating the fragments. In these experiments, a large plywood box filled with vermiculite and asphalt sheeting was used in an attempt to 'soft catch' the fragments. However, locating the fragments in the vermiculite proved to be very difficult and as a result the last experiment only used the asphalt sheeting. The shot stand and plywood fragment box are shown in Figure 4.3. In addition, sandbags were used in an attempt to minimize the movement of the fragment box.

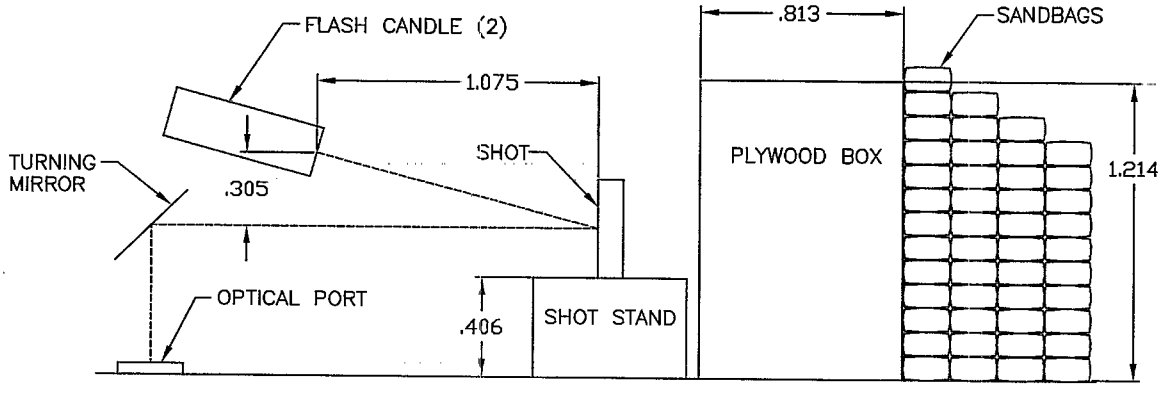

Figure 4.3: Elevation View of the Experimental Set-Up (all dimensions are in meters unless indicated)

The HE filled cylinder or shot was placed on the shot stand, which was constructed from plywood. During the event, the shot was illuminated using two flash candles. Flash candles are simply plywood boxes lined with what is known as detasheet. Detasheet is essentially paper with distinct winding patterns of HE. The HE is ignited at one end and then the HE burn follows the pattern like a fuse, resulting in bright light and

long burn times. The timing of the illumination was carefully coupled with the shutter timing on the fast framing camera. The fast framing camera was located down hole in a bunker and viewed the experiment through an optical port in the ceiling. A turning mirror, which is shown in Figure 4.3, was used to correct the line of sight. Figure 4.4 shows a plan view of the experimental set-up.

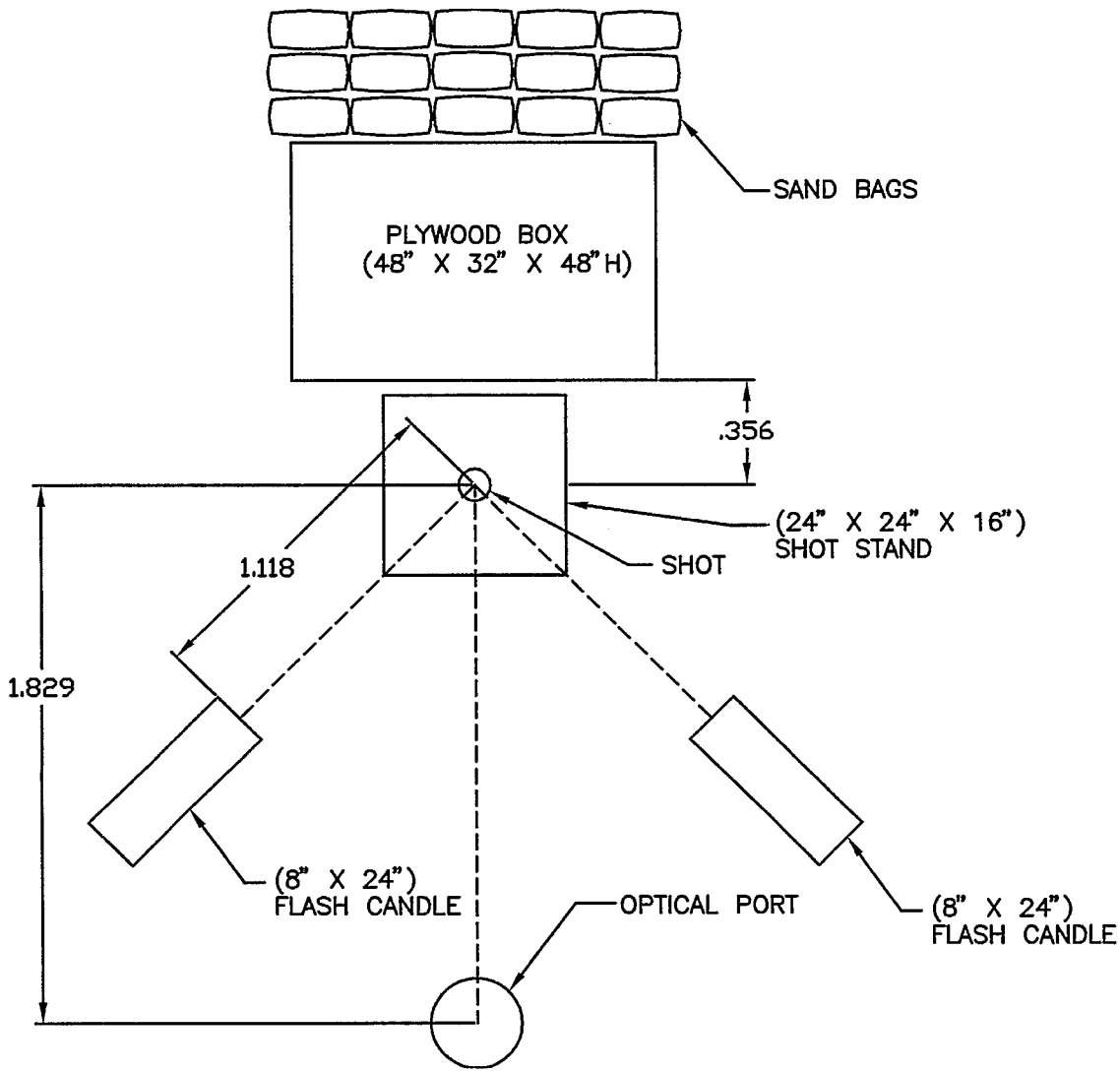

Figure 4.4: Plan View of the Experimental Set-Up (all dimensions are in meters unless indicated)

A cross-sectional view of the wooded shot stand and the placement of the cylinder are shown in Figure 4.5. The cylinder was inverted with the plane wave lens and detonator on the bottom. The spot or measurement point for the Fabry-Perot was located exactly halfway up the cylinder at 20.32 cm. A digitized picture of the entire experimental set-up and shot stand is shown in Figure 4.6.

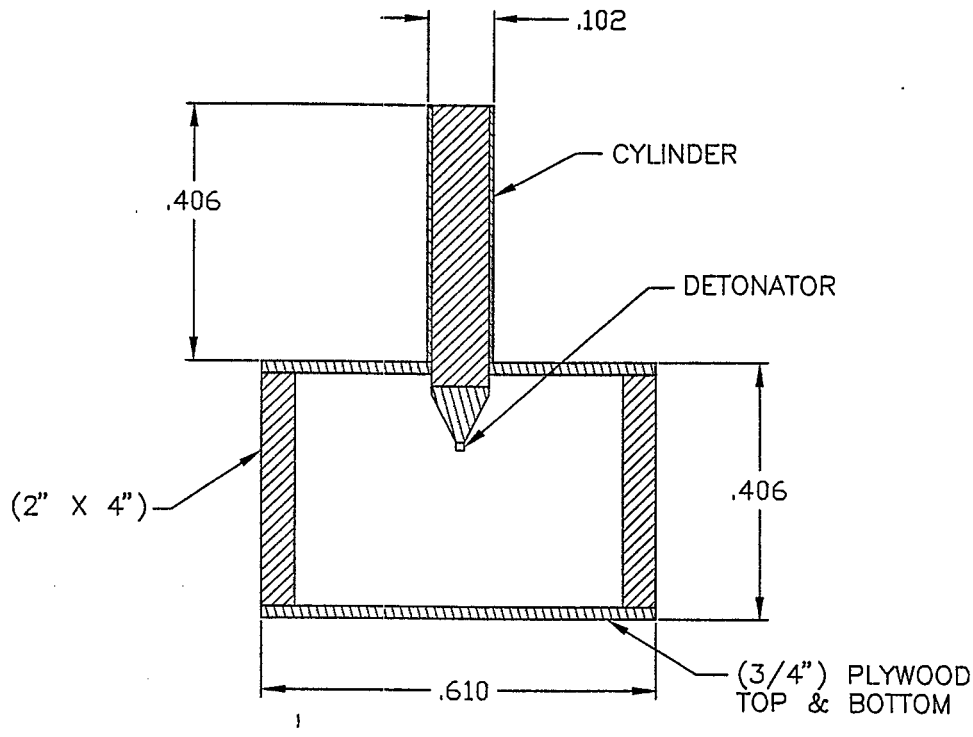

Figure 4.5: Shot Stand Used in Experimental Set-Up (all dimensions are in meters unless indicated)

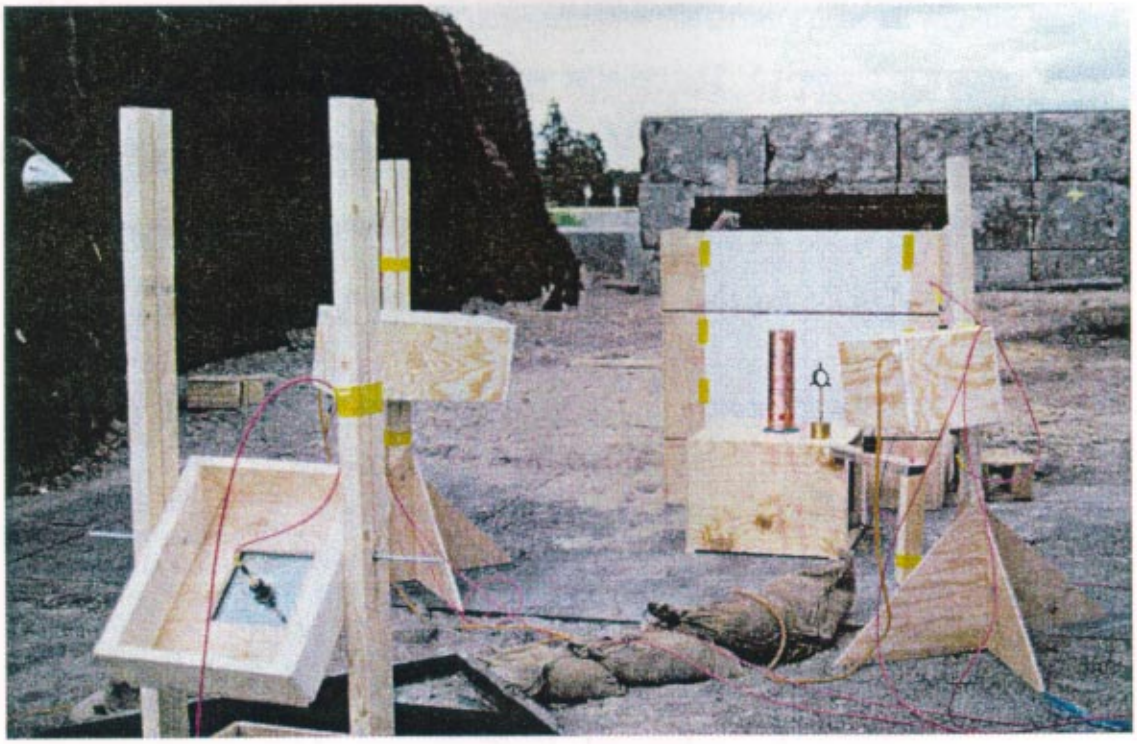

Figure 4.6: Experimental Set-Up

4.4 Preliminary Observations

The first experiment involved the thicker of the two cylinders. In this experiment, the diagnostic equipment did not perform entirely as expected. The Fabry-Perot equipment experienced a hardware failure and as a result, was not able to record data. However, the fast framing camera performed as expected. A total of 23 images with a frame interval time of 2.257 microseconds were recorded.

In the second experiment, which involved the thinner cylinder, all of the diagnostic equipment performed as expected. Again the frame interval time of the fast framing camera was 2.257 microseconds and a total of 23 images were recorded. The fast framing camera images of the thinner cylinder are shown in Figure 4.7.

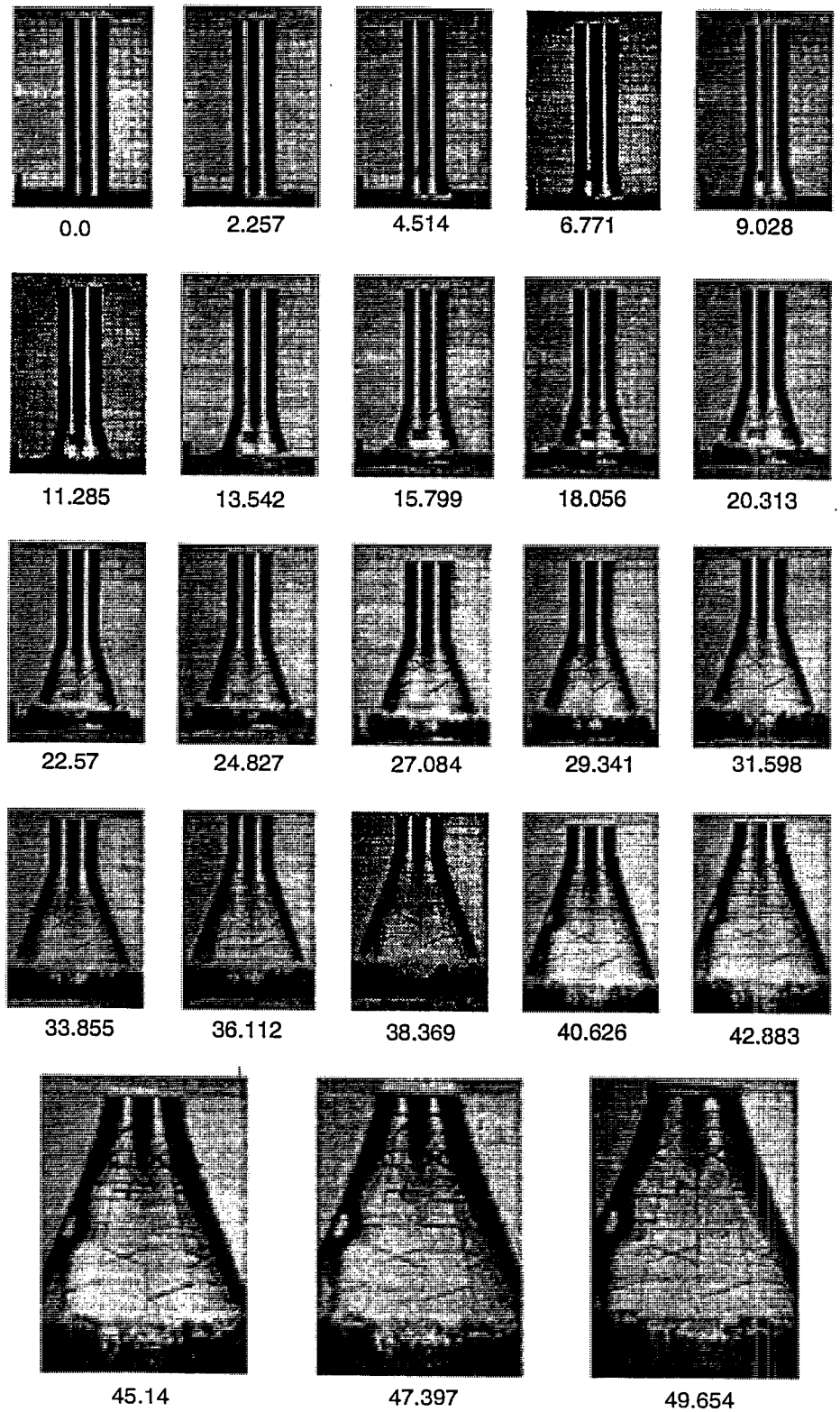

Figure 4.7: Framing Camera Images for the Thin Cylinder (Times in Microseconds)

A pattern of quasi-periodic instabilities was observed on the framing camera pictures from both experiments. However, it is more difficult to see on the thick wall cylinder. A picture of the last frame of the thin cylinder (49.6 microseconds) is shown below in Figure 4.8. The image in this figure is rotated 90° counterclockwise for illustration purposes. The quasi-periodic pattern of instabilities is most prevalent on the black lines shown inside the dark circle of this figure. The hoop strain at center of the dark circle is on the order of 1.5. The dark shaded circle on the bottom edge of the cylinder is a shadow from the Fabry-Perot optics.

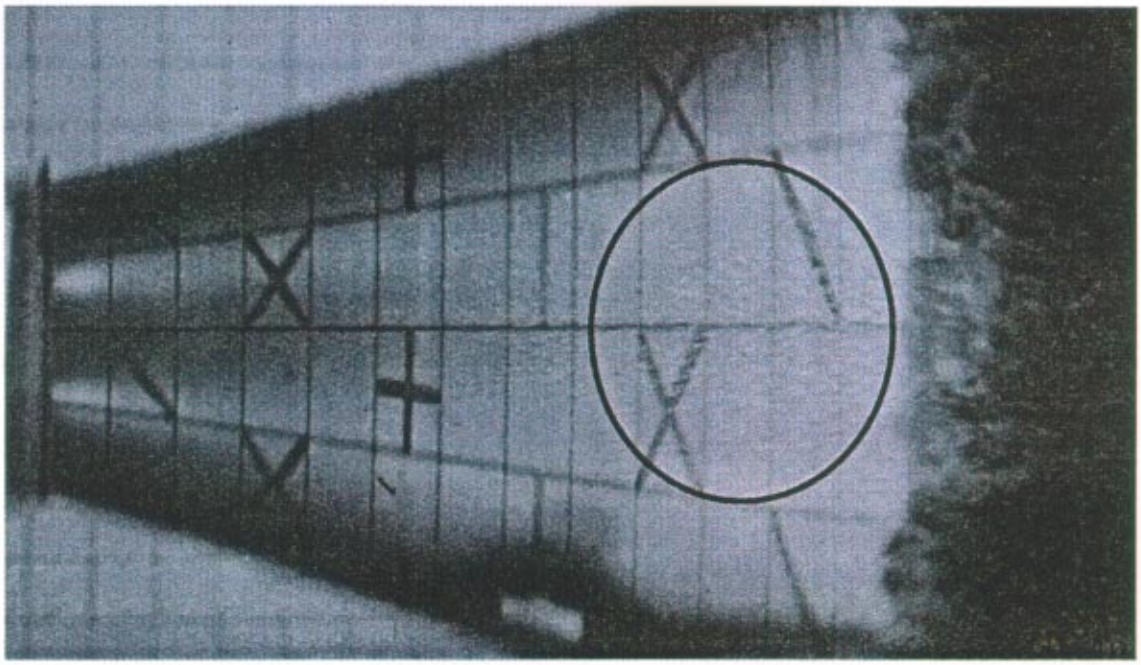

Figure 4.8: View of Instabilities on Expanding Thin Cylinder

The efforts to 'soft-catch' fragments did not work as planned. This is partially due to the destructive power of the HE. The entire experiment and shot set-up as shown in Figure 4.6 was destroyed. The only fragments that could be found were located in the asphalt sheeting and most of the sheeting was torn to shreds. The destruction and size of

the remaining pieces of hardware are illustrated in Figure 4.9. This Figure, which shows the same firing point shown in Figure 4.6, was taken after the detonation of the thick cylinder. The fragments found at the firing point were extremely small and are shown in Figure 4.10. No useful information was obtained from the fragments.

Figure 4.9: Firing Point Following Explosive Detonation of the Thick Cylinder

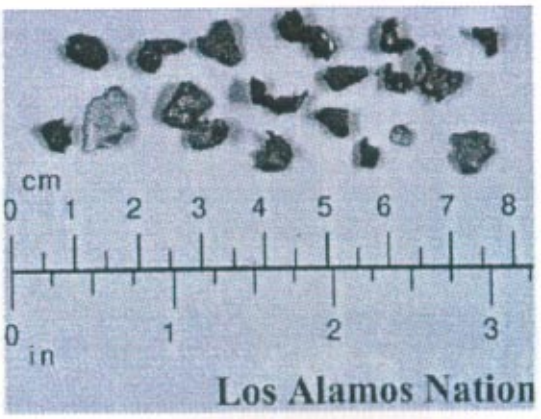

Thin Cylinder Fragments

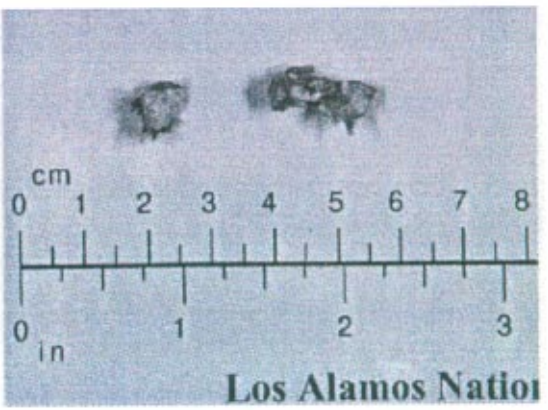

Thick Cylinder Fragments

Figure 4.10: Fragments Obtained from Explosive Detonation of Copper Cylinders

5.0 Model Verification

An axisymmetric finite element model was constructed to model the detonation and expansion of the HE and the resultant deformation of the copper cylinder. The specifics of the solid model and parameters used in the analysis are discussed in this chapter. Several figures are shown to provide a comparison of the numerical results with the experimental data. These figures indicate good agreement and add credence to the parameters supplied to the constitutive model as well as the overall development of the constitutive model.

5.1 Axisymmetric Numerical Model and Parameters

The geometry of the numerical model included the solid cylinder of HE and the copper cylinder. However, it did not include the plane wave lens or SE-1 detonator. The mesh of the HE and copper cylinder are shown below in Figure 5.1. Five elements were maintained through the thickness of the copper cylinder for both of the 2.54 and 5.08 mm thick shells. This provided a consistent qualitative comparison of the numerical results between the two cylinders and still captured the global deformation of the cylinder. The aspect ratios of the elements in the copper cylinder and HE was nearly 1:1.

The HE and the copper were separated by a 0.127 mm gap. A sliding contact surface was prescribed at this gap to model the interactions between the HE and the cylinder. The size ratio of the HE elements to the copper cylinder elements was

maintained at 2:1. Therefore, one HE element loaded two cylinder elements. The HE and copper cylinder were uniformly meshed with the same element density throughout the mesh. Four node, linear, axisymmetric elements were used throughout the analysis for both the HE and copper cylinder. The number of elements used in the HE and copper for each cylinder is shown in Table 5.1

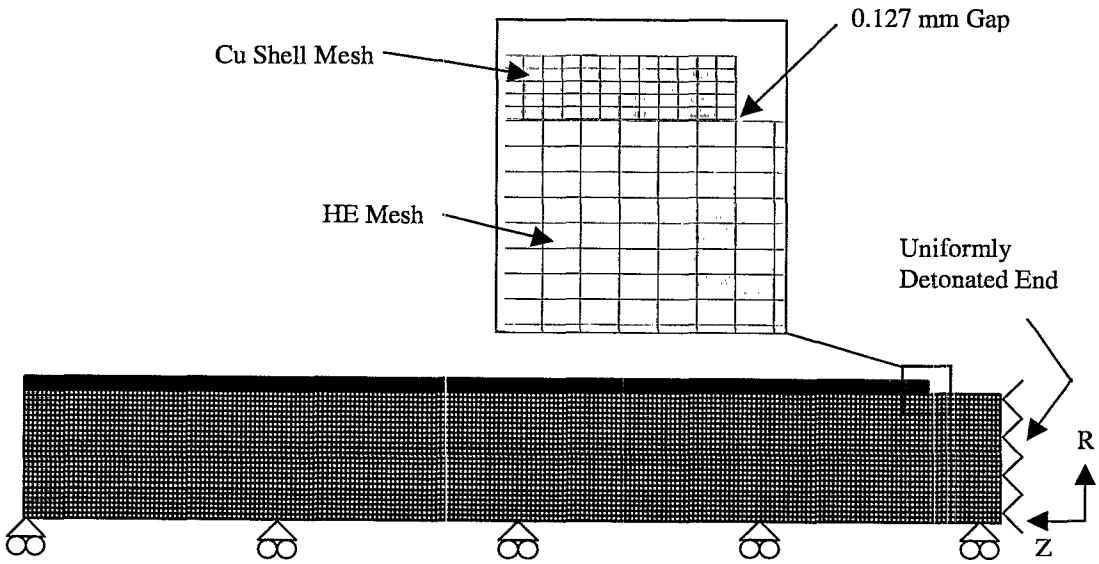

Figure 5.1: Axisymmetric Mesh of HE and Copper Cylinder

Table 5.1: Number of Elements Used in Axisymmetric Model of HE and Copper Cylinder

	Number of Elements in HE	Number of Elements in Copper
Thin Shell (2.54 mm Thick)	21,550	4,000
Thick Shell (5.08 mm Thick)	5,400	2,000

A symmetry boundary condition was applied to the bottom of the HE. This fixed the edge of the HE in the radial direction while allowing it to expand (on rollers) in the longitudinal direction. The mesh of the HE extended 50.8 mm beyond the end of the copper cylinder. This distance corresponds to the actual length of the solid HE cylinders

used in the experiments. The HE in the model was then detonated all along the right surface which numerically models the detonation front produced by the plane wave lens. The user parameters supplied to the axisymmetric model are given in Table 5.2. This table is very similar to Table 3.2 shown in Chapter 3, but is shown again for clarity.

The HE in the numerical model is detonated at time t = 0 seconds. The pressure in the model at the detonation front can be as high as 10 GPa for a very short duration. Initially, the elements at the tip of the copper cylinder can not respond to this extreme pressure loading. In fact, the actual cylinder in the experiments appears to crack in a non-ductile manner at the detonated end. The element remove subroutine, as described in Chapter 3, was implemented to handle these extreme pressures. If the equivalent plastic strain of an element exceeds 250 %, the element is removed from the numerical computation. Without the element remove subroutine, the elements distort and invert, effectively stopping the computation. The element remove subroutine only affects a few elements in the first couple of rows through the thickness. The effect of removing these elements on the overall accuracy of the solution away from the ends of the cylinders is thought to be minimal.

The plots shown in Figure 5.2 illustrate the deformation of the copper cylinder at specific periods in time. In this figure, the HE is detonated on the right hand side and the detonation wave propagates from the right to the left of the figure. The thick solid line in the plots represents the axisymmetric cylindrical shell. The dashed line in the plots represents the axis of symmetry. The expansion of the HE, which extends from the cylinder edge to the line of symmetry, is not shown for clarity.

Table 5.2: User Parameters Supplied to the Axisymmetric Model

Model	Description	Units	Value
Johnson-Cook Parameters	Material Density	kg/m^3	8945.0
	Specific Heat	J/kg-K	383.5
	Initial Temperature	K	294.26
	Room Temperature	K	294.26
	Melt Temperature	K	1355.93
	Shear Modulus	Pa	4.63×10^{10}
	Yield Stress	Pa	8.963×10^{7}
	Hardening Coef.	Pa	2.916×10^{8}
	Hardening Exp.	-	0.31
	Strain-Rate Coef.	-	0.025
	Thermal Softening Exp.	-	1.09
	Strength Cut-off	Pa	6.895×10^{10}
EOS Parameters	Bulk Modulus	Pa	1.372×10^{11}
	Sound Speed - C_0	m/s	3940.0
	Slope of U_s-U_p Curve - S	-	1.49
	Grüneisen Coef. - γ	-	1.96
	Tensile Pressure Cut-off	Pa	6.895×10^{10}
GTN Model Parameters	q_1	-	1.5
	q_2	-	1.0
	q_3	-	2.25
	f_F	-	0.85
	f_c	-	0.85
	Init. Void Vol. Fract. - f^{init}	-	0.001
	E_n	-	0.3
	S_n	-	0.1
	F_n	-	0.04
	Void Pressure Cut-off	Pa	-1.0×10^{6}
	Max. Plastic Strain	-	1.5
HE Burn Parameters	A	Pa	8.545×10^{11}
	B	Pa	2.049×10^{10}
	ω		0.25
	R_1		4.6
	R_2		1.35
	Detonation Velocity, C_d	m/s	8830.0
	Energy/Mass, E_{mo}	J/kg	5.543×10^{6}
	Pressure Cutoff, P_{cj}	Pa	0.0

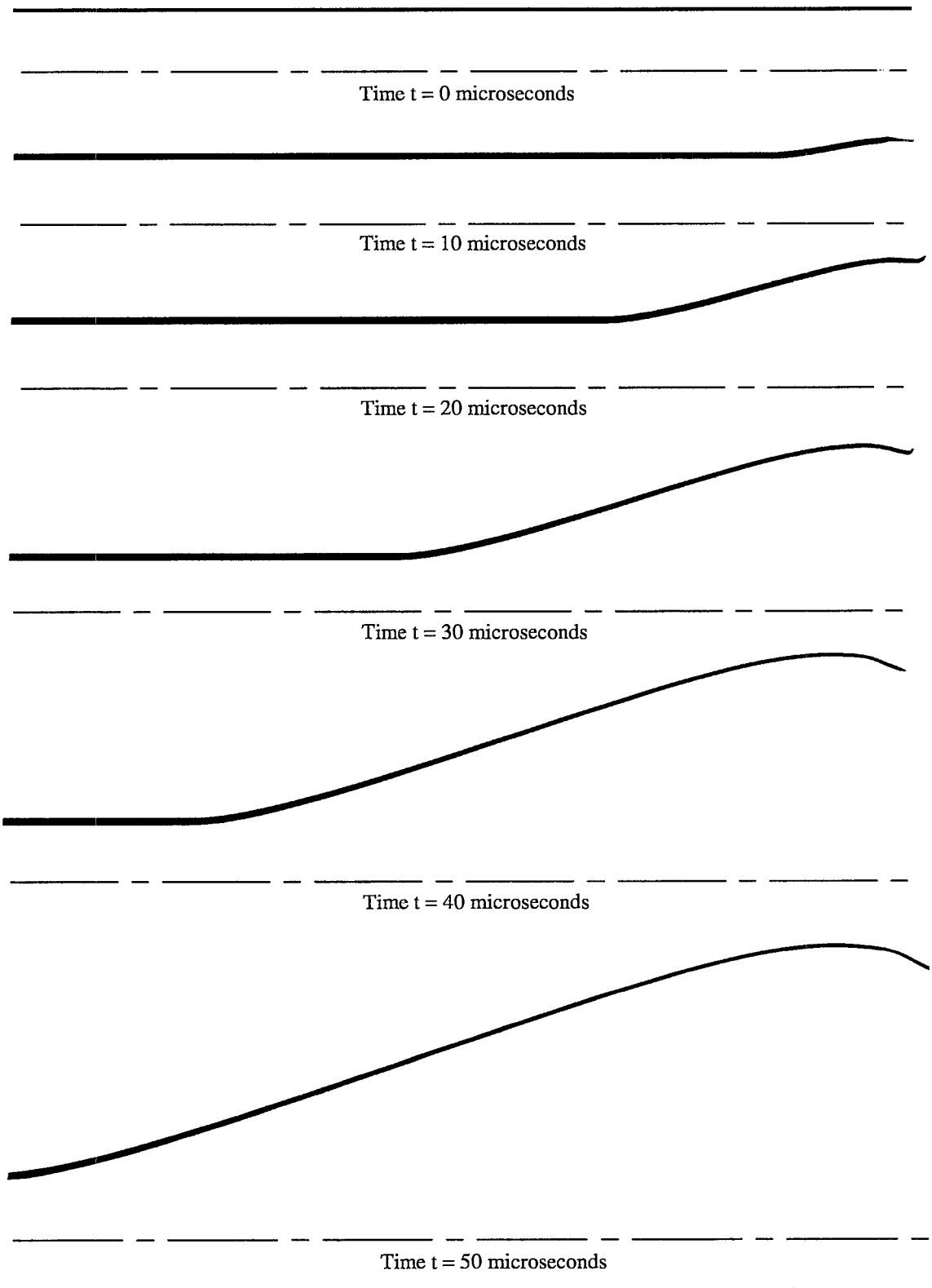

Figure 5.2: Deformed Axisymmetric Edge of the Copper Cylinder Computed from the Numerical Model (Dashed Line Indicates Axis of Symmetry)

5.2 Comparison of Numerical Results with Experimental Data

During the experiment, data from the fast framing camera and Fabry-Perot were obtained. The data from the fast framing camera are in the form of photographs from which information regarding the instabilities and cylinder deformation can be obtained. The displacement data were extracted at eight points along the longitudinal axis of the cylinder. Each point is separated by 50.8 mm, with the first point located 50.8 mm up from the detonated end. The displacement as a function of time is plotted for the following locations measured from the detonated end of the cylinder: 50.8, 101.6, 152.4, 203.2, 254.0, 304.8, 355.6, and 406.4 mm. These data points are compared with the numerical results for each corresponding cylinder.

The Fabry-Perot data were obtained at only one point on the surface of the cylinder. Recall during the experiment which involved the 5.08 mm thick cylinder, a hardware failure occurred with the Fabry-Perot instrumentation. As a result, the only useful Fabry-Perot data obtained were from the 2.54 mm thick cylinder. The velocity data from the Fabry-Perot instrumentation were taken exactly half-way up the cylinder at 203.2 mm and are compared in this section with the results from the numerical model.

A sequence of deformed geometry plots for the two cylinders are shown in Figures 5.3 and 5.4. Each figure shows two graphs, each of which contains a plot of the experimental data and the numerical results. The data and results for the 2.54 mm thick cylinder are shown in Figure 5.3. The two graphs shown in this figure are taken at 20.3 and 49.65 microseconds. The data and numerical results for the 5.08 mm thick cylinder are shown in Figure 5.4. The two graphs shown in this Figure are taken at 18.9 and 49.65 microseconds.

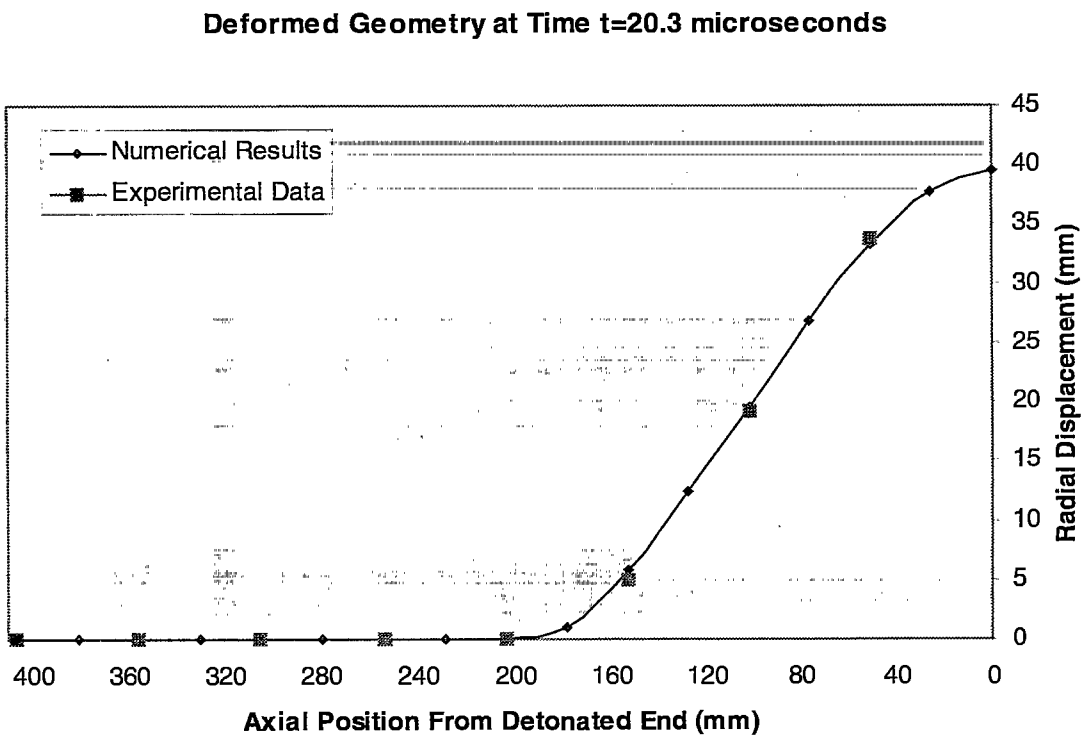

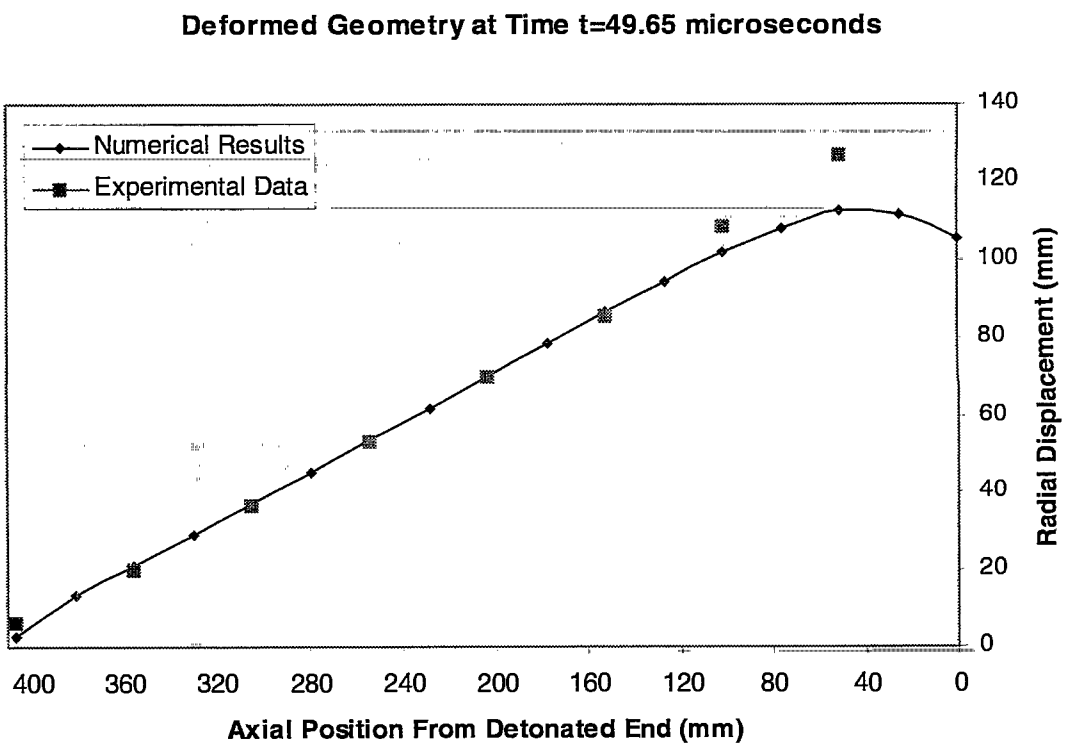

Figure 5.3: Deformed Geometry for the 2.54 mm Thick Copper Cylinder

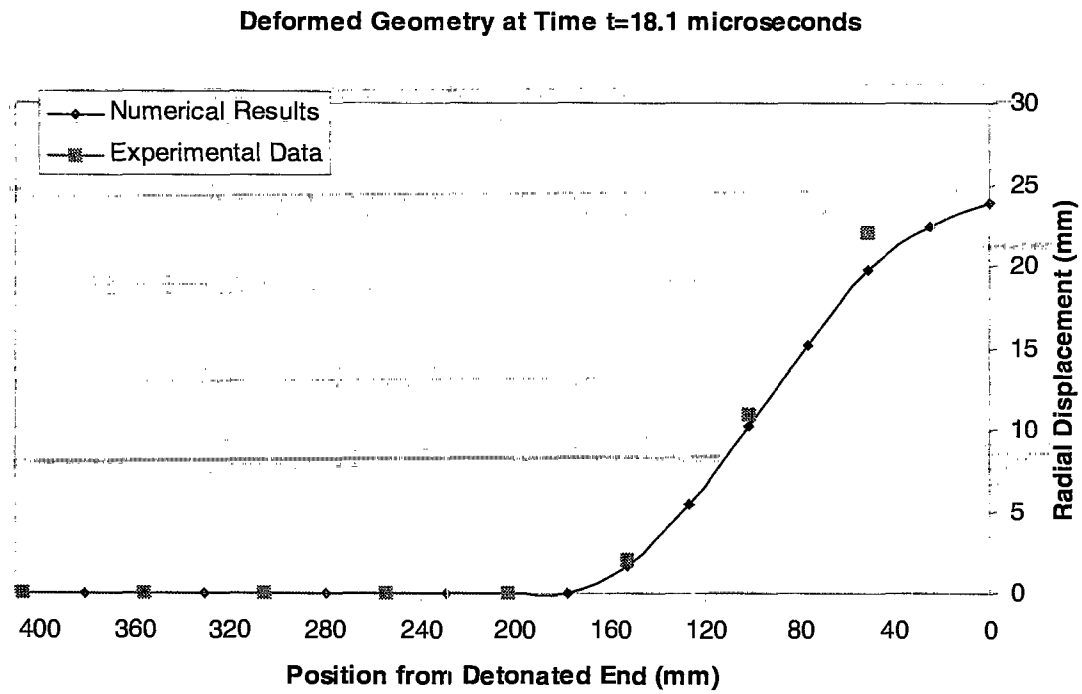

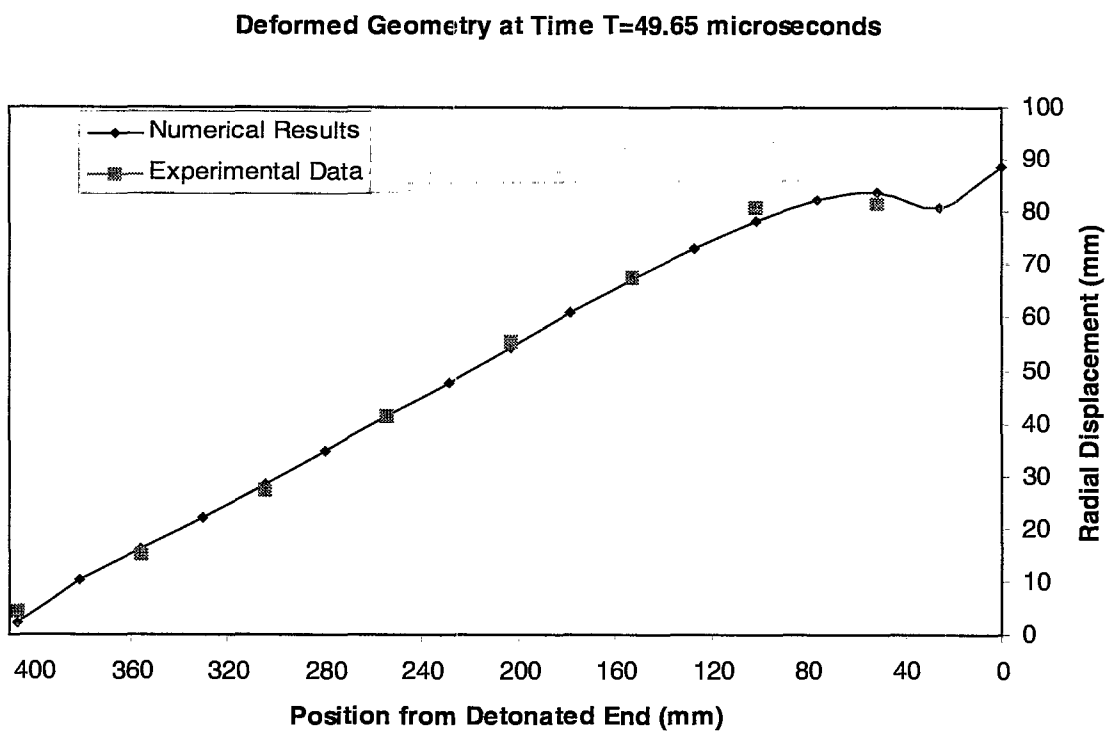

Figure 5.4: Deformed Geometry for the 5.08 mm Thick Copper Cylinder

In general, the comparisons of the deformed cylindrical shells shown in Figures 5.3 and 5.4 indicate good agreement between the experimental data and the numerical results. Some deviation is illustrated at the top and bottom end of the cylinders. This deviation is likely caused from the inability of the finite element model to respond to sudden changes in the loading. This is particularly obvious at the ends of the cylinder. The explosive gases that vent around the cylinder ends during the experiment are also not modeled correctly by the numerical model. The HE elements can not distort and behave like escaping gas. A finer mesh density and rezoning would likely improve the results in these areas. Artificial damping in the numerical model, which smears out the shock front, could also affect the displacements at the ends of the cylinder where the load is applied suddenly.

The radial displacement of each cylinder is plotted with respect to time in Figures 5.5 and 5.6. The displacement curves shown in each of these figures are taken at eight different longitudinal locations on the cylinder wall. The longitudinal location is shown in the text on the right side of the figures. The plots shown in Figure 5.5 are for the 2.54 mm thick cylinder and the plots shown in Figure 5.6 are for the 5.08 mm thick cylinder. In each figure, the plots near the center of the cylinder illustrate good agreement between the numerical results and the experimental data. However in both figures, the plots near the ends of the cylinder show a small discrepancy. This is the same discrepancy observed in Figures 5.3 and 5.4 and again, the meshing, viscosity, and rezoning of the cylinder mesh could reduce this discrepancy.

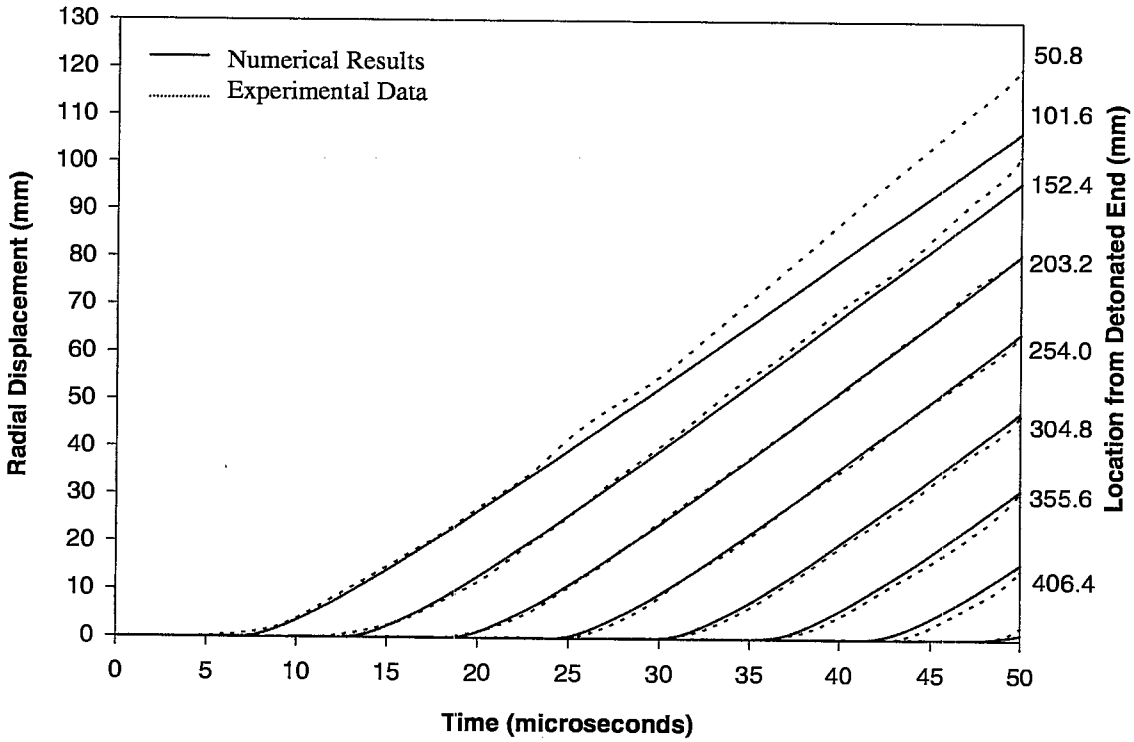

Figure 5.5: Radial Displacement as a Function of Time at Eight Locations Along the Longitudinal Axis of the 2.54 mm Thick Cylinder

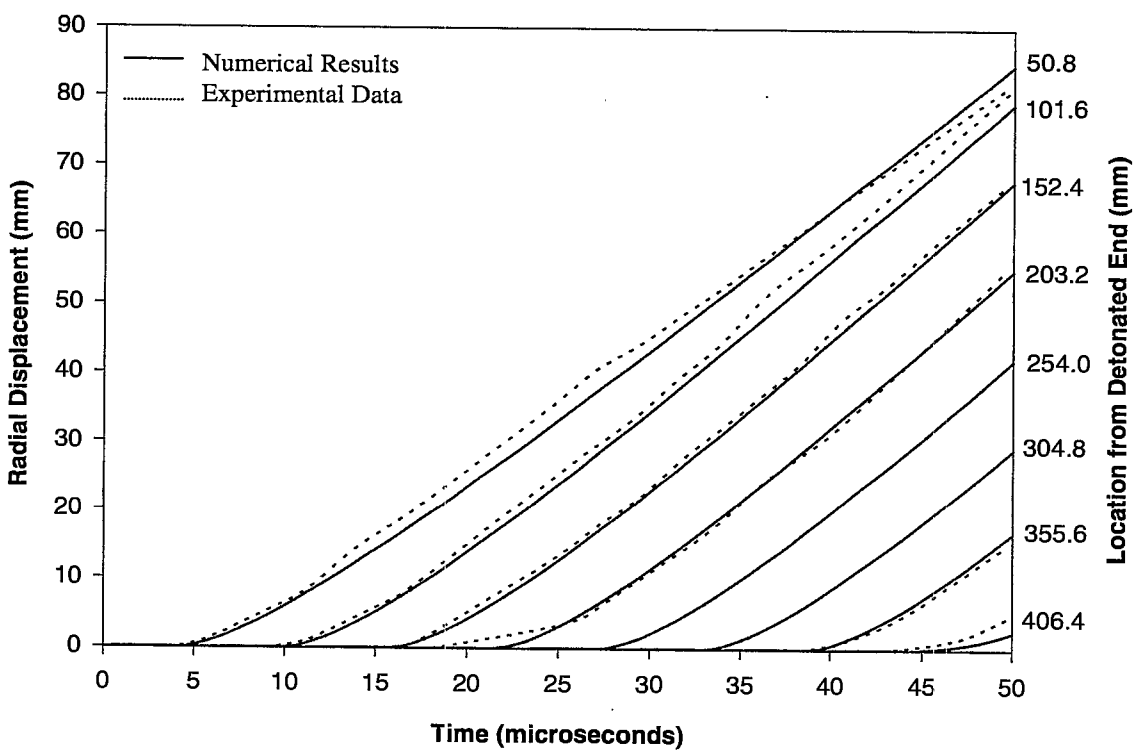

Figure 5.6: Radial Displacement as a Function of Time at Eight Locations Along the Longitudinal Axis of the 5.08 mm Thick Cylinder

In Chapter 1, a brief discussion was provided regarding an equation developed by Gurney (1943) for predicting the maximum velocity, V_{max}, of shells subjected to internal explosive detonations. Gurney's equation for a cylindrical shell is written as,

$$V_{max} = \sqrt{2E}\left(\frac{M}{C} + \frac{1}{2}\right)^{-1/2}, \tag{6.1}$$

where *M/C* is the ratio of the mass of the shell to the mass of the explosive and $\sqrt{2E}$ is called the Gurney constant. The empirical constant, $\sqrt{2E}$, was determined from experiments involving a particular type of explosive. For PBX-9501, $\sqrt{2E}$ is equal to 2900 m/s. The results shown in Table 5.3 indicate the calculated values of the Gurney velocity for the experiments conducted in this dissertation.

Table 5.3: Gurney Velocity for Cylindrical Shell Experiments

	Mass of HE (kg/m)	Mass of Shell (kg/m)	*M/C*	V_{max} (m/s)
2.54 mm Thick Shell	14.98	7.46	0.498	2902
5.08 mm Thick Shell	14.98	15.29	1.02	2351

Figures 5.7 and 5.8 show the velocity of the cylinder wall for the 2.54 and 5.08 mm thick cylinders. The plots shown in Figure 5.7 include the velocities from the empirical Gurney equation, the Fabry-Perot instrumentation, and the numerical model. The plots shown in Figure 5.8 only include the velocities from the empirical Gurney equation and the numerical model. Recall the Fabry-Perot equipment experienced a hardware failure and as a result, was not able to record data for the 5.08 mm thick cylinder. However, good agreement with the available data is shown in both figures.

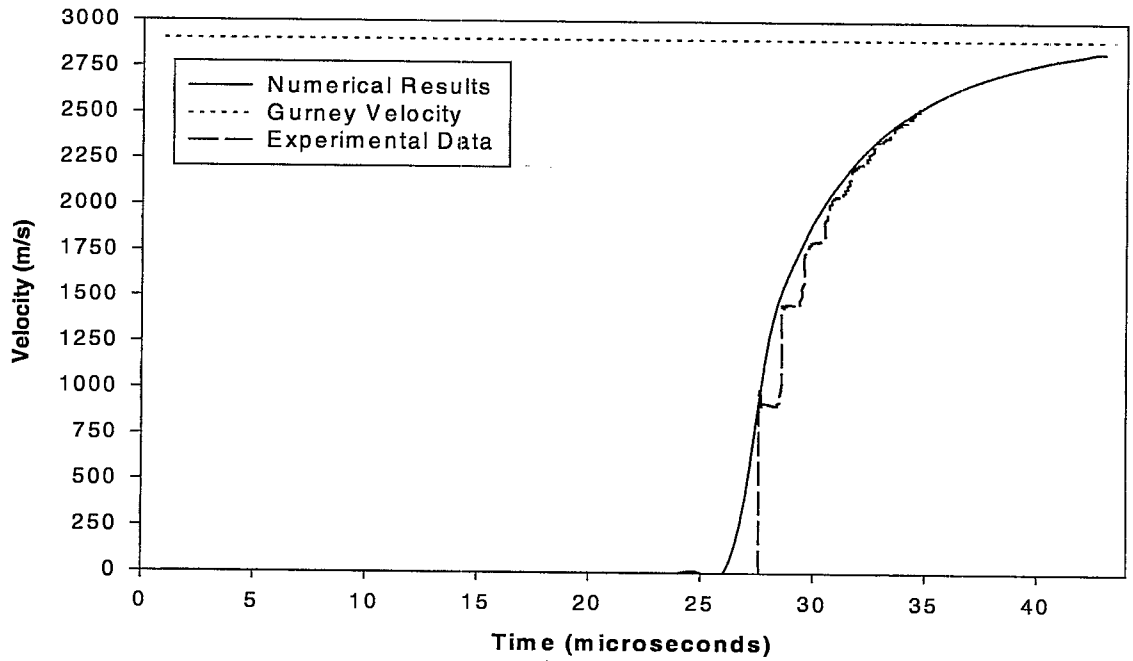

Figure 5.7: Radial Velocity as a Function of Time for the 2.54 mm Thick Cylinder

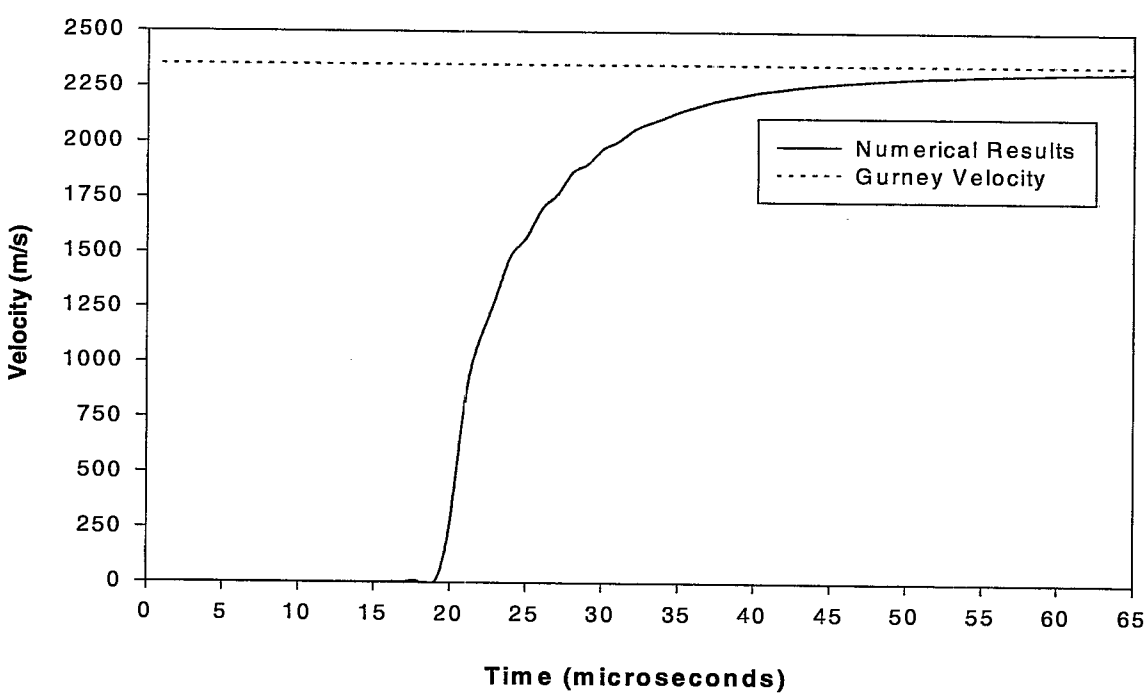

Figure 5.8: Radial Velocity as a Function of Time for the 5.08 mm Thick Cylinder

The number of instabilities and the time at which they are observed can typically be extracted from the fast framing camera pictures. In both cylinder experiments, instabilities were observed on the surface of the expanding shell. However, the resolution of the photographs was not as sharp as expected. Each photograph was digitized and enlarged to determine the number of instabilities for a small characteristic length on the surface of the cylinder. This length and the quantity of instabilities were then used to determine the total number of instabilities on the entire circumference of the shell. Unfortunately, the resolution of the photographs was not sufficient to provide information regarding the initiation time of the instabilities, average instability size, or rate of instability growth. The number of instabilities around the circumference of each cylinder is given below in Table 5.4

Table 5.4: Number of Instabilities for Each Cylinder as Determined from the Fast Framing Camera Photographs

	Number of Instabilities
2.54 mm Thick Shell	298
5.08 mm Thick Shell	343

The experiments documented in Chapter 4 of this dissertation were designed to verify the numerical model and good agreement is shown in Figures 5.3 to5.8. The deformed geometry plots in Figures 5.3 and 5.4 are reasonably close. At locations away from the cylinder ends, the correlation of the deformed shape is very good. The radial displacement plots in Figures 5.5 and 5.6 are also quite close and again a slight variation is observed at the ends of the cylinders. In Figures 5.7, excellent correlation exists between the radial velocity obtained from the experimental data and the predictions from

the numerical model. In addition, the predicted numerical velocity asymptotically approaches the Gurney velocity in both Figures 5.7 and 5.8.

The comparisons shown here illustrate that the user supplied constitutive parameters and the mesh densities used in the numerical models are reasonable. Good agreement is shown for large displacements thus indicating that the distortion of the elements in the numerical model is not affecting the solution. In addition, the fundamental work by Gurney provides a supplemental form of verification of the maximum velocity.

The instabilities observed on the surface of the expanding cylinder appear to occur and propagate down the longitudinal axis of the cylinder. The axisymmetric geometry analyzed in this chapter is not capable of predicting circumferential pattern of quasi-periodic instabilities with occurs in the longitudinal orientation. However, the credibility of the constitutive model is established based on agreement between the experimental data and numerical results for the overall deformation of the copper cylinders. With this established, the next chapter examines a plane strain geometry to determine the number of instabilities and provide insight into their development.

6.0 Dynamic Instabilities

This chapter discusses the development of the quasi-periodic instabilities, which are observed on the surface of rapidly expanding shells. For cylindrical shells, quasi-periodic instabilities appear as material separation or extreme thinning on planes of constant angle in the theta (θ) direction and propagate in the longitudinal direction, see Figure 6.1. The axisymmetric analysis presented in Chapter 5 is not capable of predicting instabilities of this type. However, the comparisons with experimental data presented in that chapter, add credence to the constitutive model. In this chapter, a plane strain analysis is performed to numerically model the development of instabilities in expanding cylindrical shells.

The quasi-periodic instabilities observed in the framing camera photographs shown in Chapter 4 appear to be perturbations on the surface. As expected, these perturbations could be initiated from inhomogeneities in the copper or the high explosive, or due to nonuniform loading. Preliminary results from this numerical analysis have verified these effects. In the analyses performed in this chapter, an extensive effort is made to minimize these incidental perturbations.

The contribution of the perturbations in the loading to the development of the instabilities is difficult to quantify. Inhomogeneities may exist in the high explosive and could cause perturbations in the loading of the shell. The work presented here assumes these inhomogeneities are not related to the instabilities. The analysis presented in this

chapter does not include the explosive burn model. Instead, the pressures resulting from the explosive detonation are applied uniformly to the inside surface of the cylinder.

Without the void model, the numerical model predicts smooth uniform expansion of the shell and instabilities do not develop. As a result, some type of damage, or void model, is necessary in the prediction of instabilities in rapidly expanding shells. The void model used in this work is based on the microvoid model by Gurson, Tvergaard, and Needleman. This model allows the user to prescribe an initial volumetric distribution of voids. Typically this distribution is thought to be uniform throughout the material. When a uniform distribution of voids is used in the numerical model, the development of instabilities occurs but it occurs much later in time and at a much larger strain. Results such as these do not correspond well with the experimental data shown in this research or in the current literature.

Recall, from Chapter 4, that the microstructure of the copper material shows a random grain structure, which varies significantly throughout the material. The current literature suggests that voids nucleate predominately at grain boundaries or secondary particles which in essence indicates random nucleation sites. As a result, a method of randomizing the initial void distribution was developed. This method is explained in Chapter 3. Using an initial random void distribution, the on set of instabilities occurs much earlier in time and the results correspond much better with experimental data.

6.1 Plane Strain Numerical Model

A plane strain finite element model was constructed to examine the development of instabilities. The user parameters supplied to the constitutive model are shown in

Table 3.2. This model has twenty elements through the thickness of the shell, and each element has a 1:1 aspect ratio for a total of 12,000 elements. These elements are two-dimensional single integration point plane strain elements. The mesh for the model is shown in Figure 6.1. The inner radius of the mesh is 5.08 cm, and the outer radius of the mesh for this analysis is 5.334 cm. Symmetry boundary conditions are applied to the edges of the mesh at 0 and 90 degrees.

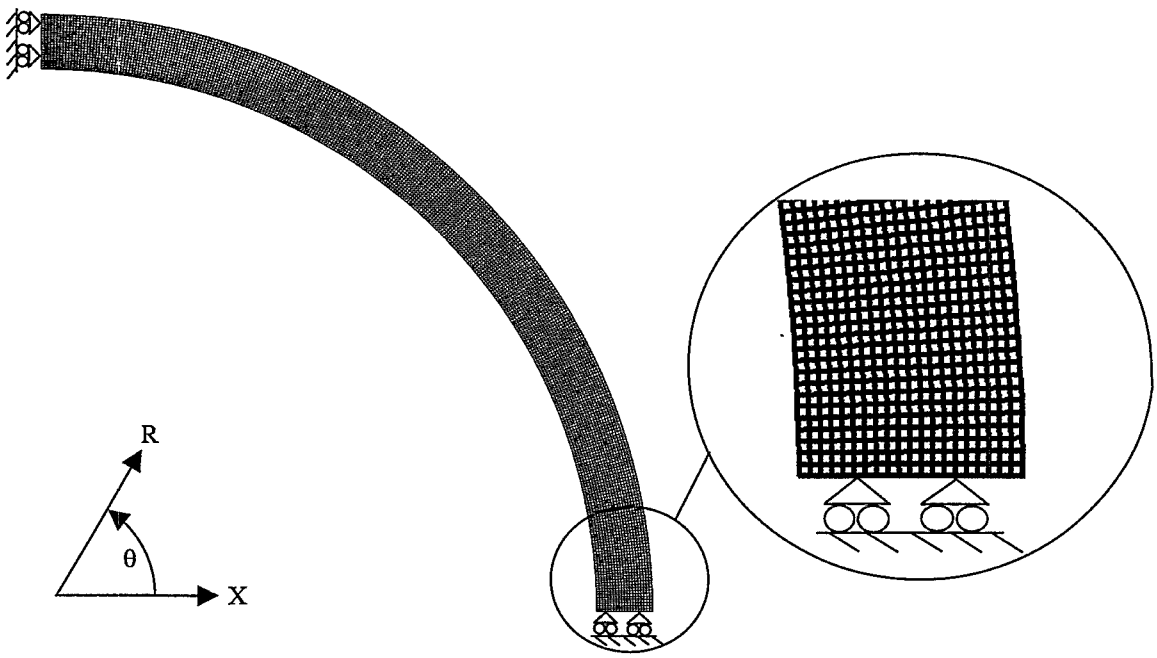

Figure 6.1: Plane Strain Mesh for Instability Investigation

As mentioned earlier in this chapter the HE was not directly included in this analysis. This minimizes the potential for numerical errors in the HE burn model and perturbations in the load transferred between the high explosive and the shell. Instead, an average pressure history at the HE-shell boundary was determined from a numerical model, which included the high explosive. This pressure history was then applied to the

inner surface of the mesh shown in Figure 6.1. Figure 6.2 shows the characteristic pressure history for the mesh shown in Figure 6.1. Notice the maximum pressure occurs early in time and then drops off rapidly. The accumulated impulse, up to 50 microseconds is approximately 67,000 Pa-sec.

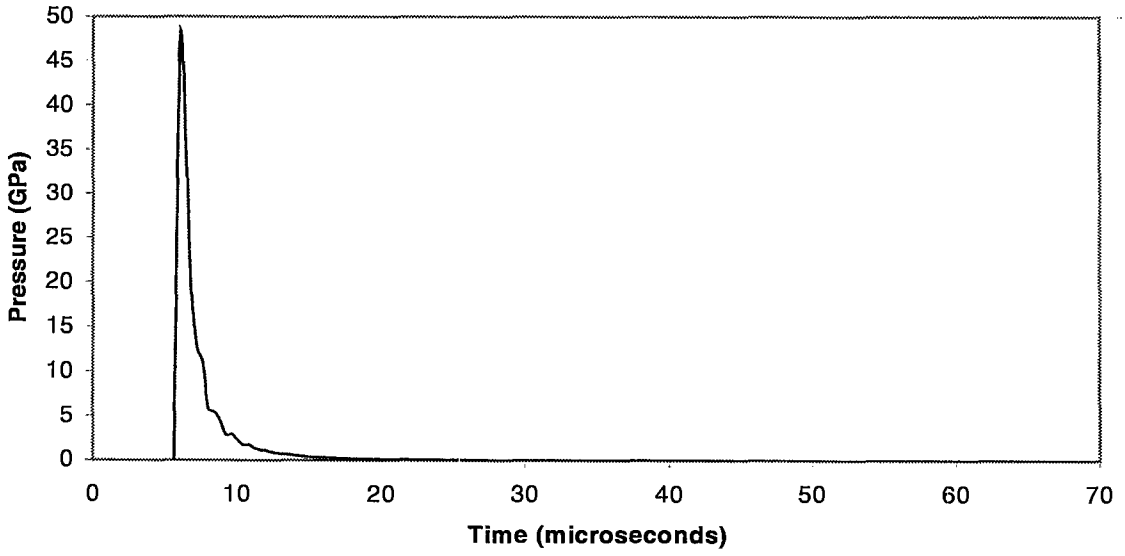

Figure 6.2: Pressure Time History for the 2.54 mm Thick Cylinder

6.2 Instability Development

From previous literature and the experiments described in Chapters 4 and 5, the instabilities developed on the surface of the shell are visible only after the shell has expanded to at least one and a half times its initial diameter. Fragments from those experiments were collected but it was difficult to determine what initiated the instabilities and how they developed.

A much less sophisticated experiment was conducted in an attempt to obtain a highly strained copper sample illustrating the development of instabilities prior to fragmentation. This experiment consisted of a 30.48 cm long OFE grade copper tube

with a 2.54 cm inner diameter and 6.35 mm thickness. The copper tube was placed on end in about 2.54 cm of sand. A slug of Composition C-4, which measured to be 7.62 cm long and 1.27 cm in diameter, was placed inside the top lip of the copper tube. The C-4 was end detonated and the explosive shock wave traveled down the inside of the tube. The shock wave reflected off the surface of the sand, resulting in an overpressure. The overpressure caused the tube to bulge and fracture but not fragment. A picture of the bulged tube is shown below in Figure 6.3. The arrows shown in this figure indicate the locations of the instabilities.

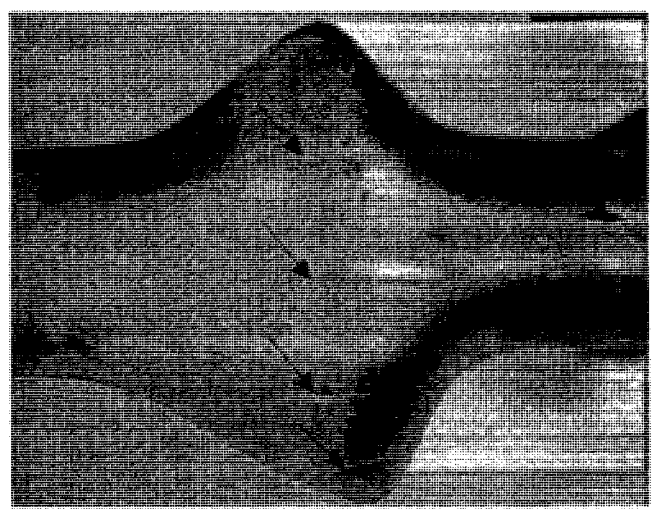

Figure 6.3: Bulged Tube from C-4 Experiment

The bulged tube shown in Figure 6.3 was cross-sectioned through the instabilities to determine how the instability formed. Examination of the section indicates the development of instabilities on both the inner and outer surfaces. However, unlike a uniaxial tensile specimen, these instabilities are offset in the theta direction and the formation of a shear band is obviously connecting the instabilities. An exaggerated illustration of the offset instabilities is shown in Figure 6.4 and a photomicrograph of the

resulting microstructure from the bulged tube section is shown in Figure 6.5. Excessive plastic deformation is visible from the elongated grains, illustrating a very ductile material response. In addition, the inner surface of the tube appears to be rougher than the outer surface indicating additional damage. This damage is possibly from localized heating and shock interactions with the high explosive.

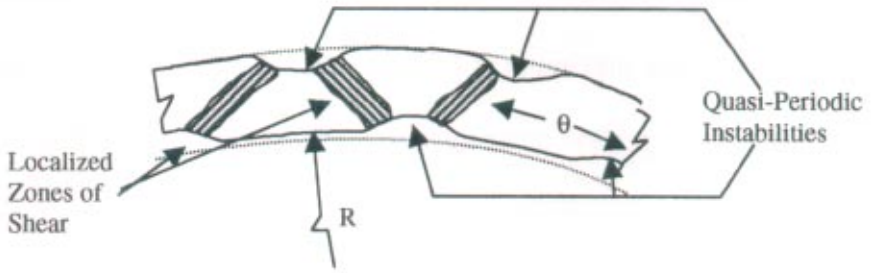

Figure 6.4: Exaggerated Illustration of Quasi-Periodic Instabilities

Outside Diameter

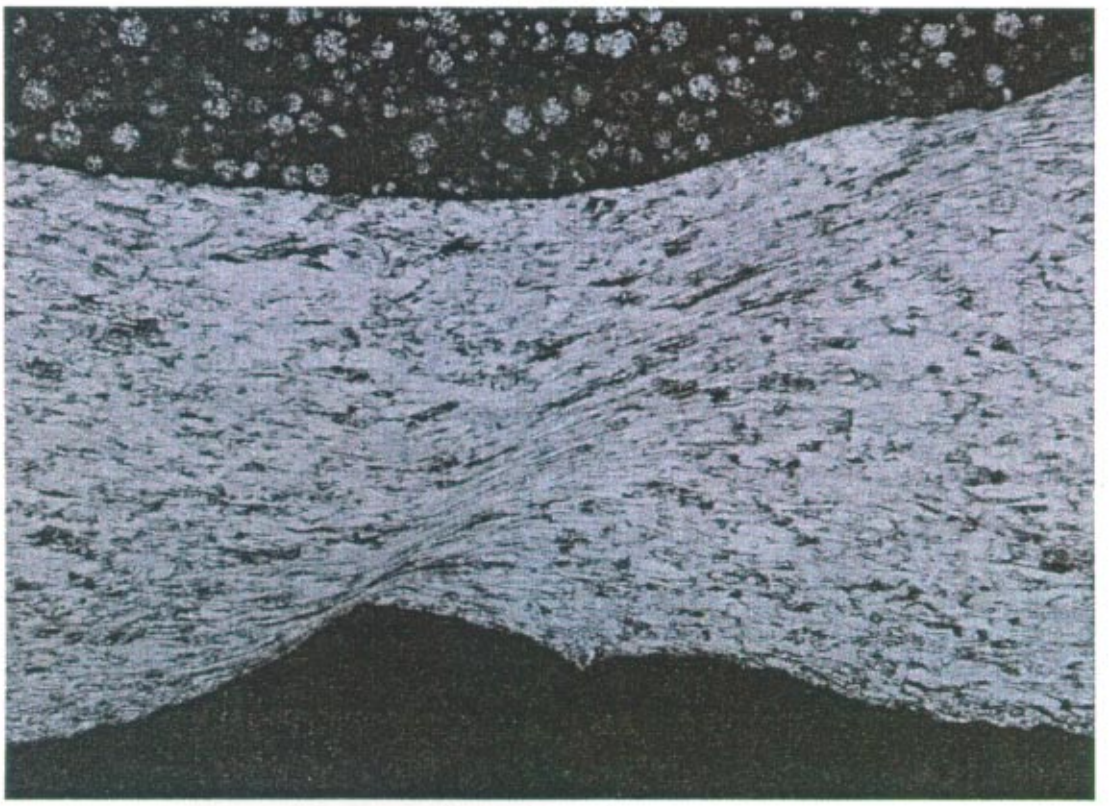

200 μm

Inside Diamter

Figure 6.5: Shear Band from Bulged Tube Experiment

The formation of localized shear is also visible in the numerical model. Figure 6.6 shows several plots illustrating the development of an instability in the copper shell. Initially at 6.7 microseconds, the equivalent plastic strain is fairly uniform in the theta direction and has a smooth gradient in the radial direction. However, an oscillatory pattern is observed in the theta direction as early as 7.6 microseconds. This pattern becomes more pronounced and by 25 microseconds, the minimum equivalent plastic strain is 0.6 and the maximum is 1.09. At this point quasi-periodic instabilities are observed on the inner and outer surfaces. These instabilities are also offset in the theta direction much like instabilities observed on the bulged tube sample and illustrated in Figure 6.4.

Initially, the hoop stress through the entire thickness of the shell is in compression. At 6.4 microseconds, the hoop stress at the outer surface of the shell becomes tensile, while the hoop stress at the inner surface of the shell does not become tensile until 14.8 microseconds. The instabilities do not appear on the surfaces of the shell until 25 microseconds, which is much later in time. However, the oscillatory pattern, which is first observed at 7.6 microseconds, does not appear to significantly grow until after 15 microseconds at which time the hoop stress is tensile throughout the thickness of the shell.

At 34 microseconds, the pattern of equivalent plastic strain is much larger. The minimum value is 0.705 and the maximum 1.65, indicating a large variation through thickness of the shell. The contours of equivalent plastic strain now illustrate the distinct formation of localized shear zones. The combination of quasi-periodic thinning and the formation of the shear zones are referred to here as quasi-periodic instabilities.

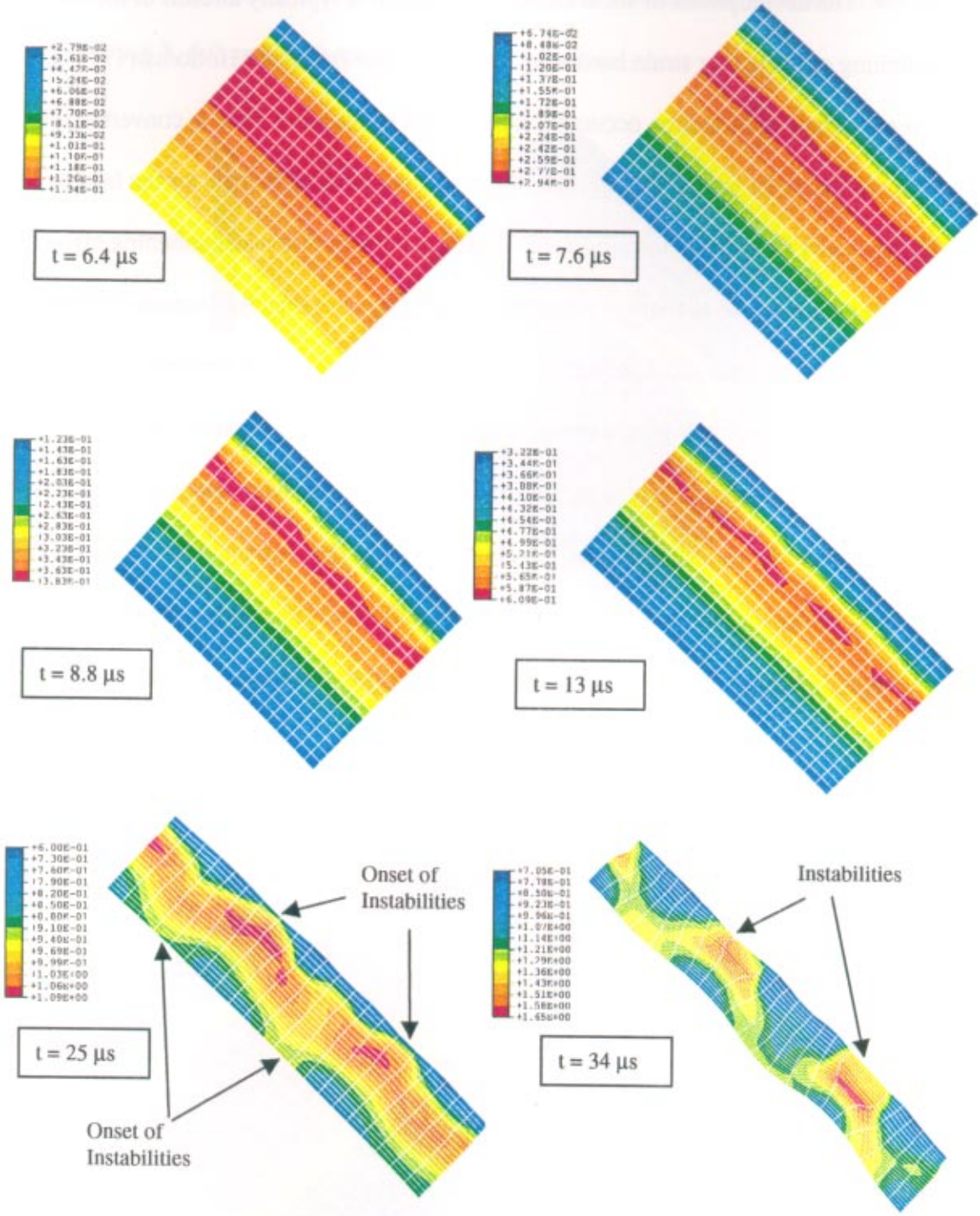

Figure 6.6: Equivalent Plastic Strain and Surface Features from the Numerical Model

The development of shear bands in a material is typically a result of thermal softening outweighing strain hardening. According to Zener and Holloman (1944), when intense plastic deformation occurs, a large portion of the work done is converted into heat. If the strain rate is high enough, there may not be enough time for the heat to diffuse away from the deforming zone. This causes a local thermal softening effect. If the strength loss due to thermal softening becomes greater than the increase in strength due to strain or strain rate hardening, the plastic deformation will become unstable. This plastic deformation will give way to a localized band-like deformation or a shear band.

As mentioned earlier, a periodic pattern in the equivalent plastic strain is observed in the numerical results as early as 7.6 microseconds. This corresponds to a strain *R/Ro* of 1.05. However, the localized shear zones are not obvious until much later in time. Figure 6.7 shows a larger image of the equivalent plastic strain at 7.6 microseconds.

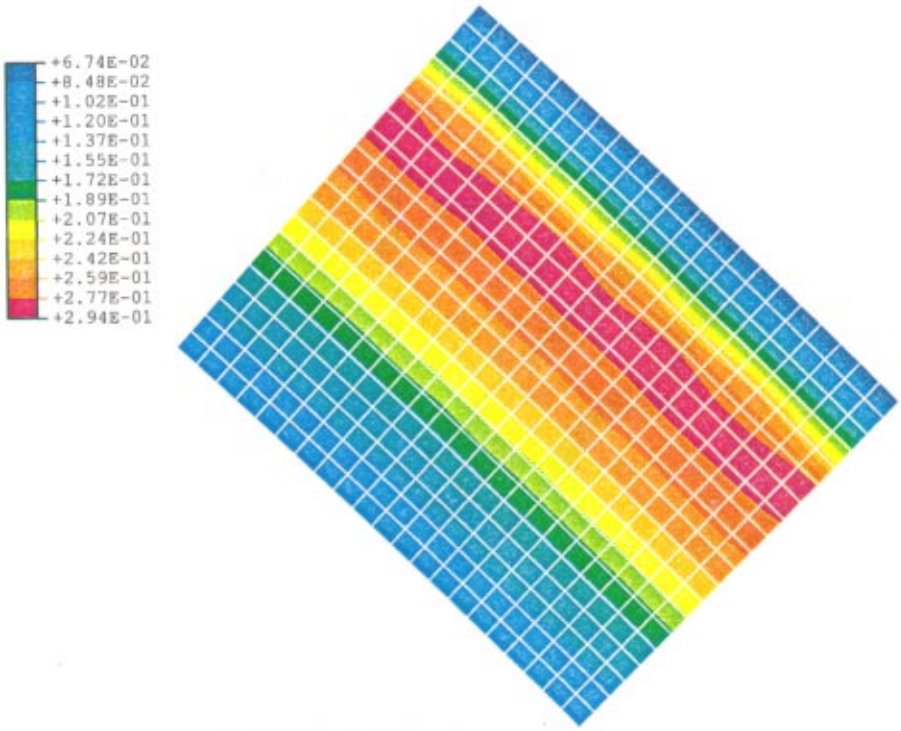

Figure 6.7: Equivalent Plastic Strain at 7.6 microseconds

The equivalent plastic strain rate, temperature, and volumetric void fraction are shown in Figures 6.8, 6.9, and 6.10 respectively.

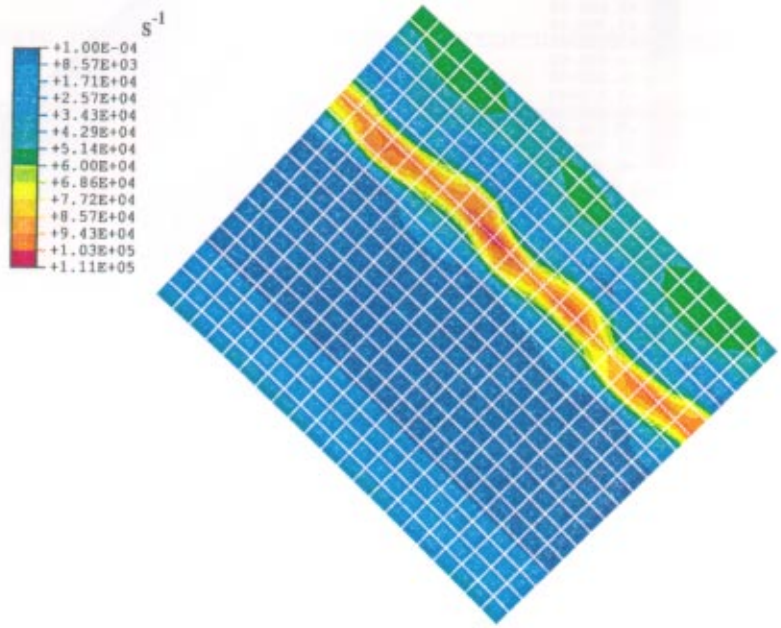

Figure 6.8: Equivalent Plastic Strain Rate at 7.6 microseconds

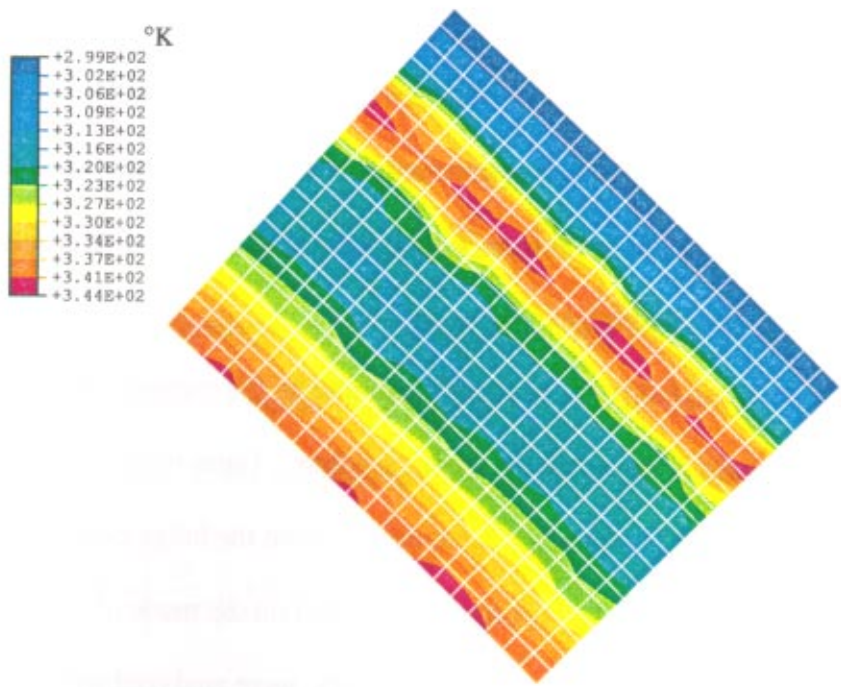

Figure 6.9: Temperature at 7.6 microseconds

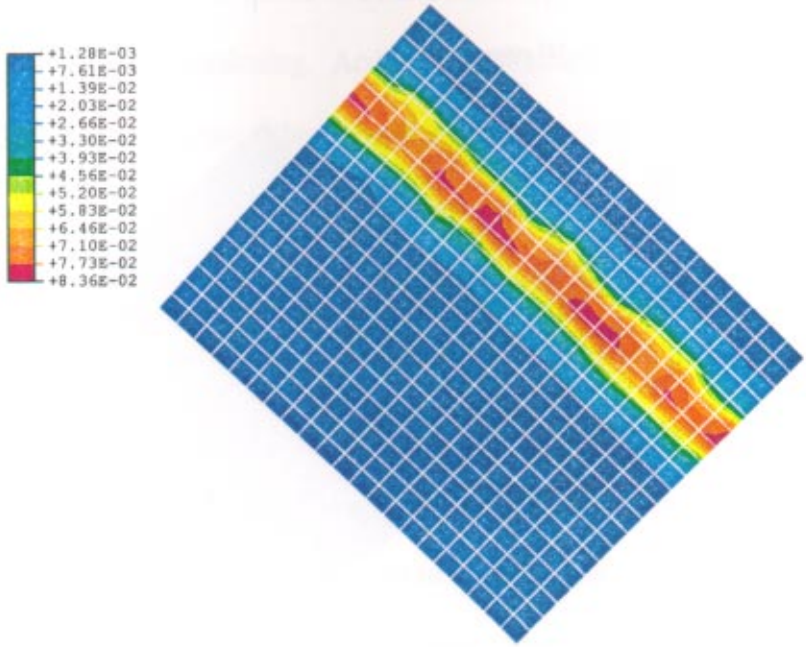

Figure 6.10: Volumetric Void Fraction at 7.6 microseconds

All four figures show some type of periodic pattern at 7.6 microseconds. In addition, the temperature fringe plot, Figure 6.9, shows a periodic pattern on the inside of the material and at the boundary between the inner radius and the HE. Specimens collected following the bulge experiment also exhibited a rough surface at the HE boundary. Again, this roughness is likely caused from excessive heating and wave interactions with the high explosive.

The localized zones of shear illustrated by the contours of equivalent plastic strain shown in Figure 6.6 indicate the mode of failure. These results agree well with the shear band illustrated in Figure 6.5, which resulted from the bulge experiment. The thickness of the cylinder appears to have a minimal effect on the mode of failure. Several cylinders, ranging from 2.54 to 7.52 mm thick, were analyzed with the numerical model and in each case, failure was indicated by the development of localized shear zones.

It is difficult at this time to theorize on the cause of the oscillatory pattern observed early in the results from the numerical model. This pattern appears before the shock waves have attenuated which suggests the accumulation of some type of damage. This damage could be due to the amplification of reverberating shock waves. Once damage is initiated, the equivalent plastic strain in the material continues to increase until the oscillatory pattern has extended to the inner and outer surfaces of the cylinder. At this point localized surface thinning begins to occur indicating the onset of the quasi-periodic instabilities. Next localized shear zones develop and the instabilities become visible on fast framing camera photographs. The zones of shear continue to grow and eventually the cylinder fragments.

6.3 Sensitivity Study

There are several user supplied parameters in the GTN model. The values for the parameters used in this analysis are based on previous literature. The f_N, ε_N, and s_N, parameters in the void nucleation rate equation appear to be more statistically and physically based than the q_1, q_2, and q_3 parameters in the yield surface equation. As a result, the sensitivity analysis presented in this section only considers the q_1 parameter in the yield surface equation for the GTN model.

Recall from eqn. (2.50), the yield surface for the GTN model is expressed as,

$$\phi = \left(\frac{\sigma}{\sigma_f}\right)^2 + 2\, q_1\, f^* \cosh\left(-\frac{3\, q_2\, P}{2\, \sigma_f}\right) - \left(1 + q_3\, f^*\right) = 0. \tag{6.1}$$

This equation has three non-physical parameters (q_1, q_2, and q_3). These parameters were introduced by Tvergaard (1981, 1982) to provide closer agreement with numerical and experimental data. The current literature by Tvergaard and Needleman suggest,

$$q_3 = q_1^2 \tag{6.2}$$

with values for q_1 ranging from 1.0 to 1.5. The value for q_2 is almost always 1.0 although some literature suggests slightly smaller values within the range of 0.9-1.0. The sensitivity analysis presented in this section considers three values of q_1: 1.0, 1.25, and 1.5.

The model considered in this study is similar to the plane strain model analyzed earlier in this chapter. Four different cylinders are considered, each with an inner radius of 5.08 cm. The wall thickness of the cylinders range from 2.54 to 7.62 mm. Again, twenty elements were maintained through the thickness of each cylinder and each element has a 1:1 aspect ratio. This resulted in a different number of elements for each analysis. The mesh is shown in Figure 6.1 and the elements used are four node, linear, plane strain elements. The boundary conditions for this analysis include symmetry planes at both ends of the mesh and a pressure loading applied uniformly to the inner surface of the cylinder. The pressure loading was determined using the procedures described above in section 6.2. The total applied impulse, from 0 to 50 microseconds, and the number of elements for each of the four cylinders are shown below in Table 6.1

Table 6.1: Impulse and Number of Elements for Four Cylinders with 50.8 mm Inside Radius

Wall Thickness (mm)	2.54	5.08	6.35	7.62
Impulse (Pa-sec)	67,000	99,600	113,000	125,400
Number of Elements	12,000	6,000	5,020	4,180

The constitutive model developed in this dissertation is unable to simulate crack behavior and is limited only to the onset of failure. In order to characterize the effects of various parameters, a failure criterion was established. This criterion was based on the change in the cylinder thickness. Consider the geometry shown in Figure 6.11.

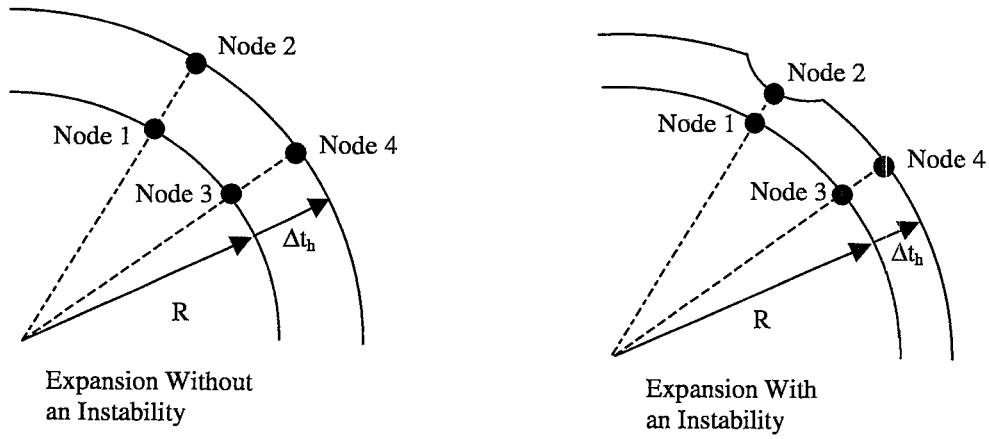

Figure 6.11: Illustration of Failure Criterion for Expanding Shell

As the cylinder expands, the wall thickness is reduced. If the cylinder expands uniformly without an instability, the cylinder wall will reduce uniformly. If an instability develops, the wall thickness at that instability will change faster than the wall thickness away from the instability. The change in the wall thickness at the instability will continue to increase while away from the instability, the change in the wall thickness will be uniform.

An 18° segment was analyzed for each cylinder. Each pair of nodes in the segment is assumed to lie along the same radial line indicating the same location in the theta direction before and after the development of instabilities, as shown in Figure 6.11.

The change in the wall thickness, Δt_h, for each nodal pair located along this 18° segment is then calculated at each time step using

$$\Delta t_h = \Delta r_i - \Delta r_o = \sqrt{\Delta x_i^2 + \Delta y_i^2} - \sqrt{\Delta x_o^2 + \Delta y_o^2}\ , \tag{6.3}$$

where,

$$\sqrt{\Delta x_i^2 + \Delta y_i^2} \tag{6.4}$$

represents the radial displacement of a node on the ID and

$$\sqrt{\Delta x_o^2 + \Delta y_o^2} \tag{6.5}$$

represents the radial displacement of a node on the OD. When the deviation of the change in thickness along the 18° segment is greater than 5% of the outer cylinder radius, failure is assumed in the cylinder. A representative plot of the change in wall thickness for an 18° segment of the 6.35 mm thick cylinder with an 5.715 cm outer radius is shown in Figure 6.12. Notice that there are several curves plotted in this figure. Each curve represents a pair of nodes whose position in the theta direction was identical at the start of the analysis. As expected, the curves shown in this figure are initially coincident, indicating that the change in wall thickness for the characteristic length of elements is initially uniform. At approximately 50 microseconds, the band of plots begins to illustrate a deviation. This deviation continues to increase and at about 65 microseconds it exceeds the previously chosen failure criterion. At this point, the instabilities are considered fully developed and failure is assumed.

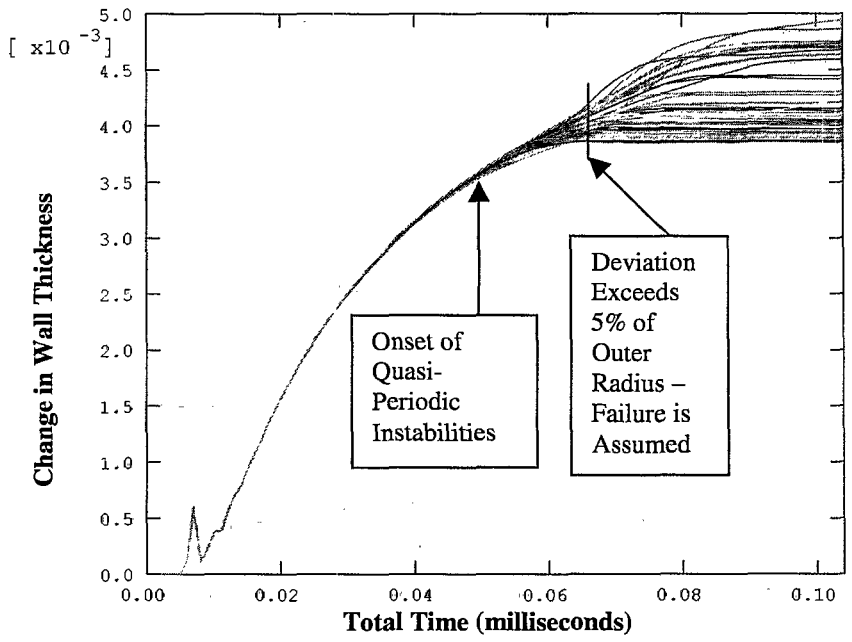

Figure 6.12: Change in Wall Thickness for Expanding Cylinder

Again, this analysis was performed for each of the four cylinders and each of the three values for q_1. Following the analysis, the time of failure was predicted using the failure criterion presented above. Then the results of the finite element model were examined to determine the maximum volumetric void concentration, equivalent plastic strain, equivalent plastic strain rate, and temperature. Plots of these values along with the failure time and strain are shown in Figures 6.13 to 6.18. It is important to note that values obtained from the fringe plots represent localized maximums and may not be representative of the global behavior.

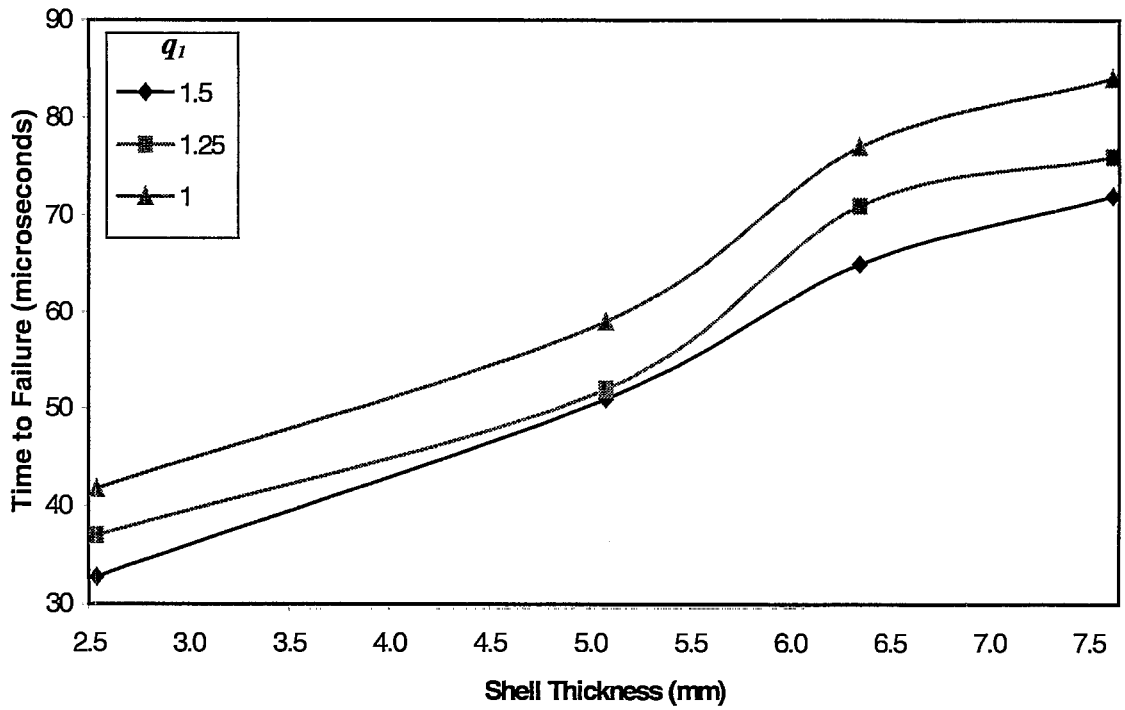

Figure 6.13: Failure Time vs Shell Thickness for Three values of q_1

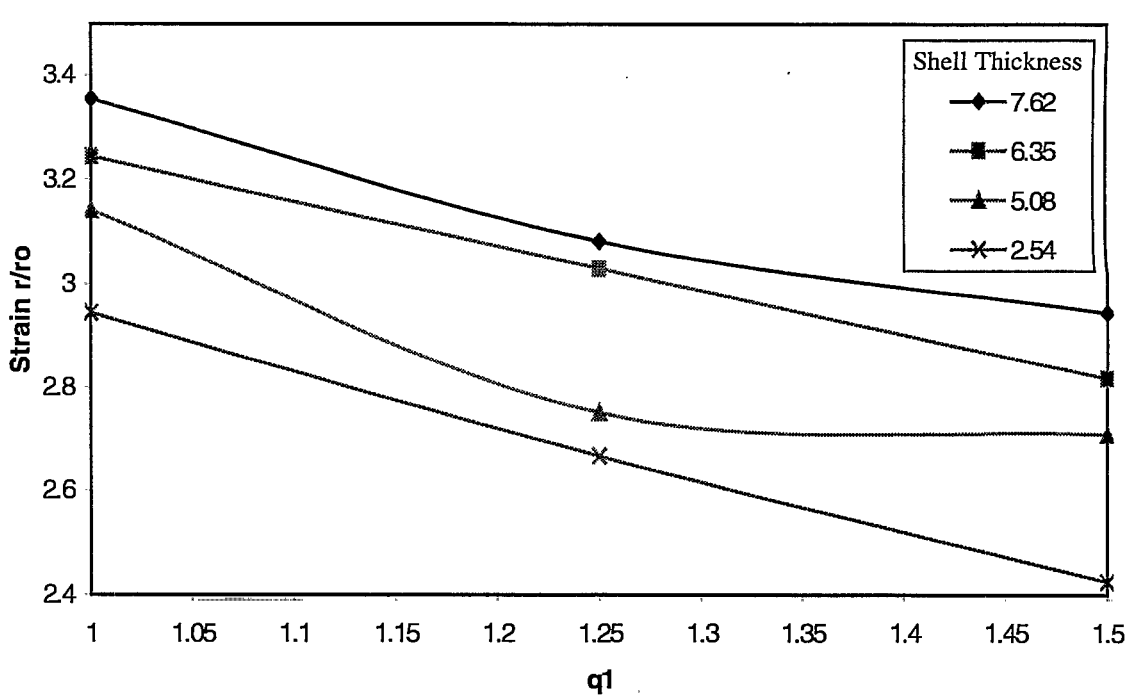

Figure 6.14: Strain at Failure vs q_1 for Four Cylinders with Different Shell Thickness

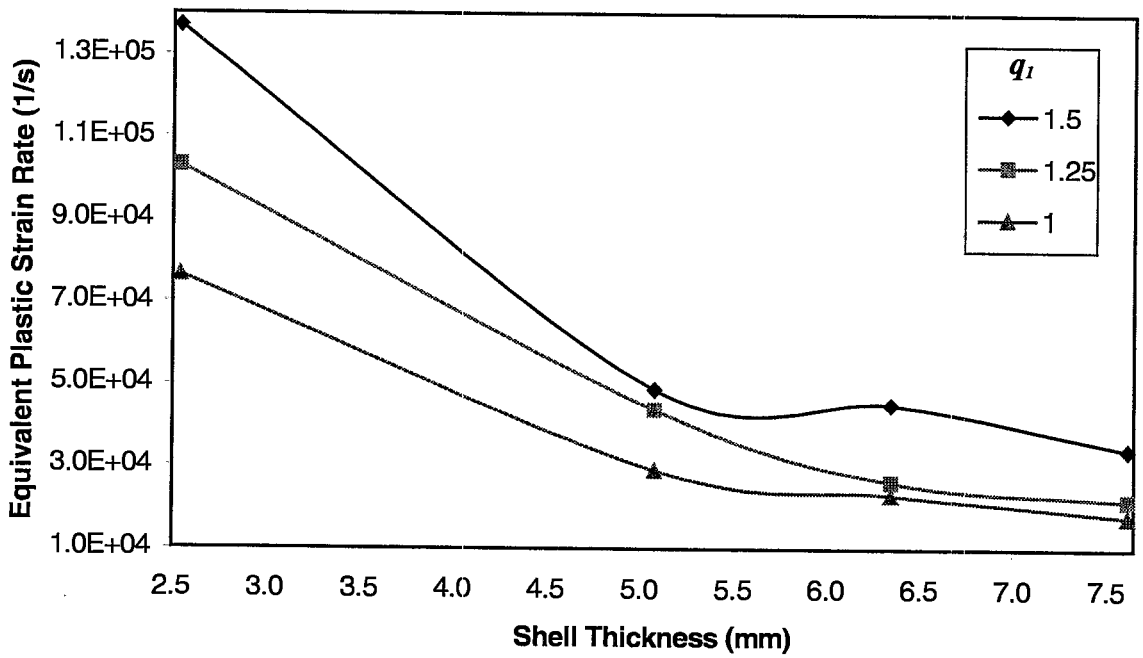

Figure 6.15: Maximum Equivalent Plastic Strain Rate at Failure vs Shell Thickness for Three values of q_1

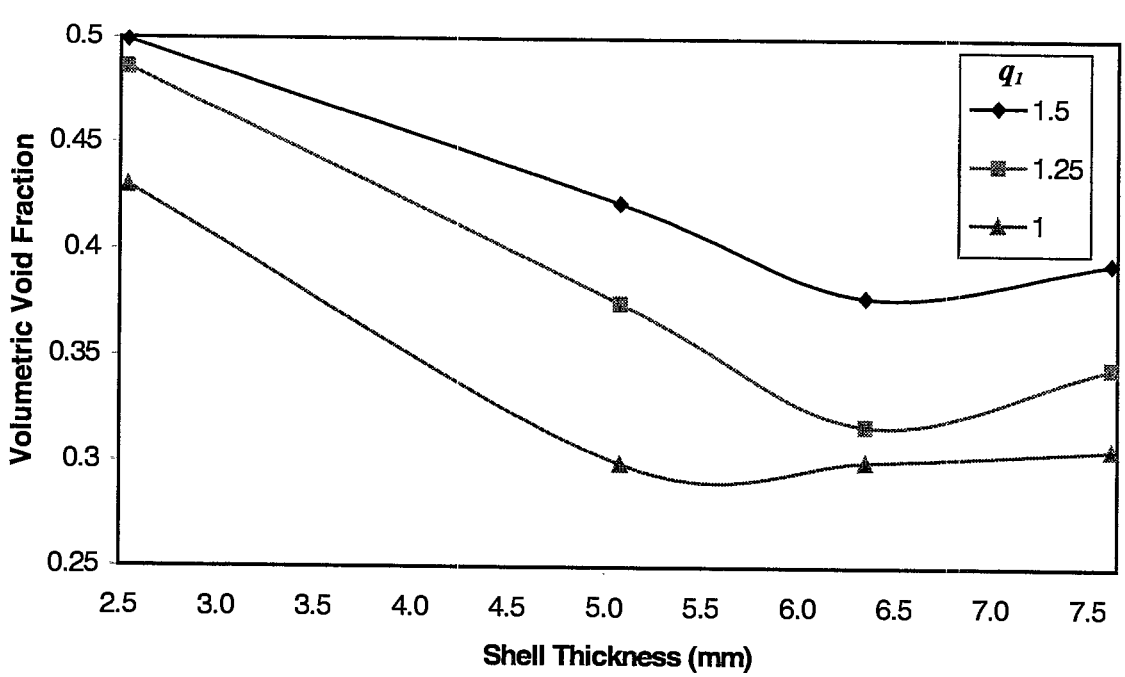

Figure 6.16: Maximum Volumetric Void Fraction at Failure vs Shell Thickness for Three values of q_1

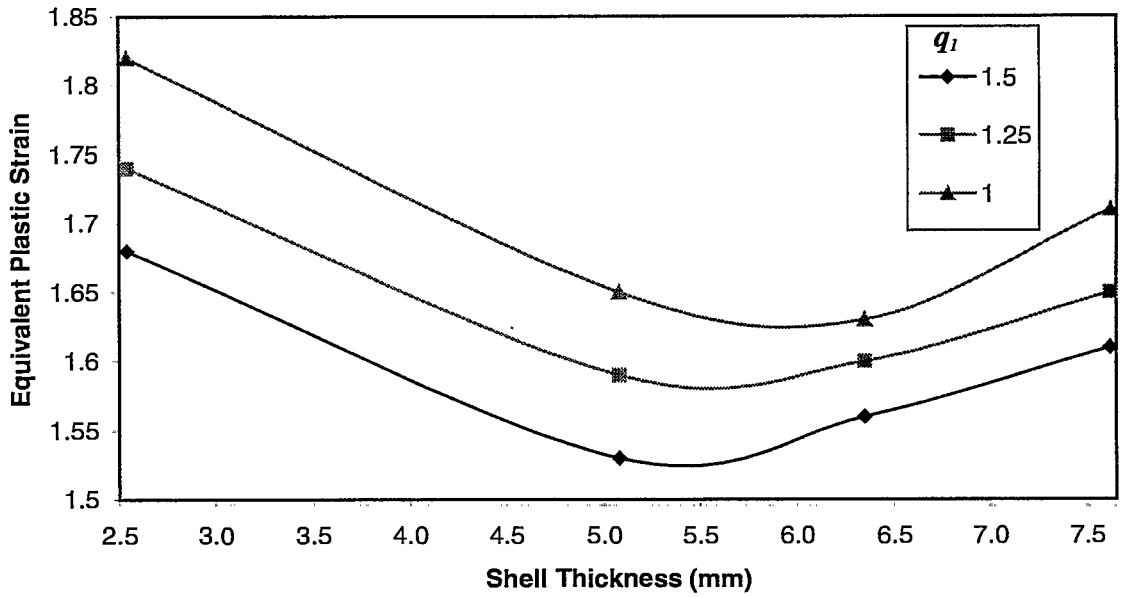

Figure 6.17: Maximum Equivalent Plastic Strain at Failure vs Shell Thickness for Three values of q_1

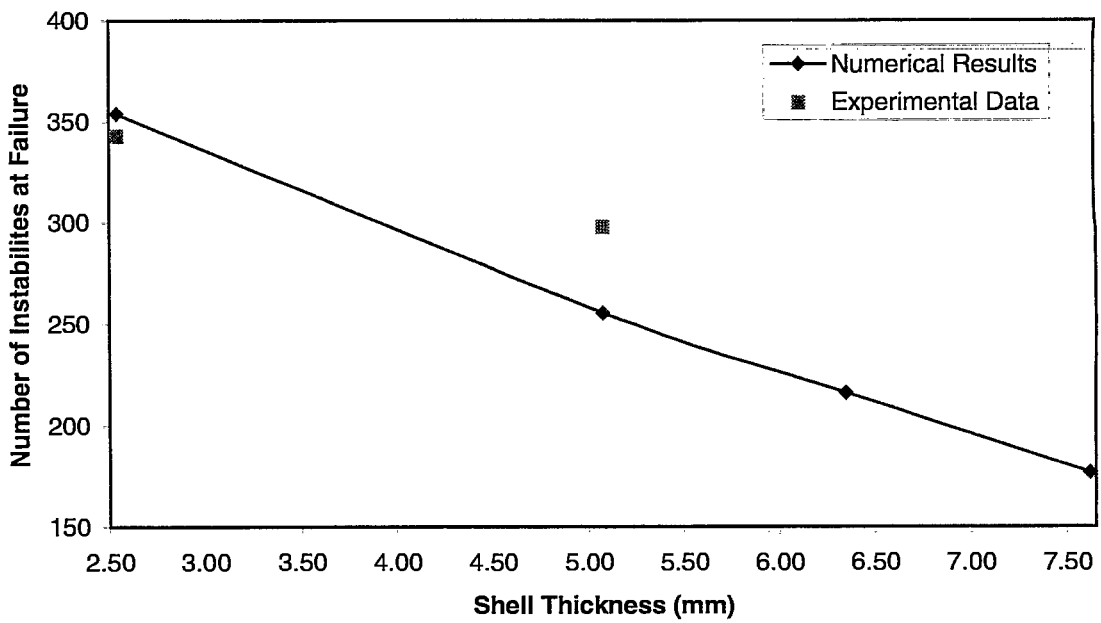

Figure 6.18: Number of Circumferential Instabilities vs Shell Thickness

Figures 6.13 through 6.14 illustrate fairly linear relations. There is a slight bend in Figure 6.13 and an even larger bend in Figures 6.16 and 6.17. The bend or change in slope in Figures 6.16 and 6.17 appear to occur at the same outer radius. This suggests a change in the failure mechanism of the cylinder. Examination of the fringe plots still suggests the development of localized shear. Recall from Figure 6.6, the area surrounding the shear zone is at a significantly lower equivalent plastic strain. This results in a large gradient between the shear zone and the surrounding material.

The plots shown in Figure 6.6 are for a cylinder with a 2.54 mm thickness. The thicker cylinders appear to have a smaller gradient in equivalent plastic strain perhaps suggesting more plastic flow and subsequent necking. The plot shown in Figure 6.18 illustrates the relationship between wall thickness and the number of instabilities. Variations in q_1 did not affect the number of instabilities observed from the model and therefore only one curve is shown in Figure 6.18. The total number of instabilities calculated by the numerical model was determined by counting the thinned regions on the 18° segment and interpolating for the entire 360° circumference. Recall that the experiments conducted had the same inner radius and a wall thickness of 2.54 mm and 5.08 mm. The estimated total number of experimentally observed circumferential instabilities was 343 and 298 for the smaller and larger cylinders respectively. This agrees reasonably with the numerical predictions as shown by the plot in Figure 6.18.

The effect of the mesh density was examined by modeling one geometry, the 5.08 mm thick shell, with two different mesh densities. This resulted in a model with 3525 elements in the first case and 6000 elements in the second case. The boundary conditions and constants on both models were identical. Values such as equivalent

plastic strain, equivalent plastic strain-rate, volumetric void fraction, and temperature were examined for each model at three different times. The results of this exercise for each mesh density are shown below in Table 6.2. The maximum values shown in this table are not identical, nor are they expected to be. Recall, the distribution of voids in the material is random, particularly the initial maximum and minimum distributions, and are expected to be different for each mesh. This will produce slight variations in the fringe plots of state variables like equivalent plastic strain, temperature, and void concentration. However, the results are within approximately 15% of each other and the hoop strain in each case is essentially identical.

Table 6.2: Results from Mesh Sensitivity Study

	Max. Equiv. Plastic Strain		Max. Void Concentration		Max. Temperature (K)		Hoop Strain	
	# of Elements		# of Elements		# of Elements		# of Elements	
Time (μs)	3525	6000	3525	6000	3525	6000	3525	6000
8.0	.148	.164	.0061	.0069	343	347	1.035	1.034
10.0	.214	.238	.0089	.0311	330	333	1.091	1.091
50.0	1.28	1.37	0.171	.210	442	454	2.663	2.663

Next the initialization of the void distribution was examined. Changing the seed of the random function changes the initial distribution of voids. The effects of seed variations were also negligible in terms of the overall failure, hoop strain, and equivalent plastic strain. However, it did have small effects, less than 10%, on the equivalent plastic strain rate, temperature, and volumetric void distribution.

In all of the preceding numerical runs, the initial range of voids in the material ranges randomly from 0.001 to 0.005. To study the effects of the initial void distribution, two different ranges were analyzed. These results are shown below in Table 6.3

Table 6.3: Results from Void Range Sensitivity Study

Initial Void Range	0.0009-0.0045	0.001-0.005
Hoop Strain at 70 μs	2.876	2.877
Hoop Strain at Failure	3.115	2.980
Max. Equiv. Plastic Strain at Failure	1.59	1.61
Max. Void Concentration at Failure	0.277	0.394
Max. Temperature at Failure	481	485
Max. Equiv. Plastic Strain Rate at Failure	2.03×10^4	3.41×10^4
Failure Time (μs)	78	73

The failure time of the model is related to the initial void distribution. The smaller the initial concentration of voids, the longer the model runs before failure and the higher the strain at failure. At 70 μs, the hoop strain for both initial void concentrations is nearly the same. In addition, at failure the equivalent plastic strain and temperature for both initial void concentrations is nearly the same. This indicates that the failure criterion is reasonable and justified when considering the mechanics involved with shear bands. There is, however, a variation in the final void concentration, equivalent plastic strain rate, and temperature. Finally, the overall number of instabilities does not appear to be affected by the mesh density, the seed, or the initial range of voids in the material

In summary, the simulations shown in this chapter illustrate the onset and development of plastic instabilities that are associated with rapidly expanding shells. The onset of a periodic pattern is observed as early as 7.6 microseconds and localized areas of intense plastic strain, which extend from the inner to the outer surfaces, are observed later at 34 microseconds. The total number of instabilities predicted by the numerical model is fairly close to the number of instabilities observed from the experimental data. In addition, several quantities such as the number of instabilities, the time to failure, and the hoop strain appear to be related to the thickness of the shell.

7.0 Summary and Conclusions

Thin cylindrical shells subjected to internal explosive detonations expand outwardly at strain rates on the order 10^4 s^{-1}. At approximately 150% strain, multiple plastic instabilities appear on the surface of these shells. These plastic instabilities develop into bands of localized shear and eventually cracks that progress in a way which causes the shell to break into fragments. Modeling this high strain rate expansion prior to fragmentation is the primary focus of this dissertation. Using the fundamental foundations of engineering mechanics, insight is also provided into the development of the instabilities through the thickness of the shell.

The multi-axial constitutive model developed for this dissertation includes modules for a hydrodynamic equation of state model, a microvoid damage model, and a rate dependent strength model. None of the constitutive models in the current literature apply all three of these components in an effort to analyze rapidly expanding shells. In addition, models in the current literature typically consider only the uniaxial stress or one of the principal stress components. The constitutive model developed in this dissertation includes the complete fundamental formulations of the entire stress and strain tensors for multi-dimensional plastic flow.

Examination of the results from the numerical model indicates that damage occurs early in time before the stress waves have attenuated. This damage does not appear to begin on the surface of the shell, but rather through the thickness of the material much

like a spall plane. However, with spall problems, damage in the form of void coalescence accumulates from waves moving transversely through the thickness of the shell. These waves load the material uniformly through its thickness and eventually cause a spall plane, which is not oscillatory or periodic. In the expanding shell problem, the periodic pattern clearly illustrates nonlinearities in the equivalent plastic strain. This periodic pattern or damage zone continues to develop and eventually extends to the outer and inner surfaces where thinning develops. Regions of intense shear eventually connect the thinned surfaces of the shell. A photomicrograph illustrating the cross-section of the thinned region around an instability is provided and is related to the numerical predictions.

In the majority of the current literature, the authors do not provide data regarding the microstructure of the material. This research provides photomicrographs illustrating the microstructure and hardness of the material prior to the experiment. The observations made from the photomicrograph of bulged samples and the results of the numerical model provide an interesting qualitative comparison of the localized thinning and shear zones that develops through the thickness of the shell.

The numerical results predicted here are compared with experimental data from this research. These experiments were designed to validate the multidimensional aspects of the constitutive model. Strain and velocity information was recorded during the experiment. Good agreement is obtained between the experimental data and the numerical results.

This research provides the scientific community with results from an additional set of sophisticated high explosive experiments that are not easily performed or recorded.

In the study of rapidly expanding shells, few authors compare their numerical results with experimental data. The authors that do provide experimental verifications are validating finite difference based models and only validate a few points on the expanding shell.

Numerical results of other quantities such as equivalent plastic strain, strain rate, and temperature are provided in this research. In addition, a limited sensitivity study is performed for parameters in the equation for the GTN yield surface. The results of this study indicate that the number of instabilities and time to failure are related to the thickness of the shell. In summary this sensitivity study indicated that the thicker the shell, the fewer instabilities and the longer the expansion. This also results in a larger strain before the onset of instabilities and larger strain at failure.

Future work in this area should focus on adaptive remeshing techniques to further study the details in the development of the instabilities predicted by the numerical model. The current model is not capable of modeling material separation. With adaptive remeshing, the growth of the instabilities and the subsequent fracture of the shell can be examined further.

The instabilities appear to be related to the periodic pattern, which is observed early in time. This periodic pattern may be initiated by an interference pattern from the reflecting stress waves in the material or by the excitation of higher order harmonics in the shell. Recall from the results presented in chapters 5 and 6 that the instabilities were not predicted for the axisymmetric model but were predicted for the plane strain model. In terms of stress wave interactions, the interference pattern developed by reflecting stress waves in the shell should be more distinct in the axisymmetric model than the plane strain model. Since the instabilities were not observed in the axisymmetric

analysis, additional research should focus on the harmonic solution and an examination of the eigenvalues.

Additional experiments should also be performed with carefully characterized bulged tests. These experiments should be designed to develop instabilities but not fragments. Should fragments be produced, enhanced fragment catching techniques should be implemented to minimize fragment damage and maximize the number of captured fragments. A less energetic explosive should also be considered in order to maximize the size of the fragments. Finally, optical resolution studies should be performed prior to the experiment to maximize the resolution of the photographs at the desired radial displacement. When the cylinder expands, the focus of the camera will either improve or diminish. A significant effort should be made to obtain the sharpest focus at the critical moment in the development of instabilities.

In summary, this research extends of the state of the art in the following ways:

1. The development of a constitutive model for multi-axial stress states, which includes modules for a hydrodynamic equation of state model, a microvoid damage model, and a rate dependent strength model.
2. The development of a constitutive model, which includes the correct fundamental formulations for multi-dimensional plastic flow, rather than the simplifying assumptions typical of hydrocodes.
3. The design, implementation, and results of experiments used to verify of the constitutive model for rapidly expanding cylindrical shells.

4. Photomicrographs illustrating the microstructure of the material before and after the experiments.

The results from this study led to the following conclusions:

1. Good correlation is shown between the numerical model and the experiments involving an explosively filled plane wave detonated copper cylinder.
2. The initiation of the periodic damage occurs early in time before the stress waves in the material have attenuated.
3. The instabilities observed on the surfaces of expanding cylindrical shells are connected by local areas of intense shear, which eventually cause failure.
4. The failure and damage accumulation in the high strain rate expansion of cylindrical shells is different from failure in spall problems.
5. The number of instabilities is related to the thickness of the shell.
6. Reasonable numerically results depend on the presence of a random distribution of microvoids at the start of the analysis.

The experimentally verified constitutive model developed in this dissertation provides a useful tool for further analytical work on the expansion of explosively expanding shells. In addition, the problems solved and the comparisons presented provide much needed insight into the development of the quasi-periodic instabilities observed on the surfaces of the expanding shells. In conclusion, the work presented in this dissertation represents an original and much needed contribution to the literature regarding the expansion of thin shells subjected to internal explosive detonations.

REFERENCES

ABAQUS, 1997, Version 5.6, Hibbit, Karlsson, and Sorenson Inc.

Ahrens, T. J., 1993, "Equations of State," High Pressure Shock Compression of Solids, Editors Asay James R. and Mohsen Shahinpoor, Springer-Verlag, New York, pp. 75-110.

Al-Hassani, S. T. S. and Johnson, W., 1969a, "The Dynamics of the Fragmentation Process for Spherical Shells Containing Explosives," *Int. J. Mech. Sci.*, Vol. 11, pp. 811-823.

Al-Hassani, S. T. S., Hopkins, H. G., Johnson, W., 1969b, "Note on the Fragmentation of Tubular Bombs," *Int. J. Mech. Sci.*, Vol. 11, pp. 545-549.

Anderson, C. E., Predebon, W. W., and Karpp, R. R., 1985, "Computational Modeling of Explosive-Filled Cylinders," *Int. J. Eng. Sci.*, Vol. 23, pp. 1317-1330.

Bai Y. and Dodd, B., 1992, Adiabatic Shear Localization, Pergamon Press. Oxford, UK.

Carrol, M. M., and Holt, A. C., 1972, "Static and Dynamic Pore-Collapse Relations for Ductile Porous Materials," *J. Appl. Phys.*, Vol. 43, pp. 1626-1636.

Chadwick, J., 1959, "The Quasi-Static Expansion of a Spherical Cavity in Metals and Ideal Soils," *J. Appl. Math. Mech.,* Vol. 12, pp. 52-71.

Christian, J. M., 1997, Interview by Rick Martineau, April 1997.

Chu, C. and Needleman, A, 1980, "Void Nucleation Effects in Biaxially Stretched Sheets," *J. Eng. Mat. Tech.*, Vol. 102, pp. 249-256.

Curran, D. R., Seaman, L., and Shockey, D. A., 1987, "Dynamic Failure of Solids," *Phys. Rep.*, Vol. 147, pp. 253-388.

Dobratz, B. M., 1981, "LLNL Explosive Handbook, Properties of Chemical Explosives and Explosive Simulants," UCRL-52997, Lawrence Livermore National Laboratory, Livermore California.

Duffey, T. A., 1989, "Dynamic Rupture of Shells," Structural Failure, Wiley, New York.

Duvall, G. E., 1961, Response of Metals to High Velocity Deformation, Editors Shewmen, P. G., and Zackay, V. F., Interscience Pub. Inc., New York, pp. 165-203.

Engelmann, B. E and Whirley, R. G., 1992, "Recent Developments in NIKE2D for Metal Forming Analysis at Low Rate Impact," *Nucl. Eng. Des.*, Vol. 138, pp. 23-35.

Ferm, E. N., 1998, Interview by Rick Martineau, January 1998.

Fung, Y. C.,1965, Foundations of Solid Mechanics, Prentice-Hall, Canada.

Follansbee, P. S., and Kocks, U. F., 1988, "A Constitutive description of the Deformation of Copper Based on the Use of the Mechanical Threshold Stress as an Internal State Variable," *Acta Metall.*, Vol. 36, pp. 81-93.

Goranson, R. W., Bancroft, D., Burton, B. L., Blechar, T., Houston, E. E., Gittings, E. F., and Landeen, S. A., 1955, " Dynamic Determination of the Compressibility of Solids," *J. Appl. Phys.*, Vol. 26, pp. 1472-1479.

Graham, R. A., 1993, "Introduction to High-Pressure Shock Compression of Solids," High Pressure Shock Compression of Solids, Editors Asay James R. and Mohsen Shahinpoor, Springer-Verlag, New York, pp. 1-6.

Gurney, R. W., 1943, "The Initial Velocities of Fragments from Bombs, Shells, and Grenades," BRL Report 405.

Gurson, A. L., 1977, "Continuum Theory of Ductile Rupture by Void Nucleation and Growth: Part I - Yield Criteria and Flow Rules for Porous Ductile Materials," *J. Eng. Mater. & Technol.*, Vol. 99, pp. 2-15.

Hall, E. O., 1951, "The Deformation and Aging of Mild Steel: III Discussion of Results," *Proc. Phys. Soc.*, Vol. B64, pp. 747-753.

Hao, S., and Brocks, W., 1997, "The Gurson-Tvergaard-Needleman-Model for Rate and Temperature-Dependent Materials with Isotropic and Kinematic Hardening", *Comp. Mech.*, Vol. 20, pp. 34-40.

Hoggatt, C. R. and Recht, R. F., 1968, "Fracture Behavior of Tubular Bombs," *J. Appl. Phys.*, Vol. 39, pp. 1856-1862.

Hopkins, H. G., 1960, Progress in Solid Mechanics 1, Editors Sneddon, I. N. and Hill, R., Interscience Publishers, Inc., New York.

Johnson, G. R. and Cook, W. H., 1983, "A Constitutive Equation and Data for Metals Subjected to Large Strains, High Strain Rates and High Temperatures," *Proc. 7th Int. Symp. Ballistics*, Am. Def. Prep. Org. (ADPA), Netherlands, pp. 541-547.

Johnson, J. N., 1981, "Dynamic Fracture and Spallation in Ductile Solids," *J. Appl. Phys.*, Vol. 52, No. 4, pp. 2812-2825.

Johnson, J. N., 1983, "Ductile Fracture of Rapidly Expanding Rings," *J. Appl. Mech.*, Vol. 50, 593-600.

Kinslow, R., High Velocity Impact Phenomena, Academic Press, 1970.

Love, A. E. H., 1944, The Mathematical Theory of Elasticity, 4th Ed. Cambridge University Press.

McClintock, F. A., 1968, "A Criterion for Ductile Fracture by the Growth of Holes," *J. Appl. Mech.*, Vol. 35, *Trans. ASME*, Vol. 90, Series E, pp. 363-371.

Mendelson, A., 1968, Plasticity: Theory and Application, Krieger, Florida.

Meyers, M. A., 1994, Dynamic Behavior of Materials, Wiley, New York.

Mott, N. R. 1947, "Fragmentation of Shell Cases," *Proc. R. Soc. London*, Vol. 189, pp. 300-308.

Necker, C., 1997, "Characterization of Copper Tubes," Internal Memo Number MST-6: 97-213, Los Alamos National Laboratory.

Needleman, A., 1987, "A Numerical Study of Void Nucleation at Carbides, Report of Brown University.

Needleman, A. and Rice, J. R., 1978, Mechanics of Sheet Metal Forming, Editors Koistinen et al., Plenum Press, New York, pp. 237-267.

Needleman, A. and Tvergaard, V., 1984, Mechanical Behavior of Materials – IV, Editors Carlsson, J. and Ohlson, N. G., Pergamon Press., Vol. 1, pp. 51-65

Ortiz, M. and Popov, E. P., 1985, "Accuracy and Stability of Integration Algorithms for Elastioplastic Constitutive Equations," *Int. J. Numer. Methods Eng.*, Vol. 21, pp. 1561-1576.

Ortiz, M. and Simo, J. C., 1986, "An Analysis of a New Class of Integration Algorithms for Elastoplastic Constitutive Relations," *Int. J. Numer. Methods Eng.*, Vol. 23, pp. 353-366.

Pack, D. C., Evans, W. M., and James, H. J., 1948, "The Propagation of Shock Waves in Steel and Lead," *Proc. Phys. Soc. London*, Vol. 60, 1-8.

Persad C., Yeoh A., Prabhu G., White G., and Eliezer Z., 1997, "On the Nature of the Armature-Rail Interface: Liquid-Metal Effects," IEEE Transactions on Magnetics, pp. 140-145.

Petch, N. J., 1953, "The Cleavage Strength o Polycrystals," *J. Iron Steel Inst.,* Vol. 174, pp. 25-28.

Prishchepenko, A. B., 1994, "A Device for Measuring the Inductance of the Winding of a Coil Explosion Magnetic Generator," *Instrum. Exp. Tech.*, Vol. 37, pp. 429-430.

Puttick, K, E. 1959, "Ductile Fracture in Metals," *Phil. Mag.*, Vol. 4, pp. 964-969.

Rice, J. R., and Tracy, D. M., 1969, "On the Ductile Enlargement of Voids in Triaxial Stress Fields," *J. Mech. Phys. Solids*, Vol. 17, pp. 201-217.

Rice, M. H., McQueen, R. G., Walsh, J. M., 1958, "Compression of Solids by Strong Shock Waves", Solid State Physics, Vol. VI, Editors F. Seitz and D. Turnbull Academic Press, New York, pp. 1-63.

Rogers, H. C., 1960, "The Tensile Fracture of Ductile Metals," Transactions of the Metallurgical Society of AIME, Vol. 218, pp. 498-506.

Shchegolevskii, M. A., 1983, "The Explosive Generator Plant – A New Technology", *Sov. Eng. Research*, Vol. 63, pp 64-66.

Shockey, D. A., Seaman, L., Dao, K. C., Curran, D. R., 1980, "Kinetics of Void Development in Fracturing A533B Tensile Bars", *Trans. ASME*, Vol. 102, pp. 14-21.

Skidmore, I. C., 1965, "An Introduction to Shock Waves in Solids," *Appl. Mater. Res.*, Vol. 4, pp. 131-147.

Slate, P. M. B, Billings, M. J. W., and Fuller, P. J. A., 1967, "The Rupture Behavior of Metals at High Strain Rates," *J. Inst. Metals*, Vol. 95, pp. 244-251.

Taylor, G. I., 1963a, "Fragmentation of Tubular Bombs," Scientific Papers of G. I. Taylor, Vol. 3, No. 44., Cambridge University Press., pp. 387-390.

Taylor, G. I., 1963b, "Analysis of the Explosion of a Long Cylindrical Bomb Detonated at One End," Scientific Papers of G. I. Taylor, Vol. 3, No. 30., Cambridge University Press., pp. 277-286.

Taylor, J. W., Harlow, F. H., Amsden, A. A., 1978, "Dynamic Plastic Instabilities in Stretching Plates and Shells," *J. Appl. Mech.*, Vol. 45, pp. 105-110.

Tipper, C. F. 1949, "The Fracture of Metals," Metallurgia, Vol. 39, pp.133-137.

Trucano, T. G., Chhabildas L. C., 1995, "Computational Design of Hypervelocity Launchers," *Int. J. Impact Eng.,* Vol. 17., pp. 849-860.

Tvergarrd, V., 1981, "Influence of Voids on Shear Band Instabilities under Plane Strain Condition," *Int. J. Fract. Mech.*, Vol. 17, pp. 389-407.

Tvergarrd, V., 1982, "On Localization in Ductile Materials Containing Spherical Voids," *Int. J. Fract. Mech.*, Vol. 18, pp. 237-252.

Tvergarrd, V., 1987, "Effect of Yield Surface Curvature and Void Nucleation on Plastic Flow Localization", *J. Mech. Phys. Solids*, Vol. 35, pp. 43-60.

Wallace, D. C., 1980a, "Irreversible Thermodynamics of Flow in Solids", *Phys. Rev.*, Vol. 22B, 1980., pp. 1477-1486.

Wallace, D. C., 1980b, "Equation of State From Weak Shocks in Solids", *Phys. Rev.*, Vol. 22B, 1980., pp. 1495-1502.

Walsh, J., and Christian, R., 1955, "Equation of State of Metals from Shock Wave Measurements," Phys. Rev., Vol. 97, pp. 1544-1556.

Wessenberg, D. L. and Sagartz, M. J., 1977, "Dynamic Fracture of 6061-T6 Aluminum Cylinders," *J. App. Mech.*, Vol. 44, pp. 643-646.

Zener, C and Hollomon, J. H., 1944, "Effects of Strain Rate Upon Plastic Flow of Steel," *J. Appl. Phys.*, Vol. 15, pp.22-32.

Zerilli, F. J. and Armstrong, R. W., 1986, "Dislocation-Mechanics-Based Constitutive Relations for Material Dynamics Calculations," *J. Appl. Phys*, Vol. 61, pp. 1816-1825.

Zukas, J.A. ed., 1991, High Velocity Impact Dynamics, Wiley, New York.

APPENDIX A

Fabrication Drawings

APPENDIX B

Fortran Source Code for VUMAT Subroutine

```
      subroutine vumat(
C Read only -
     .   nblock, ndir, nshr, nstatev, nfieldv, nprops, lanneal,
     .   stepTime, totalTime, dt, cmname, coordMp, charLength,
     .   props, density, strainInc, relSpinInc,
     .   tempOld, stretchOld, defgradOld, fieldOld,
     .   stressOld, stateOld, enerInternOld, enerInelasOld,
     .   tempNew, stretchNew, defgradNew, fieldNew,
C Write only -
     .   stressNew, stateNew, enerInternNew, enerInelasNew)

C        1         2         3         4         5         6         7
C    Written by:  Rick Martineau
C                 Submitted in partial fulfillment of the requirements for
C                 the degree of Doctor of Philosophy from Colorado State
C                 University, Fort Collins Colorado
C
      include 'vaba_param.inc'
      data iFirst/0/
C
      dimension
     *   coordMp(nblock,*), charLength(nblock), props(nprops),
     *   density(nblock), strainInc(nblock,ndir+nshr),
     *   relSpinInc(nblock,nshr), tempOld(nblock),
     *   stretchOld(nblock,ndir+nshr),
     *   defgradOld(nblock,ndir+nshr+nshr),
     *   fieldOld(nblock,nfieldv), stressOld(nblock,ndir+nshr),
     *   stateOld(nblock,nstatev), enerInternOld(nblock),
     *   enerInelasOld(nblock), tempNew(nblock),
     *   stretchNew(nblock,ndir+nshr),
     *   defgradNew(nblock,ndir+nshr+nshr), fieldNew(nblock,nfieldv),
     *   stressNew(nblock,ndir+nshr), stateNew(nblock,nstatev),
     *   enerInternNew(nblock), enerInelasNew(nblock)
C
      character*8 cmname


      dimension dsNew(nblock,6), u(nblock), dvdot(nblock),
     .   dvolInc(nblock), sbarNew(nblock), SbarOld(nblock),
     .   edev(nblock), edot(nblock), Sallow(nblock),
     .   Tstar(nblock), BulkNew(nblock)

      real  maxTen

C   general material properties are read from the input deck
```

```
      Den0    = props(1)
      SpHt    = props(2)
      Tinit   = props(3)
      Troom   = props(4)
      Tmelt   = props(5)
      Gs      = props(6)
      junk    = props(7)
      junk    = props(8)

C     Den0  MUST be the same as input on *DENSITY card
C     SpHt  -  specific heat used for temperature calcs
C    (work/mass/degree)
C     T       -  temperatures for thermal softening

C   Johnson-Cook  strength model parameters

      C1    = props(9)
      C2    = props(10)
      C3    = props(11)
      C4    = props(12)
      C5    = props(13)
      C6    = props(14)
      Smax  = props(15)
      iJC   = props(16)

C     C1 - C6 are JC strength parameters
C     C1 is commonly called A or C1 or Yield Stress
C     C2 is commonly called B or C2 or Hardening Modulus
C     C3 is commonly called n       or Hardening Exponent
C         for no strain hardening (elastic-perfectly plastic) set
C         C2=0 and C3=1.0
C     C4 is commonly called C or C3 or Strain-Rate Coefficient
C         for no strain-rate effects set C4 = 0.0
C     C5 is commonly called m or Thermal Softening Exponent
C         for no thermal softening set C5 = 0.0
C     C6 is commonly called D or C4 or Pressure Hardening Coefficient
C     Smax maximum strength - if zero, strength not limited
C           can be used like a saturation stress
C     iJC=1, do strength calc with Johnson-Cook material model
C     iJC=0  do not do strength calc

C   Grüneisen equation of state parameters

      Bulki   = props(17)
      Co      = props(18)
      S       = props(19)
      grun0   = props(20)
      maxTen  = props(21)
      b1      = props(22)
      b2      = props(23)
      iEOS    = props(24)

C    Bulki   bulk modulus for material
C    Co      Linear Acoustic Speed
C    S       Slope of the Us/Up Curve
C    grun0   Grüneisen parameter for material
C    maxTen  tensile pressure cutoff
C            for unlimited tension, set maxTen to a very large value
C    b1      Linear term of bulk viscosity - Used to reduce Ringing
C    b2      quadratic term of bulk viscosity - Used to smear shock
C            front
C    iEOS = 0,   do not do EOS or artificial vis calcs
```

```
C   iEOS = 1,   use EOS and artificial viscosity calcs

C  Gurson Void Model Parameters

      q1     = props(25)
      q2     = props(26)
      q3     = props(27)
      Ff     = props(28)
      Fc     = props(29)
      Vfract = props(30)
      En     = props(31)
      Sn     = props(32)

      Fn     = props(33)
      iVoid  = props(34)
      Vtime  = props(35)
      vmin   = props(36)
      pmax   = props(37)
      epmax  = props(38)
      ivNuc  = props(39)
      ivRand = props(40)

       iDam  = props(41)
        EPS  = props(42)
      Tkill  = props(43)

C   q#     -   parameters for Gurson Void model
C   fF     -   Ultimate Void Volume Fraction
C   fC     -   Critical Void Volume Fraction
C   Vfract -   Void Volume Fraction
C   En     -   Mean Nucleation Strain
C   Sn     -   Standard Deviation of Voids
C   Fn     -   Nucleation Void Fraction
C   iVoid  -   Void Flag
C   Vtime  -   Time at which void model starts

C   iDam   -   Turn Damage on/off
C    EPD   -   Equivalent Plastic Strain Limit
C  TKill   -   Kill Time cut-off

C   State Parameters for Void model are 36-45

      if (iJC .eq. 0) iDam = 0

      iFirst=iFirst + 1

  901 format (10i10)
  904 format (7e10.3, i3)

      if (iFirst .le. 1) then
         write(6,*)  '   begin vumat'
         write(6,*)  ' '
         write(6,*)  '********** Start Parameter Data **************'
         write(6,*)  'Den0, SpHt, Tinit, Troom, Tmelt, Gs, '
         write(6,904) Den0,SpHt,Tinit,Troom,Tmelt, Gs
         write(6,*)  'C1,    C2,    C3,    C4,    C5,  C6, Smax,  iJC'
         write(6,904) C1, C2, C3, C4, C5, C6, Smax, iJC
         write(6,*)  'Bulki, Co,    S,   grun0,   maxTen,  b1, b2 iEOS'
         write(6,904) Bulki, Co,  S, grun0, maxTen, b1, b2, iEOS
         write(6,*)  'q1,   q2,   q3,   fF,   fC,   Vfract,   En,  iVoid'
         write(6,904) q1, q2, q3, fF, fC, Vfract, En, iVoid
         write(6,*)  'Fn,   Flag, Vtime, Vmin, Pmax, EPe, Nuc, Damage'
         write(6,904) fn, iVoid, Vtime, vmin, pmax, epmax, ivNuc,Damage
```

```
         write(6,*)  'TKill'
         write(6,904) TKill
         write(6,*)  '*************** End Parameter Data **************'
         write(6,*)  ' '
         write(6,*) 'nblock, ndir, nshr, nstatev, nfieldv, nprops, annl'
         write(6,901) nblock,ndir,nshr,nstatev,nfieldv, nprops, lanneal
         write(6,*)  ' '
      endif


C   testing on element type to make sure
C   legal element types are used.
C   ndir = S11, S22, S33
C   nshr = S12, S23, S31

      if (iFirst .le. 1) then
         if (nshr .eq. 1) write(6,*)  'axisymmetric or plane strain'
         if (nshr .eq. 3) write(6,*)  '3D Solid'
      end if

C   if iEOS = 1, then update bulk modulus and calculate temperature

      if (iEOS .eq. 1) then

         if (iFirst .le. 1) then
            write(6,*)  'EOS is set to ', iEOS
            write(6,*)  'Calling EOS'
            write(6,*)  ' '
         end if

C   Note:  Specific Heat at constant Volume is passed into sub. eos
C   Uses state variables 21 and reserves 31-40.

      call EOS( nblock, dt, ndir, nshr, Den0, density, strainInc,
     .  stateOld(1,2), Bulki, S, Co, grun0, b2, SpHt, BulkNew,
     .  StateNew(1,61), StateNew(1,62), StateNew(1,63),
     .  StateNew(1,64), StateNew(1,65), StateNew(1,66),
     .  StateNew(1,67), StateNew(1,68), StateNew(1,69),
     .  StateOld(1,21), StateNew(1,21), charLength )

      else

         if (iFirst .le. 1) then
            write(6,*)  'EOS is set to ', iEOS
            write(6,*)  'NOT Calling EOS'
            write(6,*)  ' '
         end if

C    Since the EOS subroutine calculates a new bulk modulus for each
C    integration point, we need to set the array to the constant bulk
C    modulus if EOS is not called.

         do i=1, nblock
            BulkNew(i) = Bulki
         end do

      endif

C   if iJC=1 , do strength model

      if (iJC .eq. 1) then

         if (iFirst .le. 1) then
```

```
         write(6,*)  'JC is set to ', iJC
         write(6,*)  'Calling Stress'
         write(6,*)   ' '
      end if

C   Note:  Specific Heat at constant Pressure is pass into sub. stress
C   Uses State Variables 1-20, 23, 34, 45

      if (iVoid .eq. 1) then

         call Gurson( nblock, ndir, nshr, dt, stepTime, totalTime,
     .      density, strainInc, stressOld, stressNew, enerInternOld,
     .      enerInternNew, enerInelasOld, enerInelasNew, StateOld(1,1),
     .      StateNew(1,1), StateOld(1,2), StateNew(1,2), StateOld(1,3),
     .      StateNew(1,3), StateOld(1,5), StateNew(1,5), StateNew(1,6),
     .      StateNew(1,7), StateNew(1,8), StateNew(1,9), StateOld(1,10),
     .      StateNew(1,10), StateOld(1,11), StateNew(1,11),
     .      StateNew(1,12), StateNew(1,13), StateNew(1,14),
     .      StateNew(1,15), StateNew(1,16), StateNew(1,17),
     .      StateNew(1,18), StateNew(1,19), StateOld(1,20),
     .      StateNew(1,20), StateOld(1,21), StateNew(1,21),
     .      StateOld(1,22), StateNew(1,22), StateOld(1,23),
     .      StateNew(1,23), StateOld(1,24), StateNew(1,24),
     .      StateOld(1,25), StateNew(1,25), StateOld(1,26),
     .      StateNew(1,26), StateOld(1,27), StateNew(1,27),
     .      StateOld(1,28), StateNew(1,28), StateOld(1,29),
     .      StateNew(1,29), StateOld(1,30), StateNew(1,30),
     .      StateOld(1,31), StateNew(1,31), StateOld(1,32),
     .      StateNew(1,32), StateOld(1,33), StateNew(1,33),
     .      StateNew(1,34), StateNew(1,35), StateNew(1,36),
     .      StateNew(1,37), StateNew(1,38), StateNew(1,39),
     .      StateNew(1,40), StateOld(1,41),
     .      StateNew(1,45), StateNew(1,46), StateNew(1,51),
     .      StateNew(1,52), StateNew(1,53), StateNew(1,54),
     .      StateNew(1,55), StateNew(1,63),
     .      Den0, SpHt, Tinit, Troom, Tmelt, Gs, C1, C2, C3, C4,
     .      C5, C6, Smax, dsNew, sbarOld, dvdot, u, edot, Tstar,
     .      edev, BulkNew, iVoid, q1, q2, q3, vmin, pmax )

      else

         call VonMises( nblock, ndir, nshr, dt, stepTime, totalTime,
     .      density, strainInc, stressOld, stressNew, enerInternOld,
     .      enerInternNew, enerInelasOld, enerInelasNew, StateOld(1,1),
     .      StateNew(1,1), StateOld(1,2), StateNew(1,2), StateOld(1,3),
     .      StateNew(1,3), StateOld(1,5), StateNew(1,5), StateNew(1,6),
     .      StateNew(1,7), StateNew(1,8), StateNew(1,9), StateNew(1,10),
     .      StateOld(1,11), StateNew(1,11), StateNew(1,12),
     .      StateNew(1,13), StateNew(1,14), StateNew(1,15),
     .      StateNew(1,16), StateNew(1,17), StateNew(1,18),
     .      StateNew(1,19), StateOld(1,20), StateNew(1,20),
     .      StateOld(1,21), StateNew(1,21), StateOld(1,22),
     .      StateNew(1,22), StateOld(1,23), StateNew(1,23),
     .      StateOld(1,24), StateNew(1,24), StateOld(1,25),
     .      StateNew(1,25), StateOld(1,26), StateNew(1,26),
     .      StateOld(1,27), StateNew(1,27), StateOld(1,28),
     .      StateNew(1,28), StateOld(1,29), StateNew(1,29),
     .      StateOld(1,30), StateNew(1,30), StateOld(1,31),
     .      StateNew(1,31), StateOld(1,32), StateNew(1,32),
     .      StateOld(1,33), StateNew(1,33), StateNew(1,34),
     .      StateNew(1,35), StateNew(1,36), StateNew(1,37),
     .      StateNew(1,38), StateNew(1,39), StateOld(1,41),
     .      StateNew(1,45), StateNew(1,46), StateNew(1,51),
```

```
     .       StateNew(1,52), StateNew(1,53), StateNew(1,54),
     .       StateNew(1,55), StateNew(1,63),
     .       Den0, SpHt, Tinit, Troom, Tmelt, Gs, C1, C2, C3, C4,
     .       C5, C6, Smax, dsNew, SbarOld, dvdot, u, edot,
     .       Tstar, edev, BulkNew)

         end if

      else
         write(6,*)  'Strength Flag must be  1'
         stop
      endif

C   if iVoid = 1, then find void volume fraction

      if (iVoid .eq. 1) then

         if (iFirst .le. 1) then
            write(6,*)  'iVoid is set to ', iVoid
            write(6,*)  'Calling Void'
            write(6,*)   ' '
         end if

C  Uses State Variables 11, 12, 13 and reserves 41-55

         call Void(nblock, dt, ndir, nshr, stepTime, totalTime,
     .     density, strainInc, stressOld, stateNew(1,11),
     .     StateNew(1,41), StateOld(1,41), StateNew(1,42),
     .     StateNew(1,43), StateNew(1,44), StateNew(1,45),
     .     StateNew(1,46), StateNew(1,47), StateNew(1,48),
     .     StateNew(1,49), StateNew(1,50), StateNew(1,51),
     .     StateNew(1,52), StateNew(1,20), StateNew(1,54),
     .     StateNew(1,55), StateOld(1,43), StateOld(1,44),
     .     Gs, Sn, Fn, En, q1, q2, q3, fF, fC, vFract,
     .     vmin, pmax, ivNuc, ivRand )

      else

         if (iFirst .le. 1) then
            write(6,*)  'Void is set to ', iVoid
            write(6,*)  'NOT Calling Void'
            write(6,*)   ' '
         end if

      endif

C   If no damage model,
C   then set damage = zero.

      if (iDAM .eq. 0) then

         do I=1, nblock
            stateNew(i,3) = 0.0
         end do

      end if

C   Element death
C   Based on equivalent plastic strain or volumetric strain

      call death( nblock, iDam, Vdead, u, stateOld(1,1),
     .   stateNew(1,1), stateOld(1,2), stateNew(1,2),
     .   stateOld(1,3), stateNew(1,3), stateOld(1,4),
```

```
     .   stateNew(1,4), StateNew(1,41), StateNew(1,20),
     .   dt, epmax, Vfract, EPS, TKill, TotalTime)

      return
      end

cccccccccccccccccccccccccccccccccccccccccccccccccccccccccccccccccccccc
c
c     SUBROUTINE Gurson
c
c  This subroutine calculates the stresses, strains, energies, and
c  temperatures at each material point
c
c  Rick Martineau
c  Written:  05/10/97
c
cccccccccccccccccccccccccccccccccccccccccccccccccccccccccccccccccccccc

      subroutine Gurson( nblock, ndir, nshr, dt, stepTime, totalTime,
     .   density, eInc, SigOld, SigNew, eInternOld, eInternNew,
     .   eInelasOld, eInelasNew, ebarOld, ebar, dvolOld, dvol, DamOld,
     .   Dam, Oedt, State5, State6, State7, State8, State9, TanMod,
     .   State10, SallowO, State11, State12, State13, State14, State15,
     .   State16, State17, State18, State19, OPlEM, State20, TempO,
     .   State21, epo1, State22, epo2, State23, epo3, State24, epo4,
     .   State25, epo5, State26, epo6, State27, ee1, State28, ee2,
     .   State29, ee3, State30, ee4, State31, ee5, State32, ee6,
     .   State33, State34, State35, State36, State37, State38, State39,
     .   State40, VoidF, State45, State46, State51, State52, State53,
     .   State54, State55, ShockTemp,
     .   Den0, SpHeat, Tinit, Troom, Tmelt, Gs, C1, C2, C3, C4, C5, C6,
     .   Smax, dsNew, SbarOld, dvdot, u, edt, Tstar, edev, Bulk,
     .   iVoid, q1, q2, q3, Vmin, pmax )

      include 'vaba_param.inc'

      dimension density(nblock), eInc(nblock,ndir+nshr),
     .   SigOld(nblock,ndir+nshr), sigNew(nblock,ndir+nshr),
     .   eInternOld(nblock), eInternNew(nblock), Dam(nblock),
     .   eInelasOld(nblock), eInelasNew(nblock), ebarOld(nblock),
     .   ebar(nblock), dvolOld(nblock), dvol(nblock), DamOld(nblock),
     .   TempO(nblock), TempN(nblock), ShockTemp(nblock),
     .   VoidF(nblock), Oedt(nblock), TanOld(nblock)

      dimension State5(nblock), State6(nblock),
     .   State7(nblock), State8(nblock), State9(nblock),
     .   State10(nblock), State11(nblock), State12(nblock),
     .   State13(nblock), State14(nblock), State15(nblock),
     .   State16(nblock), State17(nblock), State18(nblock),
     .   State19(nblock), State20(nblock), State21(nblock),
     .   State22(nblock), State23(nblock), State24(nblock),
     .   State25(nblock), State26(nblock), State27(nblock),
     .   State28(nblock), State29(nblock), State30(nblock),
     .   State31(nblock), State32(nblock), State33(nblock),
     .   State34(nblock), State35(nblock), State36(nblock),
     .   State37(nblock), State38(nblock), State39(nblock),
     .   State40(nblock)

      dimension State45(nblock), State46(nblock), State51(nblock),
     .   State52(nblock), State53(nblock), State54(nblock),
     .   State55(nblock), ee1(nblock), ee2(nblock), ee3(nblock),
     .   ee4(nblock), ee5(nblock), ee6(nblock), Epo1(nblock),
     .   Epo2(nblock), Epo3(nblock), Epo4(nblock), Epo5(nblock),
```

```
     .    Epo6(nblock), OPlEM(nblock), Sallow(nblock)

      data iFirst/0/

      dimension dsNew(nblock,6), SbarOld(nblock), dvdot(nblock),
     .    dvbar(nblock), dvolInc(nblock), eIncAvg(nblock),
     .    edt(nblock), edot(nblock,6), edev(nblock),
     .    sbarNew(nblock), Bulk(nblock), Yfunc(nblock),
     .    TanMod(nblock), ElasMod(nblock), dsOld(nblock,6)

      dimension factor(nblock), vmises(nblock), SallowO(nblock),
     .    DelTemp(nblock), Tstar(nblock), PlastEM(nblock),
     .    PlasticWorkInc(nblock), Epdot(nblock), dsEquiv(nblock)

      dimension et(nblock,6), epeff(nblock),SigTrace(nblock),
     .    rm(nblock,6), ee(nblock,6), epInc(nblock,6), el(nblock,6),
     .    yf(nblock), VoidY(nblock), dlamda(nblock),
     .    dep(nblock,6), iconv(nblock), q2n(nblock)

      dimension v1(nblock), v2(nblock), v3(nblock), v4(nblock),
     .    xpsi1(nblock), xpsi2(nblock), h1(nblock), h2(nblock),
     .    edot1(nblock), edot2(nblock), edot3(nblock),
     .    edot4(nblock), edot5(nblock), edot6(nblock)

      dimension c11(nblock), c22(nblock), c33(nblock), c44(nblock),
     .    c12(nblock), c13(nblock), c21(nblock), c23(nblock),
     .    c31(nblock), c32(nblock), c55(nblock), c66(nblock)

      real const, yf, smean

C  cycle counter and formats for debugging

      iFirst = iFirst + 1

C  Formulate the Elastic Matrix for the Material Behavior

      do i=1, nblock
         c11(i) = (Bulk(i) - (2.0/3.0) * Gs) + 2.0 * Gs
         c22(i) = c11(i)
         c33(i) = c11(i)
         c12(i) = (Bulk(i) - (2.0/3.0) * Gs)
         c13(i) = c12(i)
         c21(i) = c12(i)
         c23(i) = c12(i)
         c31(i) = c12(i)
         c32(i) = c12(i)
         c44(i) = Gs
         c55(i) = Gs
         c66(i) = Gs
      end do

C  Set the convergence tolerance to a small number

      ctol = 0.0001

C  The strain hardening exponent must be positive

      if (C3 .le. 0.0) then
         write(6,*) 'ERROR STOP because c3 must be > 0.0'
         stop
      endif

      do i=1, nblock
```

```
         dvolInc(i) = eInc(i,1) + eInc(i,2) + eInc(i,3)
         dvol(i) = dvol01d(i) + dvolInc(i)
         dvdot(i) = dvolInc(i) /dt
         dvbar(i) = dvol(i) - dvdot(i) * dt / 2.0

C  Compute the Elastic Modulus

         ElasMod(i) = 9.0 * Bulk(i) * Gs / (3.0 * Bulk(i) + Gs)

      end do

      if (iFirst .le. 1) then
         write(6,*) 'Working on strength model'
      end if

C   ndir+nshr = 4     means 2D

      if (ndir+nshr .eq. 4) then

         if (iFirst .le. 1) then
            write(6,*) 'Working on axisymmetric strength'
         end if

         do I=1,nblock

C  Set the el equal to the previous elastic strains

            el(i,1) = ee1(i)
            el(i,2) = ee2(i)
            el(i,3) = ee3(i)
            el(i,4) = ee4(i)

            do j=1, 4

               epInc(i,j) = 0.0
               rm(i,j) = 0.0

            end do

C  Set the converged flag to 0 (false)

            iconv(i) = 0

C  Set dlamda to zero so that plastic strain starts at zero

            dlamda(i) = 0.0

C  Average normal strain increment - TOTAL
C  TOTAL means  (elastic + plastic and deviator + dilatation)

            eIncAvg(i) = (eInc(i,1) + eInc(i,2) + eInc(i,3)) / 3.0

C  Deviator strain rates

            edot(i,1) = (eInc(i,1) - eIncAvg(i)) / dt
            edot(i,2) = (eInc(i,2) - eIncAvg(i)) / dt
            edot(i,3) = (eInc(i,3) - eIncAvg(i)) / dt
            edot(i,4) = (eInc(i,4)               ) / dt

C  equivalent plastic (deviatoric) strain rate

            edt(i) = sqrt ( (2.0/9.0) * ( (edot(i,1) - edot(i,2))**2
```

```
     .          + (edot(i,2) - edot(i,3))**2 + (edot(i,3) - edot(i,1))**2
     .          + 6.0 * edot(i,4)**2 ) )

C  Calculate the old average stress for Johnson-Cook Subroutine

           SbarOld(i) = (SigOld(i,1) + SigOld(i,2) + SigOld(i,3))/3.0

C  Lower bound on strain rate for logarithm operation in flow stress calc

           if ((dt .eq. 1.0) .or. (dt .le. TotalTime)) then

              edt(i) = dmax1 (edt(i), 0.0001)

            else

              edt(i) = dmax1 (Oedt(i), 0.0001)

            end if

        end do

C  Compute flow stress  - Sallow
C  Send Ebar,

        call JC( nblock, stepTime, totalTime, OPlEm,
     .     DamOld, Tinit, Troom, Tmelt, Gs, C1, C2, C3,
     .     C4, C5, C6, Smax, SbarOld, edt, Sallow,
     .     Tstar, iFirst, TempO, DelTemp, dt )

        Converged = .False.
        j = 0

        do while (Converged .eq. .False.)

C  Increment counter

           j = j +1

           do i=1, nblock

              if (iconv(i) .eq. 0) then

C   Update the plastic strain increment

                 do k = 1, 4
                   epInc(i,k) = epInc(i,k) + dlamda(i) * rm(i,k)
                 end do

C  equivalent plastic (deviatoric) strain rate

                 edt(i) = sqrt((2.0/9.0) * (
     .                (epInc(i,1)/dt - epInc(i,2)/dt)**2
     .              + (epInc(i,2)/dt - epInc(i,3)/dt)**2
     .              + (epInc(i,3)/dt - epInc(i,1)/dt)**2
     .              + 6.0*(epInc(i,4)/dt)**2 ))

C  Lower bound on strain rate for logarithm operation in flow stress calc

                 edt(i) = dmax1 (edt(i), 0.0001)

C   Calculate the effective plastic strain change
```

```
                 epeff(i) = Sqrt(2.0/9.0)
     .              * Sqrt( ( epInc(i,1) - epInc(i,2) )**2
     .                 + ( epInc(i,2) - epInc(i,3) )**2
     .                 + ( epInc(i,3) - epInc(i,1) )**2
     .           + 6.0 *( epInc(i,4)**2 ) )

C    Update the total effective plastic strain

                 ebar(i) = ebarOld(i) + epeff(i)

C    Update the elastic strain increment
C    Elastic = OldElastic + Total Inc - Plastic

                 do k=1, 4
                    ee(i,k) = el(i,k) + eInc(i,k) - epInc(i,k)
                 end do

C    Update the volumetric increment

                 dvolInc(i) = ee(i,1) + ee(i,2) + ee(i,3)

C   Compute New stresses - For first iteration this is
C   my trial stress.

                 SigNew(i,1) = c11(i)*ee(i,1) + c12(i)*ee(i,2)
     .              + c13(i)*ee(i,3)
                 SigNew(i,2) = c21(i)*ee(i,1) + c22(i)*ee(i,2)
     .              + c23(i)*ee(i,3)
                 SigNew(i,3) = c31(i)*ee(i,1) + c32(i)*ee(i,2)
     .              + c33(i)*ee(i,3)
                 SigNew(i,4) = c44(i)*ee(i,4)

                 SbarNew(i) = (SigNew(i,1)+SigNew(i,2)+SigNew(i,3))/3.0
                 SigTrace(i)=  SigNew(i,1)+SigNew(i,2)+SigNew(i,3)

C    Reset q2
C    Basically if the element is under compression larger than pmax
C    then shut off the Gurson model.  In addition, if the bulk modulus
C    has been modified by the EOS (ie. under compression) then
C    shut off the Gurson model.

                 if (SigTrace(i) .lt. pmax) then

                    q2n(i) = abs(Sallow(i) / SigTrace(i))

                 else

                    q2n(i) = q2

                 end if

C    Find the deviatoric Stress

                 dsNew(i,1) = SigNew(i,1) - SbarNew(i)
                 dsNew(i,2) = SigNew(i,2) - SbarNew(i)
                 dsNew(i,3) = SigNew(i,3) - SbarNew(i)
                 dsNew(i,4) = SigNew(i,4)

C    Calculate the Equivalent stress from the deviatoric stress

                 dsEquiv(i) = Sqrt((1.0/2.0) * ( (dsNew(i,1)
```

```
     .                - dsNew(i,2))**2 + (dsNew(i,2)
     .                - dsNew(i,3))**2 + (dsNew(i,3)
     .                - dsNew(i,1))**2 + 6.0 * dsNew(i,4)**2) )

C  Equivalent stress

"
                   vmises(i) = sqrt( (1./2.) * (((sigNew(i,1)
"
     .                - sigNew(i,2))**2 + (sigNew(i,2)
"
     .                - sigNew(i,3))**2 + (sigNew(i,3)
     .                - sigNew(i,1))**2 + 6.0 * sigNew(i,4)**2)))

               end if
            end do


            do i=1, nblock
               if(DamOld(i) .ge. 1.0)  then
                  iconv(i) = 1
               endif
            end do

            do i=1, nblock

               if (iconv(i) .eq. 0) then

C  Determine the Tangent of the Flow Surface

                   if ( (dt .eq. 1.0) .or.
     .                 (dt .eq. TotalTime) ) then

                      TanMod(i) = Sallow(i)/(edt(i)*dt)

                   else if (abs(Sallow(i)-SallowO(i)) .lt. 0.1 ) then

                      TanMod(i) = 0.0

                   else if (epeff(i) .eq. 0.0) then

                      TanMod(i) = 0.0

                   else

                      TanMod(i) = (Sallow(i) - SallowO(i)) / epeff(i)

                   end if

C  Evaluate yield function in a non-dimensional form

                   VoidY(i) = (2.0 * q1 * Voidf(i) *
     .                Cosh(q2n(i) * SigTrace(i) / ( 2.0
     .                * Sallow(i) ))) - (1.0 + q3 * Voidf(i)**2)

                   yf(i) = (dsEquiv(i)/Sallow(i))**2 + VoidY(i)

C  Elastic stress Only and set elastic strains to total strains

                   if ( ( (yf(i) .lt. 0.0) .and. (j .eq. 1))
     .                                  .or. (dt .eq. 1.0) ) then

                      iconv(i) = 1
```

```
C  Plastic Stress and Converged

                  else if (abs(yf(i)) .lt. ctol) then

                     iconv(i) = 1

                  else

C  Calculate the Mtensor

                     vc1 = (q1 * VoidF(i)/Sallow(i)) * Sinh(q2n(i)
     .                  * SigTrace(i) / (2.0 * Sallow(i)) )
                     vc2 = 1.0 / Sallow(i)**2

                     rm(i,1) = vc2 * (3.*SigNew(i,1)-SigTrace(i))+vc1
                     rm(i,2) = vc2 * (3.*SigNew(i,2)-SigTrace(i))+vc1
                     rm(i,3) = vc2 * (3.*SigNew(i,3)-SigTrace(i))+vc1
                     rm(i,4) = vc2 * (3.*SigNew(i,4))

                     const = (VoidF(i) * TanOld(i) * q1 * SigTrace(i)
     .                  / Sallow(i)**2) * Sinh(q2n(i)*SigTrace(i) /
     .                  (2.0*Sallow(i)))

                     xpsi1(i) = -2.0 * TanOld(i)/Sallow(i)**3 *
     .                  (1.5 * (SigNew(i,1)**2 + SigNew(i,2)**2 +
     .                  SigNew(i,3)**2 + 2.0 * SigNew(i,4)**2) - 0.5
     .                  * SigTrace(i)**2) - const

                     xpsi2(i) = 2.*q1*Cosh(q2n(i) * SigTrace(i) /
     .                  (2.0*Sallow(i))) - 2.0 * q2n(i) * VoidF(i)

                     h1(i) = Sqrt((2.0/3.0) * (rm(i,1)**2 + rm(i,2)**2
     .                  + rm(i,3)**2 + 2.0*rm(i,4)**2))

                     h2(i) = (1.0 - VoidF(i)) *
     .                  (rm(i,1) + rm(i,2) + rm(i,3))

C  Compute delta

                     ct = c11(i) * (rm(i,1)**2 + rm(i,2)**2 +
     .                  rm(i,3)**2) + 4.* c44(i)*rm(i,4)**2 + 2.*c12(i)
     .                  * (rm(i,1)*rm(i,2) + rm(i,1)*rm(i,3)
     .                  + rm(i,2)*rm(i,3))

                     denom = ct - xpsi1(i)*h1(i) - xpsi2(i)*h2(i)

                     if( denom.eq.0.0) then
                        write(6,*) 'stop denom is 0'
                        stop
                     end if

                     dlamda(i) = yf(i) / denom

                     if ((denom .lt. 0.0).and.(j.gt.2)) then
                        write(6,*) '** Need to Change dlamda'
                        stop
                     end if

                  end if

                  if ((j .gt. 5) .and. (j .lt. 10000)) then
c                    write(6,*) yf(i), const, VoidY(i), dlamda(i), j
```

```
                else if (j .eq. 10000) then
                   write(6,*) 'J exceed maximum, STOP'
                   write(6,*) yf(i), const, VoidY(i), dlamda(i), j
                   write(6,*) '                                    '
                   write(6,*) 'Consider reducing the time step'
                   write(6,*) '                                    '
                   STOP
                end if
             end if
          end do

C  Check for complete convergence

          Converged = .True.

          do i=1, nblock

             if (iconv(i) .eq. 0) then
                Converged = .False.
             end if

          end do

       end do

       do i=1, nblock

C   Set dep to the plastic strain increment

          do k=1, 4
             dep(i,k) = epInc(i,k)
          end do

C   Update the new plastic strain

          epInc(i,1) = dep(i,1) + epo1(i)
          epInc(i,2) = dep(i,2) + epo2(i)
          epInc(i,3) = dep(i,3) + epo3(i)
          epInc(i,4) = dep(i,4) + epo4(i)

C   Update the Plastic Work and Inelastic Energy terms

          PlasticWorkInc(i) = (1.0/2.0) * (
     .       (SigOld(i,1) + SigNew(i,1)) * dep(i,1) +
     .       (SigOld(i,2) + SigNew(i,2)) * dep(i,2) +
     .       (SigOld(i,3) + SigNew(i,3)) * dep(i,3) +
     .       2.0 *(SigOld(i,4) + SigNew(i,4)) * dep(i,4))

          eInelasNew(i) = eInelasOld(i) +
     .       PlasticWorkInc(i) / density(i)

C   Update the Internal Energy terms

          edev(i) = (1.0/2.0) * (
     .       (SigOld(i,1) + SigNew(i,1)) * eInc(i,1) +
     .       (SigOld(i,2) + SigNew(i,2)) * eInc(i,2) +
     .       (SigOld(i,3) + SigNew(i,3)) * eInc(i,3) +
     .       2.0 *(SigOld(i,4) + SigNew(i,4)) * eInc(i,4))

          eInternNew(i) = eInternOld(i) +  edev(i) / density(i)

       end do
```

```
C   ndir+nshr = 6     means 3D

      else if (ndir+nshr .eq. 6) then

         if (iFirst .le. 1) then
            write(6,*) 'Working on solid strength'
         end if

         do I=1,nblock

C  Set the el equal to the previous elastic strains

            el(i,1) = ee1(i)
            el(i,2) = ee2(i)
            el(i,3) = ee3(i)
            el(i,4) = ee4(i)
            el(i,5) = ee5(i)
            el(i,6) = ee6(i)

            do j=1, 6

               epInc(i,j) = 0.0
               rm(i,j) = 0.0

            end do

C  Set the converged flag to 0 (false)

            iconv(i) = 0

C  Set dlamda to zero so that plastic strain starts at zero

            dlamda(i) = 0.0

C  Average normal strain increment - TOTAL
C  TOTAL means  (elastic + plastic and deviator + dilatation)

            eIncAvg(i) = (eInc(i,1) + eInc(i,2) + eInc(i,3)) / 3.0

C  Deviator strain rates

            edot(i,1) = (eInc(i,1) - eIncAvg(i)) / dt
            edot(i,2) = (eInc(i,2) - eIncAvg(i)) / dt
            edot(i,3) = (eInc(i,3) - eIncAvg(i)) / dt
            edot(i,4) = (eInc(i,4)              ) / dt
            edot(i,5) = (eInc(i,5)              ) / dt
            edot(i,6) = (eInc(i,6)              ) / dt

C  equivalent plastic (deviatoric) strain rate

            edt(i) = sqrt ( (2.0/9.0) * ( (edot(i,1) - edot(i,2))**2
     .        + (edot(i,2) - edot(i,3))**2 + (edot(i,3) - edot(i,1))**2
     .        + 6.0 * (edot(i,4)**2 + edot(i,5)**2 + edot(i,6)**2) ) )

C  Calculate the old average stress for Johnson-Cook Subroutine

            SbarOld(i) = (SigOld(i,1) + SigOld(i,2) + SigOld(i,3))/3.0

C  Lower bound on strain rate for logarithm operation in flow stress calc

            if ((dt .eq. 1.0) .or. (dt .le. TotalTime)) then

               edt(i) = dmax1 (edt(i), 0.0001)
```

```
            else

              edt(i) = dmax1 (Oedt(i), 0.0001)

            end if

        end do

C  Compute flow stress  - Sallow
C  Send Ebar,

        call JC( nblock, stepTime, totalTime, OPlEm,
     .     DamOld, Tinit, Troom, Tmelt, Gs, C1, C2, C3,
     .     C4, C5, C6, Smax, SbarOld, edt, Sallow,
     .     Tstar, iFirst, TempO, DelTemp, dt )

        Converged = .False.
        j = 0

        do while (Converged .eq. .False.)

C  Increment counter

           j = j +1

           do i=1, nblock

              if (iconv(i) .eq. 0) then

C   Update the plastic strain increment

                 do k = 1, 6
                   epInc(i,k) = epInc(i,k) + dlamda(i) * rm(i,k)
                 end do

C  equivalent plastic (deviatoric) strain rate

                 edt(i) = sqrt((2.0/9.0) * (
     .                (epInc(i,1)/dt - epInc(i,2)/dt)**2
     .              + (epInc(i,2)/dt - epInc(i,3)/dt)**2
     .              + (epInc(i,3)/dt - epInc(i,1)/dt)**2
     .              + 6.0*( (epInc(i,4)/dt)**2 + (epInc(i,5)/dt)**2
     .              + (epInc(i,6)/dt)**2) ) )

C  Lower bound on strain rate for logarithm operation in flow stress calc

                 edt(i) = dmax1 (edt(i), 0.0001)

C   Calculate the effective plastic strain change

                 epeff(i) = Sqrt(2.0/9.0)
     .              * Sqrt( ( epInc(i,1) - epInc(i,2) )**2
     .                + ( epInc(i,2) - epInc(i,3) )**2
     .                + ( epInc(i,3) - epInc(i,1) )**2
     .                + 6.0 *( epInc(i,4)**2 + epInc(i,5)**2
     .                + epInc(i,6)**2 ) )

C   Update the total effective plastic strain

                 ebar(i) = ebarOld(i) + epeff(i)

C   Update the elastic strain increment
```

```
C   Elastic = OldElastic + Total Inc - Plastic

                do k=1, 6
                   ee(i,k) = el(i,k) + eInc(i,k) - epInc(i,k)
                end do

C   Update the volumetric increment

                dvolInc(i) = ee(i,1) + ee(i,2) + ee(i,3)

C  Compute New stresses - For first iteration this is
C  my trial stress.

                SigNew(i,1) = c11(i)*ee(i,1) + c12(i)*ee(i,2)
     .             + c13(i)*ee(i,3)
                SigNew(i,2) = c21(i)*ee(i,1) + c22(i)*ee(i,2)
     .             + c23(i)*ee(i,3)
                SigNew(i,3) = c31(i)*ee(i,1) + c32(i)*ee(i,2)
     .             + c33(i)*ee(i,3)
                SigNew(i,4) = c44(i)*ee(i,4)
                SigNew(i,5) = c55(i)*ee(i,5)
                SigNew(i,6) = c66(i)*ee(i,6)

                SbarNew(i) = (SigNew(i,1)+SigNew(i,2)+SigNew(i,3))/3.0
                SigTrace(i)=  SigNew(i,1)+SigNew(i,2)+SigNew(i,3)

C   Reset q2
C   Basically if the element is under compression larger than pmax
C   then shut off the Gurson model.  In addition, if the bulk modulus
C   has been modified by the EOS (ie. under compression) then
C   shut off the Gurson model.

                if (SigTrace(i) .lt. pmax) then

                   q2n(i) = abs(Sallow(i) / SigTrace(i))

                else

                   q2n(i) = q2

                end if

C   Find the deviatoric Stress

                dsNew(i,1) = SigNew(i,1) - SbarNew(i)
                dsNew(i,2) = SigNew(i,2) - SbarNew(i)
                dsNew(i,3) = SigNew(i,3) - SbarNew(i)
                dsNew(i,4) = SigNew(i,4)
                dsNew(i,5) = SigNew(i,5)
                dsNew(i,6) = SigNew(i,6)

C   Calculate the Equivalent stress from the deviatoric stress

                dsEquiv(i) = Sqrt((1.0/2.0) * ( (dsNew(i,1)
     .             - dsNew(i,2))**2 + (dsNew(i,2)
     .             - dsNew(i,3))**2 + (dsNew(i,3)
     .             - dsNew(i,1))**2 + 6.0 * (dsNew(i,4)**2
     .             + dsNew(i,5)**2 + dsNew(i,6)**2) ) )

C  Equivalent stress

                vmises(i) = sqrt( (1./2.) * ((sigNew(i,1)
```

```
     .                - sigNew(i,2))**2 + (sigNew(i,2)
     .                - sigNew(i,3))**2 + (sigNew(i,3)
     .                - sigNew(i,1))**2 + 6.0 * (sigNew(i,4)**2
     .                + sigNew(i,5)**2 + sigNew(i,6)**2 ) ) )

                 end if
              end do

              do i=1, nblock
                 if(DamOld(i) .ge. 1.0)  then
                    iconv(i) = 1
                 endif
              end do

              do i=1, nblock

                 if (iconv(i) .eq. 0) then

C  Determine the Tangent of the Flow Surface

                    if ( (dt .eq. 1.0) .or.
     .                   (dt .eq. TotalTime) ) then

                       TanMod(i) = Sallow(i)/(edt(i)*dt)

                    else if (abs(Sallow(i)-SallowO(i)) .lt. 0.1 ) then

                       TanMod(i) = 0.0

                    else if (epeff(i) .eq. 0.0) then

                       TanMod(i) = 0.0

                    else

                       TanMod(i) = (Sallow(i) - SallowO(i)) / epeff(i)

                    end if

                    TanMod(i) = dmin1(TanMod(i), 0.001)

C  Evaluate yield function in a non-dimensional form

                    VoidY(i) = (2.0 * q1 * Voidf(i) *
     .                 Cosh(q2n(i) * SigTrace(i) / ( 2.0
     .                 * Sallow(i) ))) - (1.0 + q3 * Voidf(i)**2)

                    yf(i) = (dsEquiv(i)/Sallow(i))**2 + VoidY(i)

C  Elastic stress Only and set elastic strains to total strains

                    if ( ( (yf(i) .lt. 0.0) .and. (j .eq. 1))
     .                                  .or. (dt .eq. 1.0) ) then

                       iconv(i) = 1

C  Plastic Stress and Converged

                    else if (abs(yf(i)) .lt. ctol) then

                       iconv(i) = 1

                    else
```

```
C  Calculate the Mtensor

                    vc1 = (q1 * VoidF(i)/Sallow(i)) * Sinh(q2n(i)
     .                 * SigTrace(i) / (2.0 * Sallow(i)) )
                    vc2 = 1.0 / Sallow(i)**2

                    rm(i,1) = vc2 * (3.*SigNew(i,1)-SigTrace(i))+vc1
                    rm(i,2) = vc2 * (3.*SigNew(i,2)-SigTrace(i))+vc1
                    rm(i,3) = vc2 * (3.*SigNew(i,3)-SigTrace(i))+vc1
                    rm(i,4) = vc2 * (3.*SigNew(i,4))
                    rm(i,5) = vc2 * (3.*SigNew(i,5))
                    rm(i,6) = vc2 * (3.*SigNew(i,6))

                    const = (VoidF(i) * TanOld(i) * q1 * SigTrace(i)
     .                 / Sallow(i)**2) * Sinh(q2n(i)*SigTrace(i) /
     .                 (2.0*Sallow(i)))

                    xpsi1(i) = -2.0 * TanOld(i)/Sallow(i)**3 *
     .                 (1.5 * (SigNew(i,1)**2 + SigNew(i,2)**2 +
     .                 SigNew(i,3)**2 + 2.0 * (SigNew(i,4)**2 +
     .                 SigNew(i,5)**2 + SigNew(i,6)**2 ) ) - 0.5
     .                 * SigTrace(i)**2) - const

                    xpsi2(i) = 2.*q1*Cosh(q2n(i) * SigTrace(i) /
     .                 (2.0*Sallow(i))) - 2.0 * q2n(i) * VoidF(i)

                    h1(i) = Sqrt((2.0/3.0) * (rm(i,1)**2 + rm(i,2)**2
     .                 + rm(i,3)**2 + 2.0 * (rm(i,4)**2 +
     .                 rm(i,5)**2 + rm(i,6)**2 ) ) )

                    h2(i) = (1.0 - VoidF(i)) *
     .                 (rm(i,1) + rm(i,2) + rm(i,3))

C  Compute delta - lamda

                    ct = c11(i) * (rm(i,1)**2 + rm(i,2)**2 +
     .                 rm(i,3)**2) + 4.* (c44(i)*rm(i,4)**2 +
     .                 c55(i)*rm(i,5)**2 + c66(i)*rm(i,6)**2)+
     .                 2.*c12(i) * (rm(i,1)*rm(i,2) +
     .                 rm(i,1)*rm(i,3) + rm(i,2)*rm(i,3))

                    denom = ct - xpsi1(i)*h1(i) - xpsi2(i)*h2(i)

                    if( denom.eq.0.0) then
                       write(6,*) 'stop denom is 0'
                       stop
                    end if

                    dlamda(i) = yf(i) / denom

                    if ((denom .lt. 0.0).and.(j.gt.2)) then
                       write(6,*) '** Need to Change dlamda'
                       stop
                    end if

                 end if

                 if ((j .gt. 5) .and. (j .lt. 10000)) then
c                   write(6,*) yf(i), const, VoidY(i), dlamda(i), j
                 else if (j .eq. 10000) then
                    write(6,*) 'J exceed maximum, STOP'
                    write(6,*) yf(i), const, VoidY(i), dlamda(i), j
```

```
                write(6,*) '                                    '
                write(6,*) 'Consider reducing the time step'
                write(6,*) '                                    '
                STOP
             end if
          end if
       end do

C  Check for complete convergence

       Converged = .True.

       do i=1, nblock

          if (iconv(i) .eq. 0) then
             Converged = .False.
          end if

       end do

    end do

    do i=1, nblock

C   Set dep to the plastic strain increment

       do k=1, 6
          dep(i,k) = epInc(i,k)
       end do

C   Update the new plastic strain

       epInc(i,1) = dep(i,1) + epo1(i)
       epInc(i,2) = dep(i,2) + epo2(i)
       epInc(i,3) = dep(i,3) + epo3(i)
       epInc(i,4) = dep(i,4) + epo4(i)
       epInc(i,5) = dep(i,5) + epo5(i)
       epInc(i,6) = dep(i,6) + epo6(i)

C   Update the Plastic Work and Inelastic Energy terms

       PlasticWorkInc(i) = (1.0/2.0) * (
     .    (SigOld(i,1) + SigNew(i,1)) * dep(i,1) +
     .    (SigOld(i,2) + SigNew(i,2)) * dep(i,2) +
     .    (SigOld(i,3) + SigNew(i,3)) * dep(i,3) +
     .    2.0 *(SigOld(i,4) + SigNew(i,4)) * dep(i,4) +
     .    2.0 *(SigOld(i,5) + SigNew(i,5)) * dep(i,5) +
     .    2.0 *(SigOld(i,6) + SigNew(i,6)) * dep(i,6))

       eInelasNew(i) = eInelasOld(i) +
     .    PlasticWorkInc(i) / density(i)

C   Update the Internal Energy terms

       edev(i) = (1.0/2.0) * (
     .    (SigOld(i,1) + SigNew(i,1)) * eInc(i,1) +
     .    (SigOld(i,2) + SigNew(i,2)) * eInc(i,2) +
     .    (SigOld(i,3) + SigNew(i,3)) * eInc(i,3) +
     .    2.0 *(SigOld(i,4) + SigNew(i,4)) * eInc(i,4) +
     .    2.0 *(SigOld(i,5) + SigNew(i,5)) * eInc(i,5) +
     .    2.0 *(SigOld(i,6) + SigNew(i,6)) * eInc(i,6))

       eInternNew(i) = eInternOld(i) +  edev(i) / density(i)
```

```
         end do

      else
         write(6,*) 'No Strength Model'
         stop
      end if

C  Update the total temperature of the model

      do i=1, nblock

         TempN(i) = Tinit + eInelasNew(i) / SpHeat
     .        + ShockTemp(i)

C  Compute the equivalent Flow Stress for Void Model

         PlastEM(i) = PlasticWorkInc(i) /
     .       ( Sallow(i) * (1.0 - Voidf(i)) )

C  Calculate the trace of the plastic strain rate tensor
C  as required for the Void Model

         Epdot(i) = dep(i,1) + dep(i,2) + dep(i,3)

      end do

      do i=1, nblock

         State5(i) = edt(i)          ! Don't Change
         State6(i) = vmises(i)

         State7(i) = ebar(i)
         State8(i) = edev(i)

         State9(i) = density(i)
         State10(i) = TanMod(i)          ! Don't Change
         State11(i) = Sallow(i)          ! Don't Change

         State12(i) = epeff(i)
         State13(i) = ebar(i)/dt

         State14(i) = yf(i)

C  PlasticWorkInc = Sallow(i) * PlastEM(i)

         State15(i) = PlasticWorkInc(i)
         State16(i) = eInternNew(i)              ! Plastic E / mass

         State17(i) = VoidY(i)                   ! Yield Function Mod

         State18(i) = DelTemp(i)
         State19(i) = eInelasNew(i)

         if (dt .ne. 1.0) then
            State20(i) =  OPlEm(i) + PlastEM(i)     ! PEEQ from ABAQUS
         end if

         State21(i) = TempN(i)           ! Don't Change

         State22(i) = epInc(i,1)     ! Don't Change
         State23(i) = epInc(i,2)     ! Don't Change
         State24(i) = epInc(i,3)     ! Don't Change
```

```
         State25(i) = epInc(i,4)      ! Don't Change
         State26(i) = epInc(i,5)      ! Don't Change
         State27(i) = epInc(i,6)      ! Don't Change

         State28(i) = ee(i,1)                    ! Don't Change
         State29(i) = ee(i,2)                    ! Don't Change
         State30(i) = ee(i,3)                    ! Don't Change
         State31(i) = ee(i,4)                    ! Don't Change
         State32(i) = ee(i,5)                    ! Don't Change
         State33(i) = ee(i,6)                    ! Don't Change

         State34(i) = VoidF(i)
         State35(i) = SigTrace(i)/3.0       ! Pressure
         State36(i) = SbarNew(i)      ! Don't Change
         State37(i) = dsEquiv(i)
         State38(i) = eInelasNew(i) * density(i)! Plastic E / Volume ! PENER
         State39(i) = eInternNew(i) * density(i)
         State40(i) = SigTrace(i) / Sallow(i)

C  SDV51-SDV54 Required For Void Model

         State51(i) = Epdot(i)
         State52(i) = PlastEM(i)
         State53(i) = Cosh(q2n(i) * SigTrace(i) / ( 2.0 * Sallow(i) ))
         State54(i) = q2n(i)          ! Don't Change
         State55(i) = SigTrace(i)     ! Don't Change

      end do

      if (iFirst .le. 1) then
         write(6,*) 'End of stress returning to main'
      end if

      return
      end

CCCCCCCCCCCCCCCCCCCCCCCCCCCCCCCCCCCCCCCCCCCCCCCCCCCCCCCCCCCCCCCCCCCCCCCC
C
C     SUBROUTINE Von-Mises
C
C  This subroutine calculates the stresses, strains, energies, and
C  temperatures at each material point
C
C  Rick Martineau
C  Written:  10/10/96
C  Modified: 11/20/96      Include shock effects on Bulk and Temp.
C  Modified: 01/20/97           Converted to Cutting Plane Method to
C                               allow more general yield function
C
CCCCCCCCCCCCCCCCCCCCCCCCCCCCCCCCCCCCCCCCCCCCCCCCCCCCCCCCCCCCCCCCCCCCCCCC

      subroutine VonMises( nblock, ndir, nshr, dt, stepTime, totalTime,
     .   density, eInc, SigOld, SigNew, eInternOld, eInternNew,
     .   eInelasOld, eInelasNew, ebarOld, ebar, dvolOld, dvol, DamOld,
     .   Dam, Oedt, State5, State6, State7, State8, State9, State10,
     .   SallowO, State11, State12, State13, State14, State15, State16,
     .   State17, State18, State19, OPlEm, State20, TempO, State21,
     .   epo1, State22, epo2, State23, epo3, State24, epo4, State25,
     .   epo5, State26, epo6, State27, ee1, State28, ee2, State29, ee3,
     .   State30, ee4, State31, ee5, State32, ee6, State33, State34,
     .   State35, State36, State37, State38, State39, VoidF, State45,
     .   State46, State51, State52, State53, State54, State55,
     .   ShockTemp,
```

```
     .   Den0, SpHeat, Tinit, Troom, Tmelt, Gs, C1, C2, C3, C4, C5, C6,
     .   Smax, dsNew, sbarOld, dvdot, u, edt, Tstar, edev, Bulk)

      include 'vaba_param.inc'

      dimension density(nblock), eInc(nblock,ndir+nshr),
     .   sigold(nblock,ndir+nshr), sigNew(nblock,ndir+nshr),
     .   eInternOld(nblock), eInternNew(nblock), Dam(nblock),
     .   eInelasOld(nblock), eInelasNew(nblock), ebarOld(nblock),
     .   ebar(nblock), dvolOld(nblock), dvol(nblock), DamOld(nblock),
     .   TempO(nblock), TempN(nblock), ShockTemp(nblock),
     .   Oedt(nblock), VoidF(nblock), OPlEm(nblock)

      dimension State5(nblock), State6(nblock),
     .   State7(nblock), State8(nblock), State9(nblock),
     .   State10(nblock), State11(nblock), State12(nblock),
     .   State13(nblock), State14(nblock), State15(nblock),
     .   State16(nblock), State17(nblock), State18(nblock),
     .   State19(nblock), State20(nblock), State21(nblock),
     .   State22(nblock), State23(nblock), State24(nblock),
     .   State25(nblock), State26(nblock), State27(nblock),
     .   State28(nblock), State29(nblock), State30(nblock),
     .   State31(nblock), State32(nblock), State33(nblock),
     .   State34(nblock), State35(nblock), State36(nblock),
     .   State37(nblock), State38(nblock), State39(nblock)

      dimension State45(nblock), State46(nblock), State51(nblock),
     .   State52(nblock), State53(nblock), State54(nblock),
     .   State55(nblock), ee1(nblock), ee2(nblock), ee3(nblock),
     .   ee4(nblock), ee5(nblock), ee6(nblock), Epo1(nblock),
     .   Epo2(nblock), Epo3(nblock), Epo4(nblock), Epo5(nblock),
     .   Epo6(nblock), OldPE(nblock)

      data iFirst/0/

      dimension dsNew(nblock,6),sbarOld(nblock),dvdot(nblock),
     .   dvbar(nblock), dvolInc(nblock), eIncAvg(nblock),
     .   edt(nblock), edot(nblock,6), edev(nblock),
     .   Bulk(nblock), Yfunc(nblock),
     .   TanMod(nblock), ElasMod(nblock)

      dimension factor(nblock), vmises(nblock), Sallow(nblock),
     .   DelTemp(nblock), Tstar(nblock), PlastEM(nblock),
     .   PlasticWorkInc(nblock), SallowO(nblock),
     .   Epdot(nblock), dsEquiv(nblock)

      dimension et(nblock,6), epeff(nblock),SigTrace(nblock),
     .   rm(6), ee(nblock,6), epInc(nblock,6), el(nblock,6),
     .   ebarInc(nblock), yf(nblock), SbarNew(nblock),
     .   dep(nblock,6), etotal(nblock,6)

      real const, yf, yfc, dlamda, dlamdac, smean, yfp

C  cycle counter and formats for debugging

      iFirst = iFirst + 1

C  Set dlamda to a very small number

      epsilon = 1.0E-08

C  Set the convergence tolerance to a small number
```

```
      ctol = 0.0001

C  The strain hardening exponent must be positive

      if (C3 .le. 0.0) then
         write(6,*)'ERROR STOP because c3 must be > 0.0'
         stop
      endif

      do i=1, nblock

         dvolInc(i) = eInc(i,1) + eInc(i,2) + eInc(i,3)
         dvol(i) = dvolOld(i) + dvolInc(i)
         dvdot(i) = dvolInc(i) /dt
         dvbar(i) = dvol(i) - dvdot(i) * dt / 2.0

C  Compute the Elastic Modulus

         ElasMod(i) = 9.0 * Bulk(i) * Gs / (3.0 * Bulk(i) + Gs)

      end do

      if (iFirst .le. 1) then
         write(6,*) 'Working on strength model'
      end if

C   ndir+nshr = 4    means 2D

      if (ndir+nshr .eq. 4) then

         if (iFirst .le. 1) then
            write(6,*) 'Working on axisymmetric strength'
         end if

C   Do not have element geometry and nodal velocities, so cannot
C   compute total strain rates directly.  But do have strain
C   increment (einc).  I think this is TOTAL strain increment.
C   Assumes einc has geometry correction if required (ie axisymmetric).

         do I=1,nblock

C  Set the el equal to the previous elastic strains

            el(i,1) = ee1(i)
            el(i,2) = ee2(i)
            el(i,3) = ee3(i)
            el(i,4) = ee4(i)

C  Find the total strain

            do j=1, 4
              etotal(i,j) = el(i,j) + eInc(i,j)
            end do

C  Average normal strain increment - TOTAL
C  TOTAL means  (elastic + plastic and deviator + dilatation)

            eIncAvg(i) = (eInc(i,1) + eInc(i,2) + eInc(i,3)) / 3.0

C  Deviator strain rates

            edot(i,1) = (eInc(i,1) - eIncAvg(i)) / dt
            edot(i,2) = (eInc(i,2) - eIncAvg(i)) / dt
```

```
            edot(i,3) = (eInc(i,3) - eIncAvg(i)) / dt
            edot(i,4) = (eInc(i,4)              ) / dt

C  equivalent plastic (deviatoric) strain rate

            edt(i) = sqrt ( (2.0/9.0) * ( (edot(i,1) - edot(i,2))**2
     .        + (edot(i,2) - edot(i,3))**2 + (edot(i,3) - edot(i,1))**2
     .        + 6.0 * edot(i,4)**2 ) )

C  Lower bound on strain rate for logarithm operation in flow stress calc

            edt(i) = dmax1 (edt(i), 0.0001)

C  Calculate the old average stress for Johnson-Cook Subroutine

            sbarOld(i) = (sigOld(i,1) + sigOld(i,2) + sigOld(i,3))/3.0

C  Set edot inc to ebar from the last increment.  This is necessary
C  to correctly calculate the total increment in plastic strain

            ebarInc(i) = ebarOld(i)

         end do

C  Compute flow stress  - Sallow

         call JC( nblock, stepTime, totalTime, ebarOld,
     .      DamOld, Tinit, Troom, Tmelt, Gs, C1, C2, C3,
     .      C4, C5, C6, Smax, sbarOld, edt, Sallow,
     .      Tstar, iFirst, TempO, DelTemp, dt )

         do i=1, nblock

C  Iteration Loop to find the plastic strains using
C  the cutting plane algorithm

            Converged = .False.
            j = 0
            dlamdal = epsilon
            dlamda = 0.0
            dlamdac = 0.0

            do k=1,6
               epInc(i,k) = 0.0
            end do

            do while (Converged .eq. .False.)

C  Increment counter

               j = j +1

C   Update the plastic strain increment

               do k = 1, 4
                  epInc(i,k) = epInc(i,k) + dlamdac * rm(k)
               end do

C   Calculate the effective plastic strain change

               epeff(i) = Sqrt(2.0/9.0)
     .            * Sqrt( ( epInc(i,1) - epInc(i,2) )**2
     .                 + ( epInc(i,2) - epInc(i,3) )**2
```

```
     .                  + ( epInc(i,3) - epInc(i,1) )**2
     .            + 6.0 *( epInc(i,4)**2 ) )

C    Update the total effective plastic strain

               ebar(i) = ebarOld(i) + epeff(i)

C    Update the elastic strain increment

               do k=1, 4
                  ee(i,k) = el(i,k) + eInc(i,k) - epInc(i,k)
               end do

C    Update the volumetric increment

               dvolInc(i) = ee(i,1) + ee(i,2) + ee(i,3)

C   Compute New stresses

               sigNew(i,1) = (Bulk(i)-(2./3.)*Gs)
     .            * dvolInc(i) + 2.0 * Gs * ee(i,1)
               sigNew(i,2) = (Bulk(i)-(2./3.)*Gs)
     .            * dvolInc(i) + 2.0 * Gs * ee(i,2)
               sigNew(i,3) = (Bulk(i)-(2./3.)*Gs)
     .            * dvolInc(i) + 2.0 * Gs * ee(i,3)
               sigNew(i,4) = 2.0 * Gs * ee(i,4)

               SbarNew(i) = (SigNew(i,1)+SigNew(i,2)+SigNew(i,3))/3.0
               SigTrace(i)=sigNew(i,1)+sigNew(i,2)+sigNew(i,3)

C    Find the deviatoric Stress

               dsNew(i,1) = SigNew(i,1) - (1.0/3.0)*SigTrace(i)
               dsNew(i,2) = SigNew(i,2) - (1.0/3.0)*SigTrace(i)
               dsNew(i,3) = SigNew(i,3) - (1.0/3.0)*SigTrace(i)
               dsNew(i,4) = SigNew(i,4)

C    Calculate the Equivalent stress from the deviatoric stress

               dsEquiv(i) = Sqrt((1.0/2.0) * ( (dsNew(i,1)
     .            - dsNew(i,2))**2 + (dsNew(i,2) - dsNew(i,3))**2
     .            + (dsNew(i,3) - dsNew(i,1))**2 +
     .            6.0 * dsNew(i,4)**2) )

C   Equivalent stress - Mendelson p. 102

               vmises(i) = sqrt( (1./2.) * (((sigNew(i,1)
     .           - sigNew(i,2))**2 + (sigNew(i,2)
     .           - sigNew(i,3))**2 + (sigNew(i,3)
     .           - sigNew(i,1))**2 + 6.0 * sigNew(i,4)**2)))

C   Evaluate yield function in a non-dimensional form

               yf(i) = dsEquiv(i)/Sallow(i) - 1.0

C   Elastic stress Only and set elastic strains to total strains

               if ( ( (yf(i) .lt. 0.0) .and. (j .eq. 1))
     .                                 .or. (dt .eq. 1.0) ) then

                  Converged = .True.
                  yf(i) = 0.0
```

```
C  Plastic Stress and Converged

               else if (abs(yf(i)) .lt. ctol) then

                  Converged = .True.

               else if (j .eq. 1) then

                  Converged = .False.

                  yfc = yf(i)
                  dlamdac = dlamda1

               else if (j .gt. 1) then

                  dlamdap = dlamdac
                  yfp = yfc
                  yfc = yf(i)

                  if (yfp - yfc .ne. 0.0) then
                    dlamdac = (yfc * dlamdap) / (yfp - yfc)
                  end if

               end if

               if ((j .gt. 10) .and. (j .lt. 100)) then
                  write(6,*) yf(i), const, dlamdac, j
               else if (j .eq. 100) then
                  write(6,*) 'J exceed maximum, STOP'
                  write(6,*) yf(i), const, dlamdac, j
                  STOP
               end if

C  Calculate the Mtensor which is the deviatoric stress divided by the
C  magnitude of the equivalent stress

               smean = (1.0/3.0)*(SigNew(i,1)+SigNew(i,2)+SigNew(i,3))

               if (vmises(i) .ne. 0.0) then

               rm(1) = (SigNew(i,1) - smean) / (vmises(i)/Sqrt(3.0/2.0))
               rm(2) = (SigNew(i,2) - smean) / (vmises(i)/Sqrt(3.0/2.0))
               rm(3) = (SigNew(i,3) - smean) / (vmises(i)/Sqrt(3.0/2.0))
               rm(4) = SigNew(i,4) / (vmises(i)/Sqrt(3.0/2.0))

               end if

            end do

         end do

         do i=1, nblock

C   Set dep to the plastic strain increment

            dep(i,1) = epInc(i,1)
            dep(i,2) = epInc(i,2)
            dep(i,3) = epInc(i,3)
            dep(i,4) = epInc(i,4)

C   Update the new plastic strain

            epInc(i,1) = dep(i,1) + epo1(i)
```

```
            epInc(i,2) = dep(i,2) + epo2(i)
            epInc(i,3) = dep(i,3) + epo3(i)
            epInc(i,4) = dep(i,4) + epo4(i)

            ebarInc(i) = ebar(i) - ebarInc(i)

C   Update the Plastic Work and Inelastic Energy terms

            PlasticWorkInc(i) = dsEquiv(i) * (ebar(i) - ebarOld(i))

            eInelasNew(i) = eInelasOld(i) +
     .         PlasticWorkInc(i) / density(i)

C   Update the Internal Energy terms

            edev(i) = (1.0/2.0) * (
     .         (SigOld(i,1) + SigNew(i,1)) * eInc(i,1) +
     .         (SigOld(i,2) + SigNew(i,2)) * eInc(i,2) +
     .         (SigOld(i,3) + SigNew(i,3)) * eInc(i,3) +
     .         2.0 *(SigOld(i,4) + SigNew(i,4)) * eInc(i,4))

            eInternNew(i) = eInternOld(i) +  edev(i) / density(i)

         end do

      else
         write(6,*) 'MAJOR ERROR NO STRENGTH MODEL'
         stop
      end if

C  Update the total temperature of the model

      do i=1, nblock

         TempN(i) = Tinit + eInelasNew(i) / SpHeat
     .        + ShockTemp(i)

C  Calculate the trace of the plastic strain rate tensor
C  as required for the Void Model

            Epdot(i) = dep(i,1) + dep(i,2) + dep(i,3)

c           if (Epdot(i) .lt. 0.0) Epdot(i) = 0.0

C  Compute the equivalent Flow Stress for Void Model

            PlastEM(i) = PlasticWorkInc(i) / Sallow(i)

            if (PlastEM(i) .lt. 0.0) PlastEM(i) = 0.0

      end do

      do i=1, nblock

         State5(i) = edt(i)          ! Don't Change
         State6(i) = vmises(i)

         State7(i) = ebar(i)                     ! PEEQ
         State8(i) = edev(i)

         State9(i) = density(i)
c        State10(i) =
         State11(i) = Sallow(i)          ! Don't Change
```

```
         State12(i) = ebar(i)-ebarOld(i)
         State13(i) = ebar(i)/dt

         State14(i) = yf(i)

C  PlasticWorkInc = Sallow(i) * PlastEM(i)

         State15(i) = PlasticWorkInc(i)
         State16(i) = eInternNew(i)              ! Plastic E / mass

         State17(i) = VoidF(i)           ! VoidY

         State18(i) = DelTemp(i)
         State19(i) = eInelasNew(i)

         State20(i) = OPlEm(i) + PlastEM(i)     ! PEEQ /w voids

         State21(i) = TempN(i)           ! Don't Change

         State22(i) = epInc(i,1)      ! Don't Change
         State23(i) = epInc(i,2)      ! Don't Change
         State24(i) = epInc(i,3)      ! Don't Change
         State25(i) = epInc(i,4)      ! Don't Change
         State26(i) = epInc(i,5)      ! Don't Change
         State27(i) = epInc(i,6)      ! Don't Change

         State28(i) = ee(i,1)                   ! Don't Change
         State29(i) = ee(i,2)                   ! Don't Change
         State30(i) = ee(i,3)                   ! Don't Change
         State31(i) = ee(i,4)                   ! Don't Change
         State32(i) = ee(i,5)                   ! Don't Change
         State33(i) = ee(i,6)                   ! Don't Change

c        State34(i) =
         State35(i) = SigTrace(i)/3.0       ! Pressure
         State36(i) = SbarNew(i)
         State37(i) = dsEquiv(i)
         State38(i) = eInelasNew(i) * density(i)! Plastic E / Volume !PENER
         State39(i) = eInternNew(i) * density(i)

C  SDV51-SDV54 Required For Void Model

         State51(i) = Epdot(i)

         State52(i) = PlastEM(i)

c        State52(i) = 0.0
c        State53(i) =
c        State54(i) =
         State55(i) = SigTrace(i)

      end do

      if (iFirst .le. 1) then
         write(6,*) 'End of stress returning to main'
      end if

      return
      end

CCCCCCCCCCCCCCCCCCCCCCCCCCCCCCCCCCCCCCCCCCCCCCCCCCCCCCCCCCCCCCCCCCCCCCCCCCCCCCCCCCC
C     SUBROUTINE JOHNSON-COOK
```

```
C
C  This subroutine calculates the flow stress based on the Johnson-Cook
C  strength model.  It accounts for strain rate and temperature.
C  In addition, the capability to account for failure is include in
C  this subroutine.
C
C  Rick Martineau
C  Written:  10/10/96
C  Modified:
C
cccccccccccccccccccccccccccccccccccccccccccccccccccccccccccccccccccccc

      subroutine JC( nblock, stepTime, totalTime, ebarOld,
     .   DamOld, Tinit, Troom, Tmelt, Gs, C1, C2, C3, C4, C5,
     .   C6, Smax, sbarOld, edot, Sallow, Tstar, iFirst, TempO,
     .   DelTemp, dt )

      include 'vaba_param.inc'

      dimension ebarOld(nblock), DamOld(nblock), TempO(nblock),
     .   Sallow(nblock), Tstar(nblock), edot(nblock),
     .   DelTemp(nblock), sbarOld(nblock)

  901 format (i5, 8e10.3)
  904 format (8e10.3, i3)

      do i=1, nblock
         DelTemp(i) = TempO(i) - Tinit
      end do

      if (TotalTime .eq. dt) then
         do i=1, nblock
            DelTemp(i) = 0.0
         end do
      end if

C  Compute flow stress  - Sallow

      do i=1, nblock

C  Homologous temperature
C  The temperature rise above Troom (ambient) divided by (Tmelt - Troom)
C  Tstar is limited to values between 0.0 and 1.0

         Tstar(i) = (Tinit + DelTemp(i) - Troom) / (Tmelt - Troom)
         Tstar(i) = dmax1(Tstar(i), 0.0)
         Tstar(i) = dmin1(Tstar(i), 1.0)

C  Johnson-Cook flow stress - strain and strain-rate terms

         Sallow(i) = (C1 + C2 * ebarOld(i)**C3)
     .           * (1.0 + C4* dlog(edot(i) ) )

C  Johnson-Cook flow stress - thermal softening term

         if (C5 .gt. 0.0) then
             Sallow(i) = Sallow(i) * (1.0 - Tstar(i)**C5)
         endif

C  Johnson-Cook flow stress - pressure hardening term

         if (C6 .gt. 0.0) then
            Sallow(i) = Sallow(i) + (-sbarOld(i) * C6)
```

```
         endif

C  Johnson-Cook flow stress limited to Smax
C  If Smax=0.0, then flow stress has no upper limit.

         if(Smax .gt. 0.0) then
            Sallow(i) =  dmin1 (Sallow(i), Smax)
         endif

C  Zero flow stress if fractured element

         if(DamOld(i) .ge. 1.0)  then
            Sallow(i) = 0.0
         endif

C  Set Johnson-Cook flow stress to a positive value

         Sallow(i) =  dmax1 (Sallow(i), 0.0)

C  if data check increment, then set Sallow = Gs (shear modulus)
C  so will give elastic response.  This is required so ABAQUS will
C  compute the initial time increment properly.

         if (iFirst .le. 1) then

            if ( (stepTime .eq. 1.0)
     .                .and. (totalTime .eq. 1.0) ) then
               Sallow(i) = Gs
            endif

         endif

      end do

      return
      end

"
CCCCCCCCCCCCCCCCCCCCCCCCCCCCCCCCCCCCCCCCCCCCCCCCCCCCCCCCCCCCCCCCCCCCCCCCCCCC
"
C     SUBROUTINE EOS
"
C
"
C
"
C  Note - this routine is the same for 1D, 2D, and 3D and shell elements
C
C  This subroutine calculates the temperature rise as a result of the
C  shock.  In addition, it also calculates the change in the bulk
C  modulus as are result of the shock.
C
C  Rick Martineau
C  Written:  11/20/96
C  Modified:
C
CCCCCCCCCCCCCCCCCCCCCCCCCCCCCCCCCCCCCCCCCCCCCCCCCCCCCCCCCCCCCCCCCCCCCCCCCCCC
C123456789012345678901234567890123456789012345678901234567890123456789

      subroutine EOS( nblock, dt, ndir, nshr, Den0, density,
     .   einc, dvolOld, Bulk, S, Co, grun0, Vis, SpHt, BulkNew,
     .   State61, State62, State63, State64, State65, State66,
     .   State67, State68, State69, Temp0, TempN, CharL)
```

```
      include 'vaba_param.inc'

      dimension density(nblock), einc(nblock,ndir+nshr),
     .  State61(nblock), State62(nblock), State63(nblock),
     .  State64(nblock), State65(nblock), State66(nblock),
     .  State67(nblock), State68(nblock), State69(nblock),
     .  TempO(nblock), TempN(nblock), dvolOld(nblock),
     .  CharL(nblock)

      dimension u(nblock), dvolInc(nblock), Up(nblock),
     .   Us(nblock), ShockTemp(nblock), VisPress(nblock),
     .   factor(nblock), Ph(nblock), BulkNew(nblock),
     .   Ptemp(nblock)

C  Volumetric strain increment is the trace of the strain tensor.
C  This is a small strain approximation

      do i=1,nblock

         dvolInc(i) = eInc(i,1) + eInc(i,2) + eInc(i,3)

         if (dt .eq. TotalTime) then

            u(i) = -1.0 * dvolOld(i)

         else

            u(i) = -1.0 * ( dvolOld(i) + dvolInc(i) )

         end if

C  Calculate the particle velocity, shock velocity,
C  and Hugoniot pressure

         Up(i) = Co * u(i) / (1.0 - S * u(i))
         Us(i) = Co + S * Up(i)
         Ph(i) = (Den0 * (Co**2) * u(i))
     .       / (1.0 - S * u(i))**2

C  If particle velocity is positive then find the new bulk modulus and temp

         if (Up(i) .gt. 0.0) then

C  Compute the Bulk Modulus Factor and new bulk modulus

            factor(i) = (1.0 + u(i)*S) / (1.0 - S*u(i))**3

C  Compute the new bulk modulus based on the factor above

            BulkNew(i) = Bulk * factor(i)

C  Compute the Viscosity Pressure - ABAQUS exclusive

            VisPress(i)=(density(i)*(Vis * CharL(i) * u(i))**2)

C   Compute the temperature rise associated with the shock and
C   and the plastic work

            PTemp(i) = TempO(i) * grun0 * u(i)

            ShockTemp(i) = PTemp(i) + ( VisPress(i) * u(i) )
     .         / ( Den0 * SpHt )
```

```
         else

            VisPress(i) = 0.0
            ShockTemp(i) = 0.0
            BulkNew(i) = Bulk

         end if

      end do

C   Update state variables

      do i=1,nblock

         State61(i) = ( VisPress(i) * u(i) ) / ( Den0 * SpHt )
         State62(i) = BulkNew(i)
         State63(i) = ShockTemp(i)
         State64(i) = Up(i)
         State65(i) = Us(i)
         State66(i) = Ph(i)
         State67(i) = u(i)
         State68(i) = Den0/density(i)
         State69(i) = 1.0 - u(i)

      end do

      return
      end

CCCCCCCCCCCCCCCCCCCCCCCCCCCCCCCCCCCCCCCCCCCCCCCCCCCCCCCCCCCCCCCCCCCCCCCCCC
C
C     SUBROUTINE Void
C
C
CCCCCCCCCCCCCCCCCCCCCCCCCCCCCCCCCCCCCCCCCCCCCCCCCCCCCCCCCCCCCCCCCCCCCCCCCC

      subroutine void(nblock, dt, ndir, nshr, stepTime, totalTime,
     .   density, einc, stress, Sflow, State41, VfractOld, State42,
     .   State43, State44, State45, State46, State47, State48,
     .   State49, State50, TraceEdot, PlasticEM, TotalPlEm,
     .   q2n, SigTrace, VoidGold, VoidNold,
     .   Gs, Sn, Fn, En, q1, q2, q3, fF, fC, vFractinit,
     .   vmin, pmax, ivNuc, ivRand)

      include 'vaba_param.inc'

      dimension density(nblock), einc(nblock,ndir+nshr),
     .   stress(nblock,ndir+nshr), Sflow(nblock), State41(nblock),
     .   State42(nblock), State43(nblock), State44(nblock),
     .   State45(nblock), State46(nblock), State47(nblock),
     .   State48(nblock), State49(nblock), State50(nblock),
     .   PlasticEM(nblock), TraceEdot(nblock),
     .   VfractOld(nblock), SigTrace(nblock), q2n(nblock),
     .   VoidNold(nblock), VoidGold(nblock), TotalPlEm(nblock)

      data iFirst/0/

      dimension dvdot(nblock), sbar(nblock), dvbar(nblock),
     .   edot(nblock), sdev1(nblock), sdev2(nblock),
     .   sdev3(nblock), sdev4(nblock), sdev5(nblock),
     .   sdev6(nblock), vmises(nblock), const(nblock)
```

```
      dimension eqivplasticE(nblock), VfractNew(nblock),
     .   vgrowth(nblock), vnuc(nblock),  press(nblock),
     .   temp(nblock)

      real*8 r, rand

  901 format (10i10)
  902 format (8f15.5)
  903 format (8e15.6)

C   constants

      onethd = 1.0/3.0
      twothds = 2.0 * onethd
      twoPi = 6.28318530718
      epslon = 1.0e-10

C   Determine the void volume fraction at which there is a complete
C   loss of stress carrying capacity in the material

      fFbar = ( q1 + Sqrt(q1**2 - q3) ) / q3

C   dt = 1.0 indicates that we are in the packager

      if (dt .eq. 1.0) then
         goto 1000
      endif

C   Compute the new void volume fractions

      do i=1, nblock

C   Compute the void growth rate based on old void volume fraction

         vgrowth(i) = ( 1.0 - VfractOld(i)) * TraceEdot(i)

C   Compute the void nucleation rate

         if (iVNuc .eq. 1) then

            const(i) = (Fn / (Sn * Sqrt(twoPi))) * Exp((-1.0/2.0)
     .         * ( (TotalPlEm(i) - En)/Sn )**2 )

            vnuc(i) = const(i) * PlasticEM(i)

         else

            vnuc(i) = 0.0

         end if

C  Compute the total void volume fraction

         if ((q2n(i) .eq. q2) .and. (vgrowth(i) .gt. 0.0)) then

            temp(i) = VfractOld(i) + (vnuc(i) + vgrowth(i))

         else

            temp(i) = VfractOld(i)

         end if
```

```
      end do

      do i=1, nblock

C   Compute the vfract - Volumetric Void Fraction

         if (temp(i) .ge. fF) then

            VfractNew(i) = fFbar

         else if ( (temp(i) .gt. fC) .and. (temp(i) .lt. fF) ) then

            VfractNew(i) = fC + ((fFbar - FC)/(fF - Fc))
               * (temp(i) - fC)

         else if (temp(i) .le. fC) then

            VfractNew(i) = temp(i)

         end if

C  Verify that Vfractnew is not less than zero and the element is in
C  tension.  This is done to avoid the shock wave effects.


         if (VfractNew(i) .lt. vmin) then

            VfractNew(i) = vmin

         end if

      end do

C   Initialize the Void Volume Fraction

1000  if (TotalTime .eq. dt) then

         do i=1, nblock
            vgrowth(i) = 0.0
            vnuc(i) = 0.0

            if (iVRand .eq. 1) then

               r = rand( )
               VfractNew(i) = Vfractinit + r*Vfractinit*5.

            else

               VfractNew(i) = Vfractinit

            end if
         end do

      end if

      do i=1, nblock

         State41(i) = VfractNew(i)
         State42(i) = vgrowth(i)

         if (dt .ne. 1.0) then

            State43(i) = vgrowth(i) + VoidGold(i)
```

```
            State44(i) = vnuc(i) + VoidNold(i)

         end if

         State45(i) = Exp((-1.0/2.0)*((PlasticEM(i)*dt-En)/Sn)**2)
         State46(i) = TraceEdot(i)
         State47(i) = PlasticEM(i)
         State48(i) = const(i)

C  Volume Fract Increment

         State49(i) = temp(i)
         State50(i) = SigTrace(i)

      end do

      return

      end

CCCCCCCCCCCCCCCCCCCCCCCCCCCCCCCCCCCCCCCCCCCCCCCCCCCCCCCCCCCCCCCCCCCCCCCCCCCC
C     SUBROUTINE DEATH
CCCCCCCCCCCCCCCCCCCCCCCCCCCCCCCCCCCCCCCCCCCCCCCCCCCCCCCCCCCCCCCCCCCCCCCCCCCC

      subroutine death( nblock, iDam, Vdead, u, ebarOld, ebar,
     .   dvolOld, dvol, DamOld, Dam, deadOld, dead, VoidF, EffPe,
     .   dt, Epmax, Vfract, EPS, TKill, TotalTime )

      include 'vaba_param.inc'

      dimension ebarOld (nblock), ebar(nblock), dvolOld(nblock),
     .   dvol(nblock), DamOld(nblock), Dam(nblock), EffPe(nblock),
     .   deadOld(nblock), dead(nblock), VoidF(nblock)

      data iFirst/0/

      dimension u(nblock)

      iDead = 0

      Do I=1,nblock

C   Initialize all elements to "live"

         dead(i) = 1

C   If iDead flag set, check strain criteria to see if
C   element should be deleted.

          if ((iDam .eq. 1) .and. (dt .ne. 1.0))  then
             if (TotalTime .lt. TKill) then
                if (ebar(i) .ge. EPS)  dead(i) = 0
C               if (dvol(i) .ge. Edead)  dead(i) = 0
c               if (EffPe(i) .ge. Epmax) dead(i) = 0
C               if (ebar(i) .ge. Epmax)  dead(i) = 0
c               if (VoidF(i) .gt. Vdead)  dead(i) = 0
             end if
          endif

      end do

      return
      end
```

This report has been reproduced directly from the
best available copy.

It is available to DOE and DOE contractors from
the Office of Scientific and Technical Information,
P.O. Box 62,
Oak Ridge, TN 37831.
Prices are available from
(615) 576-8401.

It is available to the public from the
National Technical Information Service,
US Department of Commerce,
5285 Port Royal Rd.
Springfield, VA 22616.

Los Alamos
NATIONAL LABORATORY
Los Alamos, New Mexico 87545